



Cleveland State University
EngagedScholarship@CSU

ETD Archive

Spring 5-26-2022

Targeting Heat Shock 27 Kda Protein Induces Androgen Receptor Degradation

Yaxin Li

Follow this and additional works at: <https://engagedscholarship.csuohio.edu/etdarchive>

 Part of the [Biochemistry Commons](#), and the [Chemistry Commons](#)

How does access to this work benefit you? Let us know!

TARGETING HEAT SHOCK 27 kDa PROTEIN INDUCES ANDROGEN RECEPTOR
DEGRADATION

YAXIN LI

Bachelor of Science in Pharmaceutical Engineering
Tianjin University of Commerce, China
June 2014

Master of Science in Nutrients of Science
Tianjin University of Commerce, China
June 2017

Submitted in partial fulfillment of requirements for the degree
DOCTOR OF PHILOSOPHY IN CLINICAL AND BIOANALYTICAL CHEMISTRY
at the
CLEVELAND STATE UNIVERSITY
May 2022

We hereby approve this doctoral dissertation for

YAXIN LI

Candidate for the Doctor of Philosophy in Clinical-Bioanalytical Chemistry Degree for

the Department of Chemistry

and

CLEVELAND STATE UNIVERSITY'S

College of Graduate Studies by

Date: _____

Bin Su, Ph.D., Chairperson (Advisor) Dissertation Committee.

Department of Chemistry, Cleveland State University

Date: _____

Aimin Zhou, Ph.D., Dissertation Committee Member;

Department of Chemistry, Cleveland State University

Date: _____

David J. Anderson, Ph.D., Dissertation Committee Member;

Department of Chemistry, Cleveland State University

Date: _____

Xuelong Sun, Ph.D., Dissertation Committee Member;

Department of Chemistry, Cleveland State University

Date: _____

Girish C. Shukla, Ph.D., Dissertation Committee Member;

Department of Biological, Geological and Environmental Sciences, Cleveland State
University

Date of Defense: May 26, 2022

ACKNOWLEDGEMENTS

It is a genuine pleasure to express my deep appreciation and gratitude to my advisor, Dr. Bin Su, who has supported me throughout my research study with his patience and steadfast encouragement. He provided me with the guidance and feedback throughout the whole projects. The completion of this project could not have been possible without the expertise of Dr. Bin Su. He was always accessible and willing to help with my research, manuscript writing and encouraging me reading. Moreover, Dr. Bin Su is very supportive for my future job career. He always gave me lots of suggestions and always urge me to be prepared for my next stop. Thank him for all the supports he gave me in the past five years.

I also would like to express my special appreciation to my advisory committee, Dr. Aimin Zhou, Dr. David Anderson, Dr. Xuelong Sun and Dr. Girish Shukla. For their advice and feedbacks in my projects. They provided tons of helpful comments on my research project and presentation. Especially, Dr. Aimin Zhou, who influences me with very positive attitudes into research, which is very helpful for my research progress. He also supported me for my future job career by sharing the own experiences and writing the reference letters. Dr. David Anderson who introduced me to the clinical chemistry field, gave me vigorous supports for my career progression and insightful advice. He is so patient to prepare my reference letter for the clinical chemistry fellowship application.

I would like to thank Dr. Sihe Wang, Mrs. Tracy Frankowski and Dr. Carolyn Friedrich's help during my internship study at Akron's Children's Hospital. Dr. Wang is so nice and supper supportive. During the 6-week internship there, Dr. Wang and Dr.

Friedrich shared with me many clinical experiences of their career. I learned more about how clinical lab works with their vigorous support.

I thank profusely all my colleagues for their kind help and co-operation throughout my study period. Wenjing Zhang is helpful for my research work. She helped me a lot on my cell studies and data analysis. I can say I cannot complete all my research projects that fast without her help. Cody Orahoske, is one of my best friends also, provides me a lot of assistance during my Ph.D.'s periods. He helped me in animal research studies, manuscript writing, organic synthesis, etc. I can say, I cannot complete all my projects in 5 years without his help. Moreover, Cody taught me oral English and American cultures. He improved my English communication skills, which is very important to survive here. We also hung out together to relax ourselves at our leisure time, which is also very helpful for my projects.

I also want to thank my friends, including Anran Zhao, Danting Liu, Gang Xu, Ruhan Wei, Yu Zhao, Guanmin Chen and Xiaotong Zhao for their assistances. Anran Zhao taught me how to run organic synthesis when I just joined in Dr. Su's lab, also he is the person to provide me guidance to know more about the city and the university. Danting Liu helped me a lot in moving in and, she answered me many questions in my projects. Gang Xu and Yu Zhao helped me a lot in mass spectrometry. I cannot finish my projects without their help. Guanmin Chen and Xiaotong Zhao are also super supportive in many aspects.

Finally, I want to thank my parents. I do not know how to express my appreciation. Without their love and constant support, none of this would indeed be possible.

TARGETING HEAT SHOCK 27 kDa PROTEIN INDUCES ANDROGEN RECEPTOR
DEGRADATION

YAXIN LI

ABSTRACT

Glioblastoma (GBM) is the most common and aggressive brain tumor, with very poor prognosis. Androgen receptor (AR) plays a significant role in the progression of GBM, and anti-androgen agents have the potential to be used for the treatment of GBM. However, AR mutation commonly happens in GBM, which makes the anti-androgen agents less effective. Heat shock 27 kDa protein (HSP27) is a well-documented chaperone protein to stabilize AR. Inhibition of HSP27 results in AR degradation regardless the mutation status of AR, which makes HSP27 a good target to abolish AR in GBM.

Identified compound **I** (*(N-(3-((2,5-dimethoxybenzyl)oxy)-4-(methylsulfonamido)phenyl)-4-methoxybenzamide)*) inhibits GBM cell growth with IC₅₀s around 5 nM, and also shows significant inhibition in an *in vivo* GBM xenograft model at 20 mg/kg. Furthermore, it does not show toxicity to mice up to 80 mg/kg, 4-fold higher than the active *in vivo* dose. The compound significantly induces AR degradation in GBM cells *via* the proteasomal pathway. These results suggest that targeting HSP27 chaperone function to induce AR degradation in GBM is a promising and novel treatment.

Additionally, a sensitive and rapid high-performance liquid chromatography-tandem mass spectrometry (HPLC-MS/MS) method was developed and validated to investigate the pharmacokinetics and brain distribution of compound **I** in mice. The

method was successfully applied to evaluate the pharmacokinetic of compound **I** in mouse plasma and brain tissue. The apparent elimination half-life ($t_{1/2}$) was 4.06 h. The C_{\max} of compound **I** in brain tissue was 0.88 $\mu\text{g/g}$. The results indicated that compound **I** was rapidly distributed and compound **I** could cross the blood-brain barrier (BBB). The pharmacokinetic profile summarized provides valuable information for the further investigation of compound **I** as a potential anti-glioblastoma agent.

Ligand based structural optimization in the project identified two novel compounds (compounds **4** and **26**) which have potent anti-GBM activity and significantly increased BBB permeability in comparison to the lead compound **I**. This study indicated that compounds **4** and **26** could be the promising drugs to treat AR over expressed GBM, also provided a meaningful insight for the further structural modification to retain or improve the potency and BBB permeability.

TABLES OF CONTENTS

	Page
ABSTRACT.....	v
LIST OF TABLES.....	xii
LIST OF FIGURES.....	xiii
CHAPTER	
I. INTRODUCTION.....	1
1.1 Glioblastoma.....	1
1.2 Current strategies for GBM treatment.....	2
1.3 Current GBM treatment challenges.....	3
1.4 Androgen receptor: a potential therapeutic target for GBM.....	5
1.5 HSP27 and AR relationship.....	6
1.6 Targeting HSP27: a novel approach for the treatment of GBMs.....	7
II. STATEMENT OF THE RESEARCH AND SPECIFIC AIMS.....	9
2.1 The Research Problem.....	9
2.2 Specific Aims.....	10
III. SMALL MOLECULE HSP27 INHIBITOR ABOLISHES ANDROGEN RECEPTOR IN GLIOBLASTOMA.....	11
3.1. Introduction.....	11
3.2. Materials and methods.....	14

3.2.1. Reagents	14
3.2.2. Cell culture	15
3.2.3. Compounds I-IV	15
3.2.4. Cell viability analysis	15
3.2.5. Experimental animals	16
3.2.6. Maximum Tolerated Dose (MTD) study	16
3.2.7. Western blotting	17
3.2.8. Tubulin polymerization assay	17
3.2.9. HSP27 chaperone activity assay	18
3.2.10. Quantitative real-time polymerase chain reaction (qRT-PCR) analysis	18
3.2.11. Immunofluorescence assay	19
3.2.12. Computational study	20
3.2.13. Cyclooxygenase-2 (COX-2) inhibition assay	20
3.2.14. <i>In vivo</i> xenograft study	21
3.2.15. Statistical analysis	21
3.3. Results and discussion	22
3.3.1. AR and mutated AR are detected in GBM cell lines	22
3.3.2. Four drug candidates showed promising selectivity and activity inhibiting the growth of AR overexpressed GBM cells	23
3.3.3. N-methyl group is the key moiety of the compounds causing <i>in vivo</i> toxicity	25

3.3.4. Compound I inhibits chaperone activity of HSP27.....	28
3.3.5. Compound I dose dependently decreases AR and mutated AR protein levels in GBM cells	31
3.3.6. MG132 reverses the effect of compound I on AR in both U87 and T98G cells	32
3.3.7. Compound I also suppresses AR transcription in GBM cells.....	33
3.3.8. Dihydrotestosterone (DHT) dissociates AR from HSP27 and decreases compound I induced AR degradation.....	35
3.3.9. Compound I inhibits tubulin polymerization via interfere with colchicine binding domain.....	38
3.3.10. Compound I does not inhibit cyclooxygenase 2 (COX-2)	40
3.3.11. Compound I significantly reduces the growth of human GBM and AR level in the xenograft tumor model	42
3.4. Conclusion.....	44
IV. PHARMACOKINETIC AND BRAIN DISTRIBUTION STUDY OF AN ANTI- GLIOBLASTOMA AGENT IN MICE BY HPLC-MS/MS	46
4.1. Introduction.....	46
4.2. Materials and methods	48
4.2.1. Chemicals and reagents.....	48
4.2.2. Animals.....	48
4.2.3. Instrumentations and HPLC-MS/MS conditions	48

4.2.4. Preparation of standards and samples.....	49
4.2.5. Method validation.....	51
4.2.6. Pharmacokinetic study.....	52
4.2.7. Data analysis.....	53
4.3. Results and discussion.....	53
4.3.1. Optimization of chromatography conditions and MS conditions.....	53
4.3.2. Method validation.....	54
4.3.3. Pharmacokinetic study and brain tissue determination.....	58
4.4. Conclusions.....	59
V. SYNTHESIS AND ANTI-GLIOBLASTOMA EFFECT EVALUATION OF HSP27	
INHIBITORS.....	61
5.1. Introduction.....	61
5.2. Materials and Methods.....	63
5.2.1. Reagents.....	63
5.2.2. Chemistry.....	64
5.2.3. Cell culture.....	83
5.2.4. Cell viability analysis.....	83
5.2.5. Experimental animals.....	83
5.2.6. Maximum Tolerated Dose (MTD) study.....	84
5.2.7. Western blotting.....	85

5.2.8. HSP27 chaperone activity assay	85
5.2.9. Immunofluorescence assay	86
5.2.10. <i>In vivo</i> xenograft study	86
5.2.11. Determination of anti-glioblastoma agents in mouse plasma and brain.....	87
5.2.12. Statistical analysis	88
5.3. Results and discussions	89
5.3.1. Lead optimization and summarization of the structure-activity relationship (SAR).....	89
5.3.2. Compounds 4 and 26 inhibit the chaperone activity of HSP27.....	97
5.3.3. Compounds 4 and 26 dose-dependently decrease AR and mutated AR protein levels in GBM cells	99
5.3.4. AR downregulation effect of compounds 4 and 26 was confirmed with immunofluorescence imaging	100
5.3.5. Compounds 4 and 26 significantly shrunk the GBM growth and AR level in the xenograft tumor model	102
5.3.6. Compounds 4 and 26 could cross blood brain barrier	104
5.3.7. Compounds 4 and 26 do not show <i>in vivo</i> toxicity with high dose exposure	106
5.4. Conclusion.....	109
VI. CONCLUSIONS AND FUTURE DIRECTIONS	112
BIBLIOGRAPHY.....	116

LIST OF TABLES

Table	Page
1. The growth inhibitory effects of the four compounds in GBM cells.....	25
2. Comparative hematology (Mean \pm SD) between different groups.....	27
3. Intra- and inter-assay precision, accuracy for the determining compound I in mouse plasma and brain tissue.....	56
4. Extraction recovery and matrix effect of compound I in mouse plasma and brain tissue.	57
5. Stability of compound I in mouse plasma and brain tissue	58
6. Non-compartmental pharmacokinetic parameters of compound I in mouse after IP administration.....	59
7. Growth inhibitory effects of the new compounds in GBM cells.....	91
8. Non-compartmental pharmacokinetic parameters of compounds 4 and 26 in mouse after IP administration.....	105
9. Comparative hematology (Mean \pm SD) between different groups.....	109

LIST OF FIGURES

Figure	Page
1. The timeline of GBM therapy.....	3
2. Schema demonstrating AR and HSP27 interactions.....	7
3. AR, mutated AR (AR-V7) and HSP27 expression in four GBM cell lines.....	23
4. The chemical structures of compounds I-IV	24
5. Effect of compounds I-IV on body weight.....	26
6. The inhibition of compound I to HSP27 chaperone function.....	29
7. Binding of compound I with HSP27.....	30
8. Compound I abolishes AR/mutated AR in GBM.....	32
9 The downregulation of AR by compound I is through the proteasome pathway.....	33
10. Transcriptional regulation of AR related gene expression..	35
11. The expression and location of AR and HSP27 after T98G and U87 cells treated with compound I or DHT or combination, then the cells were analyzed by immunofluorescence assay.	37
12. Tubulin polymerization in the presence of different concentrations of compound I . 39	
13. Interaction of compound I with tubulin at the colchicine binding pocket (1SA0.pdb).	40
14. Compound I does not change Prostaglandin E ₂ (PGE ₂) production..	42
15. <i>In vivo</i> efficacy of compound I in human glioblastoma.	44
16. Full-scan product ion spectrum and proposed fragmentation pathways of (A) compound I and (B) compound 14 (IS).....	54

17. Typical chromatograms of different samples.	55
18. Plasma (A and B) and brain (C and D) tissue concentration-time profiles of compound I with IP administration in mice.	59
19. Core structure of the new derivatives.	89
20. AR downregulation effect of compounds 1-42 at 100 nM for 12 h in T98G cells.	96
21. AR downregulation effect of promising compounds at 50 nM for 12 h in T98G cells.	97
22. Inhibition of Compounds 4 and 26 chaperone function.....	98
23. AR and or mutated AR (AR-V7) was abolished with compound 4 or 26 treatment in T98G cells and U87 cells.	100
24. Expression and location of AR with DMSO or compounds treatment in T98G cells and U87 cells.....	101
25. <i>In vivo</i> efficacy of compound 4 and 26 in human GBM.....	103
26. Plasma and brain tissue concentration-time profiles of compound 4 (A and B) and 26 (C and D) with IP administration in mice.....	105
27. Body weight (A) and microscope images of the kidney, spleen, lung, liver and heart stained with H&E staining after compounds 4 or 26 treatment (B).	108

CHAPTER I

INTRODUCTION

1.1 Glioblastoma

Glioblastoma multiforme (GBM) is the most common and malignant tumor of the brain, with about 12,000 cases diagnosed in the United States annually ^{1,2}. GBM is also referred to as a grade IV astrocytoma, a cancer that forms from astrocytes. This type of cancer usually starts in the cerebrum, the largest part of brain in adults. GBM is a devastating brain cancer that can result in death in 6 months or less if untreated ³. GBM has an incidence of 3.21 per 100,000 people. Median age of diagnosis is 64 years, and it is more common in men as compared to women. Survival is poor with approximately 40% survival in the first-year post diagnosis and 17% in the second year. GBM symptoms might different when it locates different locations of brain, but usually includes constant headaches, seizures, vomiting, changes in mood or personality, etc.

The prognosis of GBM remains poor, despite with the development of advanced new surgical techniques combined with radiotherapy and chemotherapy ⁴. The median length of survival after a diagnosis is 15-18 months ². The current mainstay of treatment

for GBM patients is surgery, followed by radiation therapy with temozolomide (TMZ, an oral alkylating chemotherapy medicine) ⁵. However, GBM usually recurs within couple months after the surgery. Identification of new molecular targets to develop more effective drugs for GBM treatment is very urgent, the current mainstay treatment protocol caused the low median survival rate for GBM patients.

1.2 Current strategies for GBM treatment

A brief summary of existing treatment options for GBM is shown in **Figure 1**. The current standard treatment for GBM is surgery. The primary goal of surgery is to remove as much of the tumor as possible without injuring the surrounding normal brain tissue needed for normal neurological function ⁶. However, glioblastomas are surrounded by a zone of migrating tumor cells that invade surrounding tissues, making it nearly impossible to remove the entire tumor ⁷. Surgery provides the ability to reduce the amount of solid tumor tissue within the brain, removing those cells in the center of the tumor that may be resistant to radiation or chemotherapy. Overall, surgery prolongs the lives of some patients and improves the quality of remaining life but does not cure the patients. Chemotherapy was first introduced at 1970s, Carmustine (BCNU) was the first chemotherapy drug reported which could cross blood brain barrier (BBB) and kill GBM cells directly ⁸. In 1979, Salazar et al employed radiation therapy in GBM treatment, which proved to be effective ⁹. Targeting therapy was introduced in 2008. Avastin targeted the blood vessels by inhibiting angiogenesis in order to block the nutrition supply to brain tumor to kill the cancer. Currently, the mainstay of treatment of glioblastoma is surgery, followed by radiation and chemotherapy. Radiation therapy uses high-energy beams, such as X – rays to kill cancer cell. For people who cannot undergo

surgery, radiation therapy is used as the primary treatment. In some cases, thin, circular wafers containing chemotherapy medicine may be placed in the brain during surgery. The wafers dissolve slowly, releasing the medicine which kills the cancer cells. Currently, TMZ was introduced in 1999, still the first line to treat the glioblastoma. Tumor treating fields (TTFields) is a new non-invasive strategy that involves provision of low intensity (1-2 V/cm) and intermediate frequency (100 kHz to 1 MHz) electric fields to the tumor. TTFields interfere with mitotic processes within rapidly dividing GBM cells, causing cell death¹⁰. TTFields are applied by placing electrodes on the shaved skull, does cause mild dermatitis and local skin irritation are commonly reported side effects¹¹. TTFields have been approved for both newly diagnosed and recurrent GBM in 2011 and 2015, respectively^{7,12}. Seviteronel, an antiandrogen drug, was considered to be a promising anti-androgen receptor expressed GBM agent¹³. Unfortunately, seviteronel treatment of GBM patients was terminated after phase II trials in 2021¹⁴.

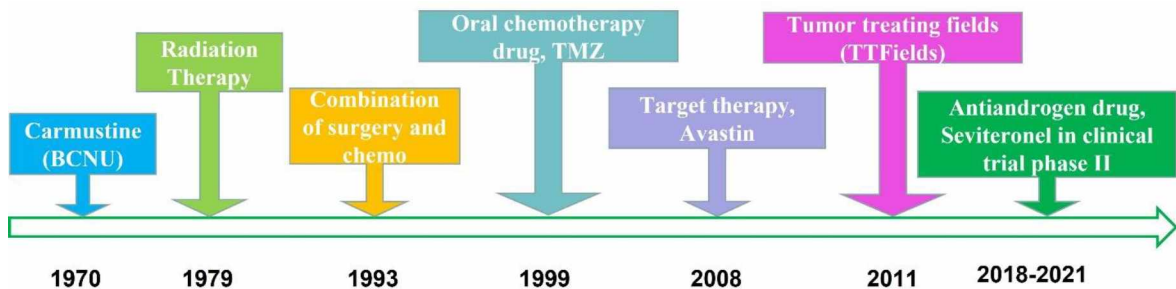


Figure 1. The timeline of GBM therapy.

1.3 Current GBM treatment challenges

There are three main challenges involved in the treatment of GBM. These are heterogeneity within the same tumor which facilitates the selection of resistant subpopulations, the fortified location of tumor which hinders delivery of therapeutics, as

well as the induction of strong local immunosuppression that promotes immune evasion and restricts the efficacy of emerging immunotherapies.

First, the proliferative property of GBM cells cause the fast resistance development and eventual relapse ^{15,16}. Studies proved that GBMs have specific local tumor microenvironments (TME) that determine the ability of a specific tumor region to invade surrounding tissues and resist conventional radiotherapy and chemotherapy ¹⁷. Second, GBM induced immunosuppression may further contribute to treatment failure. Multiple pathways have been reported to contribute to immunosuppression, including the recruitment of tumor associated macrophages which promote immune evasion, tumor growth, invasion and angiogenesis ¹⁸.

Second, in brain tumors, delivery and penetration of therapeutic agents is further restricted by the presence of the blood-brain barrier (BBB). The BBB is a highly complicated and structured neurovascular entity responsible for controlling neural homeostasis and penetration of substances into the brain. The BBB includes cerebral endothelial cells, pericytes, astrocytes, microglial and smooth muscle cells ¹⁹. The BBB has unique structure, which including tight junctions and absence of fenestrations lead to an impenetrable barrier ²⁰. Therefore, only selective substances such as small (< 500 Da) molecules can passively diffuse across the BBB ²¹. It has been reported that almost all large molecular weight drugs and about 98% of small active pharmaceutical ingredients (API) are unable to permeate the BBB ^{22,23}. The BBB plays an important role in protecting the brain from toxins and other harmful substances, but this is a double-edged sword as it also impedes the delivery of therapies to the tumor ²¹.

Third, drug resistant is common in the treatment of GBMs. The oral chemotherapy drug TMZ is often used during and after surgery and radiation therapy. Clinical evidence showed that TMZ treatment can extend patient's post-operative survival, but most cases eventually demonstrate resistance to TMZ. O⁶-methylguanine produced by TMZ mis pairs with thymine during DNA replication, alerting DNA mismatch repair. Mismatch repair recognizes the mis paired thymine on the daughter strand and excises it. However, O⁶-methylguanine persists in the template strand, so cycles of thymine reinsertion and excision result in DNA strand breaks, causing the cell death. However, O⁶-methylguanine- methyltransferase repairs the main cytotoxic lesion, as O⁶-methylguanine, generated by TMZ, can be the main mechanism of the drug resistance.

1.4 Androgen receptor: a potential therapeutic target for GBM

A statistical data indicated that the incidence of glioma in men is higher than that in women ²⁴. This indicates that glioblastoma is sex related. Sex hormone or its relevant signal pathway might be involved in moderating glioblastoma occur in our human body. It is well known that the androgen receptor (AR) is a ligand, which is an activated nuclear receptor that plays a critical role in normal prostate physiology, as well as in the development and progression of prostate cancer ²⁵. The ligand – induced conformational change facilitates the formation of AR homodimer complexes that can then bind to androgen response elements in the promoter regions of targets. Recently, studies showed that AR has high expression in glioblastoma cells, while having minimum expression in normal tissue ²⁶. Moreover, downregulating AR gene level can induce glioblastoma cell death *in vitro* ²⁷. This research indicated that AR play an important role in regulating GBM proliferation. It is well known that AR is activated by binding its ligand, androgen.

Thus, AR antagonist competes with androgen binding to AR to inhibit AR signaling, making it a potential drug to treat GBM. However, mutant AR was detected in glioblastoma, even targeting AR still promising²⁷. This AR variant, AR-V7, which lacks the ligand-binding domain, which indicating, AR antagonist will not be effective in downregulating AR-V7. This might explain that why Seviteronel failed in the clinical trials phase II for the treatment of GBM.

1.5 HSP27 and AR relationship

Heat shock 27 kDa protein (HSP27) plays an important role in the folding, activation and regulation of transcriptional activity of many steroid receptors such as AR²⁸. The overexpression of HSP27 is vital to stabilize AR. AR is in the cytoplasm in the absence of ligand, forming a complex with chaperones and co-chaperones like heat shock proteins. Upon ligand binding, AR undergoes conformational changes and translocates to the nucleus, where it binds to the androgen response elements (AREs), which activate the expression of AR target genes to induce cell proliferation, differentiation, and survival (Figure 2).

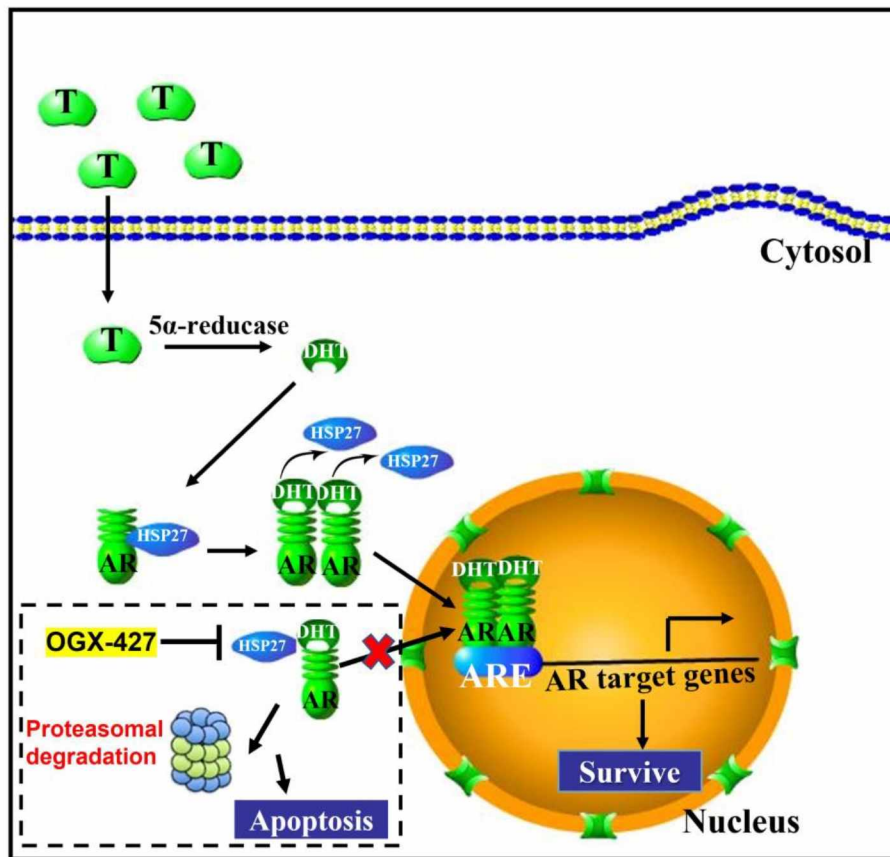


Figure 2. Schema demonstrating AR and HSP27 interactions: Testosterone (T) was reduced by 5- α reductase, produced dihydrotestosterone (DHT). DHT binding to AR recruit HSP27 escort the dimer complex translocate into nucleus, triggering ARE gene induce cell proliferation. However, with the presence of OGX-427, a HSP27 antisense oligonucleotides (ASO), could interrupt HSP27, induce AR degradation via ubiquitin proteasomal pathway.

1.6 Targeting HSP27: a novel approach for the treatment of GBMs

Recently, many researches indicate that targeting HSP27 can induce AR degradation in prostate cancer ²⁷⁻²⁸. Zoubeidi et al introduce HSP27 antisense oligonucleotides (ASO), OGX-427 to disrupt HSP27 in prostate cancer (Figure 2). The effects of OGX-427 on AR degradation was verified *in vitro* and *in vivo*. In prostate cancer, AR is critically important. OGX-427 induces HSP27 level decrease, thus, destabilizes AR and induce its ubiquitination and degradation. However, GBM is unique

type of cancer, which is different to prostate cancer due to the presence of BBB. ASO and siRNA HSP27 inhibitors are not applicable in GBM because of the poor BBB penetration of their biological agents. It is impossible to study the transient dynamic characteristics between HSP27 and Ars with HSP27 gene silencing techniques because they do not directly interfere with Ars and HSP27 inhibitors without the administration difficulties and high potential to pass the BBB would demonstrate promise for great clinical outcomes in GBM treatment.

In the following chapters, my research will demonstrate that targeting HSP27 has the significance of inhibiting GBM growth *in vitro* and *in vivo*. In our previous study, compound **I** is a HSP27 inhibitor that significantly induces AR degradation in GBM cells via the proteasomal pathway. It selectively inhibits AR overexpressed GBM cells growth with IC₅₀ values around 5 nM. Compound **I** also significantly inhibit *in vivo* GBM xenograft at 20 mg/kg and does not cause toxicity to mice up to 80 mg/kg ²⁹. These results indicate that targeting HSP27 to induce AR degradation in GBM is a promising and novel treatment approach.

CHAPTER II

STATEMENT OF THE RESEARCH AND SPECIFIC AIMS

2.1 The Research Problem

Glioblastoma (GBM), referred to as a grade IV astrocytoma, is the most common and malignant brain cancer and is considered the most aggressive malignant brain cancer in adults. It invades the nearby brain tissue, but generally does not spread to distant organs. GBM can develop in the brain from the lower grade astrocytoma. In adults, GBM occurs most often in the cerebral hemispheres, especially in the frontal and temporal lobes of the brain. GBM is a devastating brain cancer, and the median overall survival is only 20.9 months. The incidence of GBM is 50% greater in men than in women. GBM has an incidence of 3.21 per 100,000 people. Median age of diagnosis is 64 years, and it is more common in men as compared to women. The current mainstay of treatment of GBM is surgery, followed by radiation and chemotherapy. The primary aim of surgery is to remove as much of tumor as possible without damaging the surrounding normal brain tissue. However, GBM invades surrounding tissues, making it impossible to ever remove the tumor entirely. After surgery, the oral chemotherapy drug temozolomide (TMZ) is often used during and after radiation therapy. Clinical evidence showed that TMZ

treatment can extend patient's post-operative survive but most cases eventually demonstrate resistance to TMZ. Therefore, identification of new molecular targets to develop more effective drugs for GBM treatment is very urgent.

The Statistical data showed that the incidence of GBM in men is about 1.6 folds higher in men than in women. Furthermore, it is reported that androgen and the androgen receptor (AR) correlated pathway play important in GBM proliferation. Thus, targeting AR could a potential approach in GBM treatment. However, mutant AR commonly occurred in GBM, which makes the antiandrogen agents less effective. Heat shock 27 kDa protein (HSP27) is a well-documented chaperone protein to stabilize AR. Inhibition of HSP27 results in AR degradation regardless of the mutation status of AR, which indicates that HSP27 could be a potential target to abolish AR in GBM.

2.2 Specific Aims

1. To identify small molecules HSP27 inhibitors could inhibit androgen receptor and suppress glioblastoma.
2. To verify the small molecule identified could cross blood-brain barrier.
3. To synthesize new derivatives by structural modification to the compound I, identified HSP27 inhibitor. To determine the anti-glioblastoma activity *in vitro* and *in vivo* of the new compounds.
4. To verify the toxicity *in vivo* and the permeability of blood brain barrier of the new candidates.

CHAPTER III

SMALL MOLECULE HSP27 INHIBITOR ABOLISHES ANDROGEN RECEPTOR IN GLIOBLASTOMA

3.1. Introduction

GBM is the most common and malignant tumor of the brain. The prognosis of GBM patients remains poor, even with the progress in the development of new surgical techniques and the standard chemotherapy of TMZ combined with radiotherapy³⁰⁻³². TMZ is an alkylating agent that is considered the most efficient chemo drug in GBM therapy due to its good capability to pass BBB. However, *de novo* and acquired resistance to TMZ treatment are very common in GBM patients, resulting in a poor outcome³². Identification of new molecular targets to develop more effective drugs for GBM treatment is very urgent. On the other hand, the incidence of GBM in men is higher than that in women, which also is associated with men experiencing poorer outcome^{33,34}. Moreover, there are well reported cellular, molecular and imaging alterations that

underline these sex differences^{34,35}. These findings suggest that involvement in sex hormones could play a role in GBM development.⁷ To elucidate this sex disparity, studies found that AR is overexpressed in GBM and androgens contribute to the GBM tumor progression^{27,36-39}. The overexpression of AR and the role of androgen in GBM are consistent to the gender-related discrepancy of this disease. Therefore, targeting AR becomes a novel approach in GBM and an AR inhibitor Seviteronel has been investigated in clinical trials for AR overexpressed GBM patients⁴⁰. Unfortunately, AR mutation happens in 30% of the AR overexpressed GBM patients²⁷, which very likely limits the effectiveness of AR targeting agents in the treatment of GBM. It is critical to find alternative approach to diminish AR activity in GBM.

In fact, AR is correlated to a small chaperone protein HSP27 that exists in multiple oligomeric states within the cells. Overexpression of HSP27 increase the stability of its client proteins and protects cancer cells from various treatment induced cell death⁴¹. The critical connection between HSP27 and AR is AR is a well-documented HSP27 client protein^{28,41}. HSP27 is responsible for AR stability and seems a good direct target for HSP27-AR pathway in GBM. HSP27 functions through an ATP-independent mechanism and therefore could not be inhibited with geldanamycin derivatives that target the ATP-binding site of chaperone proteins⁴²⁻⁴⁴. Strategies to inhibit HSP27 at the mRNA level are alternative approaches to suppress the protein activity^{41,45}. Gene silencing strategies using short interfering RNA (siRNA) and antisense oligonucleotides (ASO) to disrupt HSP27 have been investigated and AR level was consequently reduced^{28,41,46}. Unfortunately, GBM is different from other cancer types due to the BBB protection. ASO and siRNA HSP27 inhibitors are not applicable in GBM due to the poor BBB penetration

of these biological agents. In addition, it is impossible to study the transient dynamic characteristics between HSP27 and AR with HSP27 gene silence techniques, since they don't directly interfere with AR and HSP27 at protein level. Small molecule HSP27 inhibitors without the administration difficulties and high potential to pass BBB would demonstrate promise for great clinical outcomes in GBM treatment. They can also be used to investigate the transient changes of HSP27-AR interaction following rapid HSP27 inhibition.

In our previous study, we developed dual HSP27 and tubulin inhibitors based on nimesulide (COX-2 inhibitor) as a lead compound ⁴⁷. The derivatives showed both inhibitory activity to HSP27 chaperone function and tubulin polymerization ⁴⁸. Some of the compounds showed great potency against cancer cell growth with IC₅₀s at the low nanomoles ^{48,49}. Due to the HSP27 targeting effect, we hypothesize that the small molecules could affect the stability and function of AR, which could make these compounds potential candidates to target AR overexpressed GBM ^{48,49}. In the present study, we systematically investigated a promising lead compound for the *in vitro* and *in vivo* anti-glioblastoma activity. The targeting effect of the compound to AR stability via HSP27 inhibiting was confirmed. The compound showed selectivity to AR overexpressed GBM cells and also induced AR degradation in both *in vitro* and *in vivo* GBM models. Via the toxicity study, we identified the structure moieties that are critical to the low toxicity profile and provided a new direction for future structural modification. Our results indicate that the HSP27 inhibitor has great potential to be a group of novel agents for the treatment of AR overexpressed GBM.

3.2. Materials and methods

3.2.1. Reagents

Compounds **I-IV** were prepared by our own lab. Prostaglandin E₂ ELISA kit (Cayman Chemical Company, 514010). Thiazolyl Blue tetrazolium bromide, 98% (Alfa Aesar, P31B064). Tubulin (> 99% pure) was isolated from bovine brain (Cytoskeleton, TL238). GTP (Cytoskeleton, BST06). Tubulin glycerol buffer (Cytoskeleton, BST05-001). Tubulin general buffer (Cytoskeleton, BST01-010). Insulin (Sigma Aldrich, 91077C). α -Crystallin (Sigma Aldrich, C4163). Dithiothreitol (DTT) (Amresco, EC# 222-468-7). MG132 (Sigma Aldrich, C2211). DMEM (Cleveland Clinic media laboratory, 11-500p). RPMI 1640 (Cleveland Clinic, 10-500p). FBS (Atlanta Biologicals, S11150). Pen/Strep solution (Cleveland Clinic, 725-100p). Anti- β -actin antibody (Cell Signaling Technology, 4967S). RiboZol Reagent (VWR, 97064-952). DNase I (Promega, M6101). ImProm-IITM Reverse Transcription System (Promega, A3800). 4% paraformaldehyde (VWR, J61899-AK). Bovine serum albumin (Millipore Sigma, 2905-OP). DAPI (VWR, 95059-474). Anti-HSP27 antibody (Cell Signaling Technology, 2402S). Anti-Androgen Receptor antibody (Cell Signaling Technology, 5153S). Anti-AR-V7 antibody (Cell Signaling Technology, 68492S). Anti-Rabbit IgG (Cell Signaling Technology, 7074S). Anti-Rabbit Alexa Fluor 488 secondary antibody (Thermo Scientific, A-21206). Anti-Mouse Alexa Fluor 594 secondary antibody (Thermo Scientific, SA5-10168). Non-Fat dry milk (Rockland, B51-0500). Chemiluminescent Substrate (Thermo Scientific, 34577). All the other chemicals are analytical grade.

3.2.2. Cell culture

T98G, A172, U87 and U251 cells were from ATCC. The cells were maintained in RPMI1640 or DMEM supplemented with 10% fetal bovine serum (FBS), 100 U/mL penicillin and 100 mg/mL streptomycin in a humidified incubator with 5% CO₂ at 37 °C.

3.2.3. Compounds I-IV

The synthesis of the four compounds has been published in our previous studies.^{21,22} All the final compounds exhibited purities above 97%. The chromatographic separation was performed on a C₁₈ column (2.0 mm × 150 mm, 5 μm) from Phenomenex (Torrance, CA). Two mobile phases (H₂O/CH₃OH; H₂O/CH₃CN) were employed for isocratic elution with a flow rate of 0.2 mL/min. The injection volume was 20 μL and the UV detector was set up at 256 and 290 nm.

3.2.4. Cell viability analysis

MTT assay was used to evaluate the effect of dual HSP27 and tubulin inhibitors on the growth of T98G, A172, U87 and U251 cells in eight replications. 3000 cells per well were seeded with RPMI1640 or DMEM in 96-well flat-bottomed plates for 24 h and were then exposed to various concentrations of test compounds dissolved into DMSO (highest final concentration 0.1%) in the medium for 48 h. controls received DMSO at a same concentration as that in highest does drug-treated cells. Cells were incubated in 100 μL 1 mg/mL of MTT reagent diluted in fresh media at 37 °C for 2 h. Supernatants were removed from the wells, and the precipitated MTT dye was dissolved in 200 μL/well

DMSO. Absorbance at 570 nm was determined on a SpectraMax Plus 384 spectrophotometer (Molecular Devices).

3.2.5. Experimental animals

Male CD-1 mice and nude mice were purchased from Taconic lab. Mice were housed in Plexiglas cages, kept on a 12/12 -h light-dark cycle, and received food and water *ad libitum* in a temperature- and humidity- controlled environment. All the experimental procedures involving animals were performed in accordance with the guide for the Care and Use of The Cleveland State University (CSU) Institutional Animal Care and Use Committee (IACUC).

3.2.6. Maximum Tolerated Dose (MTD) study

20 CD-1 mice were randomly divided into five groups. Mice were injected with vehicle (DMSO) or compounds **I-IV** (80 mg/kg in PBS) by intraperitoneal injection (IP) three times weekly. Mice would be euthanized once the toxicity (e.g., dehydration, lethargy, disorientation, hunched posture and ruffled coat) was observed. Body weights were determined at the start dosing day and the end dosing day. Non-fasted blood samples were collected from the heart immediately for hematology analysis after the euthanizing. Hematology analysis was performed with a hematology analyzer—Element HT5 (Heska Corporation, USA).

3.2.7. Western blotting

Cells were cultured in 6-well culture plates and incubated with DMSO or inhibitors and then lysed with RIPA (Thermo Scientific, Prod# 89900) supplemented with a protease inhibitor cocktail (Thermo Scientific, Prod# 1861278). After incubating the cells on ice for 10 min, lysates were collected into a 1.5 mL centrifuge tube, then, the supernatant would be collected after centrifuged at 10,000 g for 10 min. Protein concentrations were determined by the Bradford Protein Assay kit (Bio-Rad). Fifty micrograms of total protein lysate for each sample were boiled with 1x loading buffer for 10 min. Samples were then separated on a 10% SDS-polyacrylamide gel and transferred to polyvinylidene fluoride (PVDF) membrane (Bio-Rad). The membrane was blocked for 2 h with 5% non-fat milk in 1x TBS-T (150 mM NaCl, 10 mM Tris, pH7.4, 0.1% Tween 20) at room temperature and then incubated with primary antibody at 4°C overnight. After the membrane was incubated with the primary antibody and washed three times with 1x TBS-T for 10 min each wash, it was incubated with the secondary antibody for 60 min at room temperature. The membrane was washed three times again for 10 min each time with 1x TBS-T. Eventually, the membranes were incubated with SuperSignal West Pico Chemiluminescent Substrate (Pierce) according to the protocol of the manufacturer.

3.2.8. Tubulin polymerization assay

A mixture of 100 μ L of microtubule-associated protein-rich tubulin (2 mg/mL, Bovine brain, Cytoskeleton) in buffer containing 80 mM PIPES (pH 6.9), 2 mM MgCl₂, 0.5 mM EGTA, and 5% glycerol was mixed with DMSO (as control) or various concentrations of compound **I** in DMSO and incubated at 37 °C. Then 1 μ L of 100 mM

GTP was added to the mixture to initiate the tubulin polymerization and the absorbance at 340 nm was monitored every single minute continuously for 45 min using Molecular Devices SpectraMax Microplate reader.

3.2.9. HSP27 chaperone activity assay

24 μ L 1 mg/mL insulin stock solution was added to the single well of 384 well plate, 3 μ L 5 mg/mL α -crystallin (a segment of HSP27 responsible for the chaperone function of HSP27), 71 μ L PBS with 10 μ M compound I dissolved inside were added as well. The mixture was thoroughly mixed and incubated at 37 °C for 5 min, then 2 μ L of 1 M DTT in water was added to initiate the insulin aggregation. The mixture of insulin in the absence or presence of α -crystallin with 0.1% DMSO was used as control. The absorbance at 400 nm was monitored every three minutes continuously for 2 h using Molecular Devices SpectraMax Microplate reader.

3.2.10. Quantitative real-time polymerase chain reaction (qRT-PCR) analysis

T98G and U87 cells were seeded at a density of 2×10^5 cells per well in a 6-well plate. Leave cells in incubator overnight to adhere and treat with compound I at 25 nM for 12 h. Total RNA was isolated via using RiboZol reagent according to the manufacturer's instructions. RNA yield and purity were determined spectrophotometrically at 260–280 nm and the integrity of RNA verified by electrophoresis through denaturing agarose gels stained with ethidium bromide. To remove DNA contamination from the RNA samples, 10 μ g of total RNA was incubated with 10 units of RNase-free DNase I at 37°C for 30 min, followed by Phenol/Chloroform

Extraction and Ethanol Precipitation. Then, 1 µg of DNase I treated RNA was reverse transcribed into cDNA using the ImProm-II™ Reverse Transcription System according to the protocols. The iTaq Universal Sybr Green Super mix was obtained from Bio Rad and used for setting up real-time PCR reactions. And the specific primers for real-time PCR were designed using the Primer Express software (v3.0; Applied Biosystems). The relative levels of each gene mRNA transcripts to 18S were determined. The primer sequences for AR, PSA, NKX3.1 and 18S were as follows: AR: GGCCAGGAAAGCGACTTCA (forward); CCCATTTGCTTTTGACACA (reverse). PSA: TGTGCTTCAAGGTATCACGTCAT (forward); CTTGATCCACTTCCGGTAATGC (reverse). NKX3.1: CTTGGAGAAGCACTCCTCTTG (forward); CGCAGTACAGGTATGGGT AGTA (reverse). 18S: TCGGAACTGAGGCCATGATT (forward); CTTTCGCTCTGGTCCGTCTT (reverse). The comparative cycle of the threshold fluorescence method was applied, and the relative transcript amount of the target gene was normalized to that of 18S using the $2^{-\Delta\Delta C_t}$ method. Three replicates were performed per cDNA sample.

3.2.11. Immunofluorescence assay

T98G and U87 Cells were seeded in 6-well plates. Cover slips were placed into the wells and the cells could attach naturally. After 24 h, cells were treated with compound I at 100 nM, DHT at 10nM or combination for 12 h. Then, cells were fixed with 4% paraformaldehyde for 20 min, permeabilized with 0.1% Triton X-100 for 10 min, blocked with 1% bovine serum albumin for 30 min. Several washing steps with TBST-BSA (5%)

occurred in between fixation, permeabilization and blocking. Then, incubation with the AR and HSP27 primary antibodies for 1 h. Followed by washing with TBST-BSA (5%) then fluorescein-labeled secondary antibodies for 1 h DAPI was incubated for 10 min to stain the nucleus. Images were visualized and analyzed using GE Launches DeltaVision™ Ultra Microscopy System.

3.2.12. Computational study

Docking studies were done using the molecular modeling program MOE version 2019.0102 (Chemical Computing Group). Each protein target, HSP27 (6DV5.pdb) and tubulin (1SA0.pdb) were prepared for docking using the QuickPrep function, which adds hydrogens, and optimizes the hydrogen orientation for pH 7.4; additionally, any missing loops or crystallographic steric clashes were fixed. The binding pocket of HSP27 was identified from the literature,⁵⁰ and for tubulin, the colchicine binding site was chosen as per our previous work.⁴⁸ For the docking study, an induced-fit docking model was used, since compound binding to proteins may induce changes in the amino acid orientation to allow for optimal binding between ligand and protein. For each protein, 10 binding poses were generated, and visually inspected for optimal binding interaction.

3.2.13. Cyclooxygenase-2 (COX-2) inhibition assay

From our previous research, all four inhibitors in this paper are derivative from COX-2 inhibitor nimesulide ⁴⁷, and their COX-2 inhibition activity still remain to be determined. Prostaglandin E₂ production is an indicator of COX-2 activity since COX-2 could catalyzes the conversion of substrate arachidonic acid to prostaglandins ⁴⁶. In this

study, compound I (10 nM) were treated in U87 cells for 12 h, and nimesulide (10 μ M) was the positive control. After the treatment, the cell media was taken to determine prostaglandin E₂ content via prostaglandin E₂ ELISA kit (Cayman Chemical, USA).

3.2.14. *In vivo* xenograft study

U87 cells were re-suspended in sterile PBS (100 μ L) and injected (5×10^6 cells/injection) subcutaneously at the left and right flank of a male nude mouse (5-6 weeks, n = 4/group, 2 tumors per mouse and 8 tumors per group). Tumors and body weight were monitored with Vernier calipers three times weekly, and tumor volume was calculated by the following formula: $V = \frac{2}{3} d_1 \times d_2^2$, where d_1 is the larger diameter and d_2 is the smaller diameter. When the tumor volume reached approximately 50 mm³, mice were injected with vehicle (DMSO) or compound I (20 mg/kg in PBS) by IP or oral administration three times weekly for 14 days, and the tumor size were monitored and measured at the same time. In the end, mice were euthanized by exposure to excess CO₂ and the tumors were removed, weighted. And every two tumors from every single one mouse was mixed and homogenized with RIPA buffer (Protein inhibitors and PMSF were added) to prepare the tumor lysates after tumor were weighted.

3.2.15. Statistical analysis

Statistical and graphical information was determined using GraphPad Prism software (GraphPad Software Incorporated) and Microsoft Excel (Microsoft Corporation). Gray values from western blot were determined via Quantity One Software (Bio-Rad). The determination of IC₅₀s was performed using nonlinear regression analysis.

Statistically significant differences were calculated with the two-tailed unpaired Student's *t*-test and *p* values reported at 95% confidence intervals.

3.3. Results and discussion

3.3.1. AR and mutated AR are detected in GBM cell lines

It has been demonstrated that AR is highly expressed in some of the GBM patients and contributes to higher disease accidents in men than in women^{27,35,36}. Due to the high mutation of AR in GBM, AR antagonists could not be very effective for the treatment of GBM in this regard^{27,37}. Abolishing the AR protein in glioblastoma cells has more advantages, because both wild type and mutated AR could be both eliminated by this strategy^{27,37-40}. Therefore, we initiated the novel approach to induce AR degradation via inhibition of HSP27 in glioblastoma cells, because AR is a well-documented client protein of HSP27, and its stability is dependent on HSP27.

Multiple glioblastoma cell lines are used in our study for the potential drug candidate mechanism and efficacy evaluation. To examine the AR and HSP27 status in these glioblastoma cells, we used western blotting assay to check the protein levels in the four cell lines including, T98G, U251, A172 and U87 (**Figure 3**). Highest AR expression in T98G cells is observed, and U87 shows weaker expression, whereas U251 and A172 do not show clear AR expression compared to other two cell lines. To further explore the mutated AR (AR-V7, N terminus truncated AR with a molecular weight of 87 kDa) in these cells, we used antibody specific for mutated AR and found that only T98G cells express the mutated version of AR. The other three cell lines do not show clear protein bands. HSP27 is observed in three cell lines with the higher levels in T98G and A172

cells, whereas U251 cells do not express detectable HSP27. It seems that when AR and HSP27 are co-expressed in the cells, higher HSP27 could contribute to higher AR, as indicated by T98G cells. When AR is not expressed in the cells, higher HSP27 may contribute to the stability of its other client proteins, which is not our focus of the study. T98G and U87 cells both show detectable HSP27 and AR, and they could be good models for the investigation if targeting HSP27 could induce AR degradation.

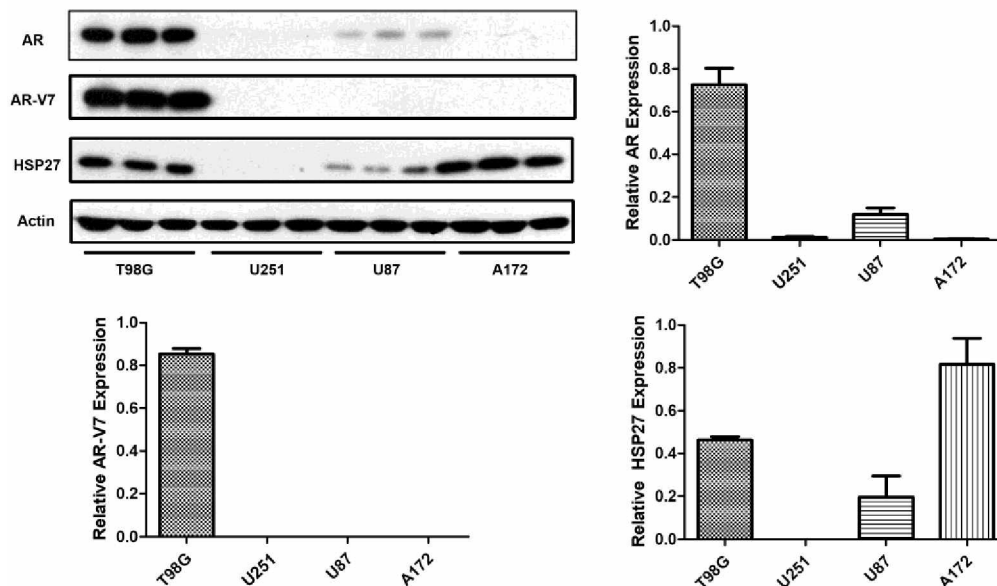


Figure 3. AR, mutated AR (AR-V7) and HSP27 expression in four GBM cell lines. The proteins were analyzed by western blot with specific antibodies, and the results are the representative images and quantification. Data are expressed as Means \pm SD (n=3).

3.3.2. Four drug candidates showed promising selectivity and activity inhibiting the growth of AR overexpressed GBM cells

To identify the most promising compounds targeting GBM, we investigated the *in vitro* activity of the four nimesulide analogs developed from our previous studies (Figure 4)^{48,49}. These compounds were discovered as dual HSP27 and tubulin inhibitors and showed inhibitory activity to the *in vitro* chaperone activity of HSP27. The HSP27

inhibition of the compound trigger our interest to investigate if the compound could target the AR function of the GBM cells. First, we examined if the compound could inhibit the growth of the GBM cells with cell proliferation assay. The IC_{50} s of the compounds against the proliferation of the four GBM cell lines were determined with multiple doses, and the results are exhibited in **Table 1**. All the IC_{50} s are less than 20 nM, indicating the great potency of the compounds in the *in vitro* cell proliferation assay. Together, all four compounds showed relatively better potency to T98G cells that express higher level of AR expression, suggesting that the selectivity of the compounds is correlated to the AR expression in the cells. Overall, compounds with ethyl sulfonamide moiety are less active than methyl sulfonamide compounds, suggesting this domain may fit into a small pocket of the molecular target.

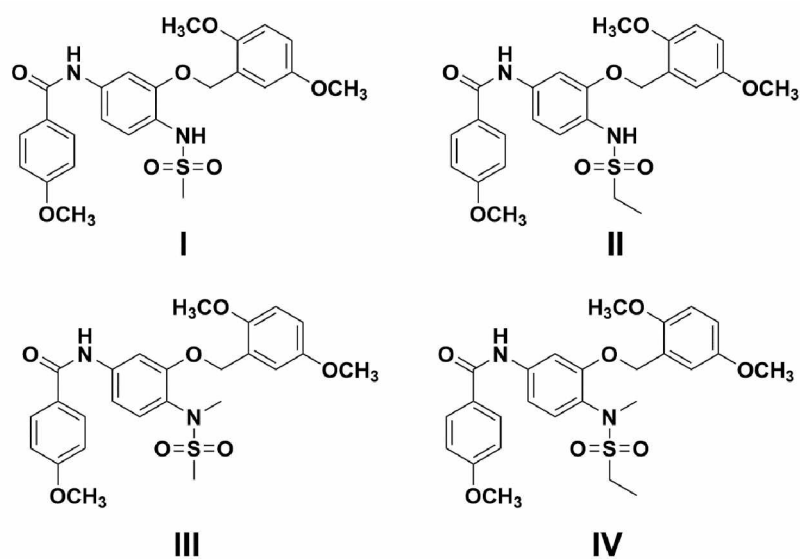


Figure 4. The chemical structures of compounds I-IV.

Table 1. The growth inhibitory effects of the four compounds in GBM cells.

Compounds	IC _{50s} (nM)			
	T98G	U251	A172	U87
I	2.01±0.64	4.00±1.20	6.24±1.06	4.78±1.62
II	4.87±2.04	6.39±1.94	11.96±2.77	6.74±2.73
III	1.85±0.81	1.57±0.33	3.13±0.78	3.05±1.16
IV	5.71±1.99	6.97±1.08	8.21±2.26	7.83±3.81

3.3.3. N-methyl group is the key moiety of the compounds causing *in vivo* toxicity

To identify the most promising drug candidate from the four compounds for further investigation, we used *in vivo* toxicity as a criterion. Mice were exposed with the four compounds at 80 mg/kg per day to evaluate the toxicity. For compounds **III** and **IV**, mice started to show dehydration and reduced food consumption after 5 days and 7 days, respectively, and were euthanized accordingly. For compounds **I** and **II**, mice did not show any syndromes of toxicity such as acute pain or distress, weight loss even at day 10. All the rest of the mice were euthanized at day 10. To quantitatively determine the *in vivo* toxicity, the weight of the mice weight was analyzed. Compounds **III** and **IV** (N-methyl group) significantly ($p < 0.05$) decreased the body weight of mice by the 5th and 7th day of exposure, while compounds **I** and **II** (N-hydrogen group) had no weight changing compared to control group (**Figure 5**). And the hematology results of all the mice are listed in **Table 2**. There is no significant change for the profile of the blood even for compounds **III** and **IV** that showed toxicity to the mice. The results reveal that compounds **I** and **II** without the N-methyl group are less toxic to the animals compared to

the compounds with the N-methyl group, suggesting that the methyl group seems play a critical role for this toxicity. Considering the *in vitro* selectivity, activity and *in vivo* toxicity, compound **I** has more potential to be a better drug candidate. Therefore, we focused on the molecular mechanism investigation of compound **I** in AR overexpressed GBM cells.

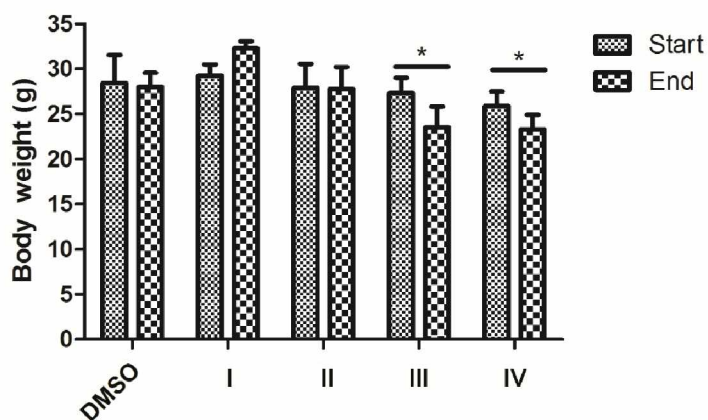


Figure 5. Effect of compounds **I-IV** on body weight with the intraperitoneal injection at dose of 80 mg/kg. CD-1 mice were exposure to both compounds **I** and **II**, **III** and **IV** for 10, 5 and 7 days, respectively. Body weight were measured at the beginning and the end of the experiment. Data are expressed as Means \pm SD (n=4). * $p < 0.05$, ** $p < 0.01$ compared to DMSO group with unpaired *t* test.

Table 2. Comparative hematology (Mean \pm SD) between different groups.

Parameters	Group					Reference
	Control	C1	C2	C3	C4	Range
WBC (10 ³ / μ L)	2.15 \pm 0.63	8.71 \pm 2.71	14.33 \pm 3.3	2.72 \pm 1.4	7.30 \pm 0.96	0.80-10.6
Neu (10 ³ / μ L)	0.27 \pm 0.30	4.07 \pm 2.09	8.09 \pm 2.62	0.86 \pm 0.6	4.32 \pm 1.75	0.23-3.60
Lym (10 ³ / μ L)	1.64 \pm 0.41	3.95 \pm 0.56	5.20 \pm 0.57	1.10 \pm 0.6	1.87 \pm 0.59	0.60-8.90
Mon (10 ³ / μ L)	0.10 \pm 0.05	0.22 \pm 0.05	0.61 \pm 0.15	0.16 \pm 0.1	0.65 \pm 0.04	0.04-1.40
Eos (10 ³ / μ L)	0.12 \pm 0.12	0.36 \pm 0.10	0.28 \pm 0.03	0.46 \pm 0.1	0.23 \pm 0.06	0.00-0.51
Bas (10 ³ / μ L)	0.02 \pm 0.02	0.12 \pm 0.03	0.16 \pm 0.06	0.14 \pm 0.1	0.24 \pm 0.19	0.00-0.12
Neu (%)	12.43 \pm 3.34	44.65 \pm 9.19	55.90 \pm 5.1	29.67 \pm 7	58.00 \pm 16	6.50-50.0
Lym (%)	76.75 \pm 6.2	47.05 \pm 8.16	36.80 \pm 4.6	40.13 \pm 2	26.35 \pm 11	40.0-92.0
Mon (%)	4.75 \pm 1.44	2.55 \pm 0.33	4.20 \pm 0.14	6.17 \pm 1.0	8.95 \pm 0.64	0.90-18.0
Eos (%)	5.18 \pm 3.75	4.30 \pm 1.52	2.00 \pm 0.71	19.30 \pm 11	3.25 \pm 1.20	0.00-7.50
Bas (%)	0.90 \pm 0.70	1.45 \pm 0.25	1.10 \pm 0.14	4.73 \pm 1.7	3.45 \pm 3.04	0.00-1.50
RBC (10 ⁶ / μ L)	7.24 \pm 2.08	7.64 \pm 0.64	7.59 \pm 1.21	9.41 \pm 2.1	8.33 \pm 0.13	6.80-12.00
HGB (g/dL)	13.10 \pm 3.13	13.96 \pm 0.60	13.50 \pm 2.1	17.47 \pm 3	15.40 \pm 0.3	10.5-19.0
HCT (%)	36.48 \pm 10.6	39.65 \pm 2.53	38.80 \pm 5.5	47.20 \pm 11	40.85 \pm 1.2	37.2-58.0
MCV (fL)	50.43 \pm 0.90	51.95 \pm 1.59	51.2 \pm 0.85	50.00 \pm 2	49.05 \pm 0.6	42.6-55.6
MCH (pg)	18.38 \pm 1.45	18.28 \pm 0.90	17.85 \pm 0.1	18.63 \pm 0	18.50 \pm 0.0	13.0-19.8
MCHC (g/dL)	36.45 \pm 2.61	35.18 \pm 1.07	34.85 \pm 0.5	37.30 \pm 2	37.70 \pm 0.6	26.0-37.9
RDW-CV (%)	12.58 \pm 0.46	13.78 \pm 0.37	13.40 \pm 0.7	17.50 \pm 1	14.40 \pm 0.1	11.1-21.1
PLT (10 ³ / μ L)	180.3 \pm 191	983.8 \pm 392	977.5 \pm 419	551 \pm 101	1075 \pm 585	565-1849
MPV (fL)	5.70 \pm 0.22	5.95 \pm 0.24	6.15 \pm 0.07	6.47 \pm 0.3	7.40 \pm 0.28	3.6-6.8

*Reference ranges obtained from Heska hematology analyzer based on the age, sex of species

3.3.4. Compound I inhibits chaperone activity of HSP27

This group of compounds were previous identified to bind to both HSP27 and tubulin ⁴⁷. Therefore, we determined if compound I affect the chaperone activity of HSP27. Our hypothesis is that the compound has the potential to downregulate AR via HSP27 inhibition. It is well documented that HSP27 plays a vital role in the prevention of cell apoptosis and effectively prevents the aggregation or degradation of its client proteins ⁵⁰. The cellular protective functions of HSP27 in the apoptotic pathway are regulated by its chaperone activity, and this activity contributes to the protection of cells from stress stimuli ⁵¹. To examine the *in vitro* chaperone activity, insulin is often used as a model substrate protein to mimic the protein aggregation and HSP27 serve as the chaperone to prevent the aggregation ^{52,53}. In this study, DTT could denature insulin, which induces insulin B chain to aggregate. We used alpha crystallin that is the chaperone function domain of HSP27 to perform the chaperone assay ⁵⁴. In the presence of the chaperone protein, the aggregation of insulin can be suppressed due to the formation of stable complexes between the chaperone and the unfolded B chain ⁵⁵. Aggregated insulin could be examined via the absorbance at 400 nm. The capability of compound I to modulate the *in vitro* chaperone activity of HSP27 was evaluated by monitoring the DTT-induced insulin aggregation in the presence of alpha crystallin, with or without compound I. As shown in **Figure 6**, alpha crystallin exhibits significant potency against DTT-induced insulin aggregation. Compound I does not interfere with DTT-induced insulin aggregation directly. When compound I and α -crystallin are combined, the chaperone function of α -crystallin is reduced. Therefore, more insulin aggregation is observed, and the curve is shifted up compared to the only α -crystallin

with DTT induced insulin aggregation. The results demonstrate the inhibitory activity of compound **I** to the *in vitro* chaperone function of HSP27.

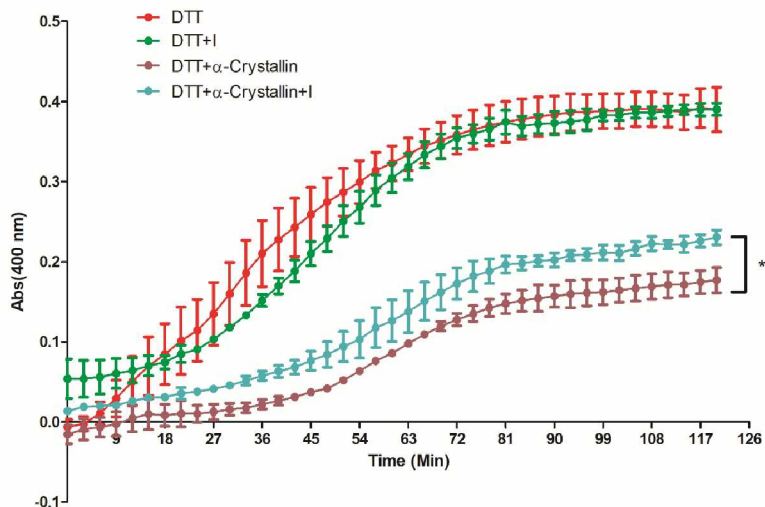


Figure 6. The inhibition of compound **I** to HSP27 chaperone function. α -Crystallin lost the activity to prevent DTT induced insulin aggregation in the presence of compound **I**. The kinetics of the DTT-induced insulin aggregation was monitored in the absence of a chaperone protein, or in the presence of a chaperone protein without or with compound **I**. The mixture of insulin and DTT with or without other components in the assay buffer was incubated for 45min at 37 °C and the absorbance at 400 nm was measured. The compound at this concentration or below did not interfere with DTT and insulin interaction. The results are representative of three independent experiments and each curve was measured in triplicate and the mean was used to generate the curve. The representative one of the three experiments are presented. The statistical analysis was performed for the end reading of the curve with unpaired *t* test, $p < 0.05$ with compound **I** vs without compound **I**.

To investigate molecular interaction of compound **I** with HSP27, we performed a docking study with the published crystal structure of HSP27 (6DV5.pdb), similar to previous studies recently published (Figure 7)⁵⁵. The crystal structure of HSP27 is a multimeric system, of which a biologically relevant phosphorylation site is located between two monomers, with S78 and S82 important for HSP27 phosphorylation⁵⁵. We found that compound **I** is able to bind to this site, and block S78 by a hydrogen-bond between the serine residue and the nitrogen from the sulfonamide moiety. This

interaction is likely contributing to the biological profile of compound I, as preventing phosphorylation of HSP27 thereby preventing HSP27 interaction with the misfolded proteins in the cellular environment. The docking result is consistent to the chaperone inhibition study of compound I.

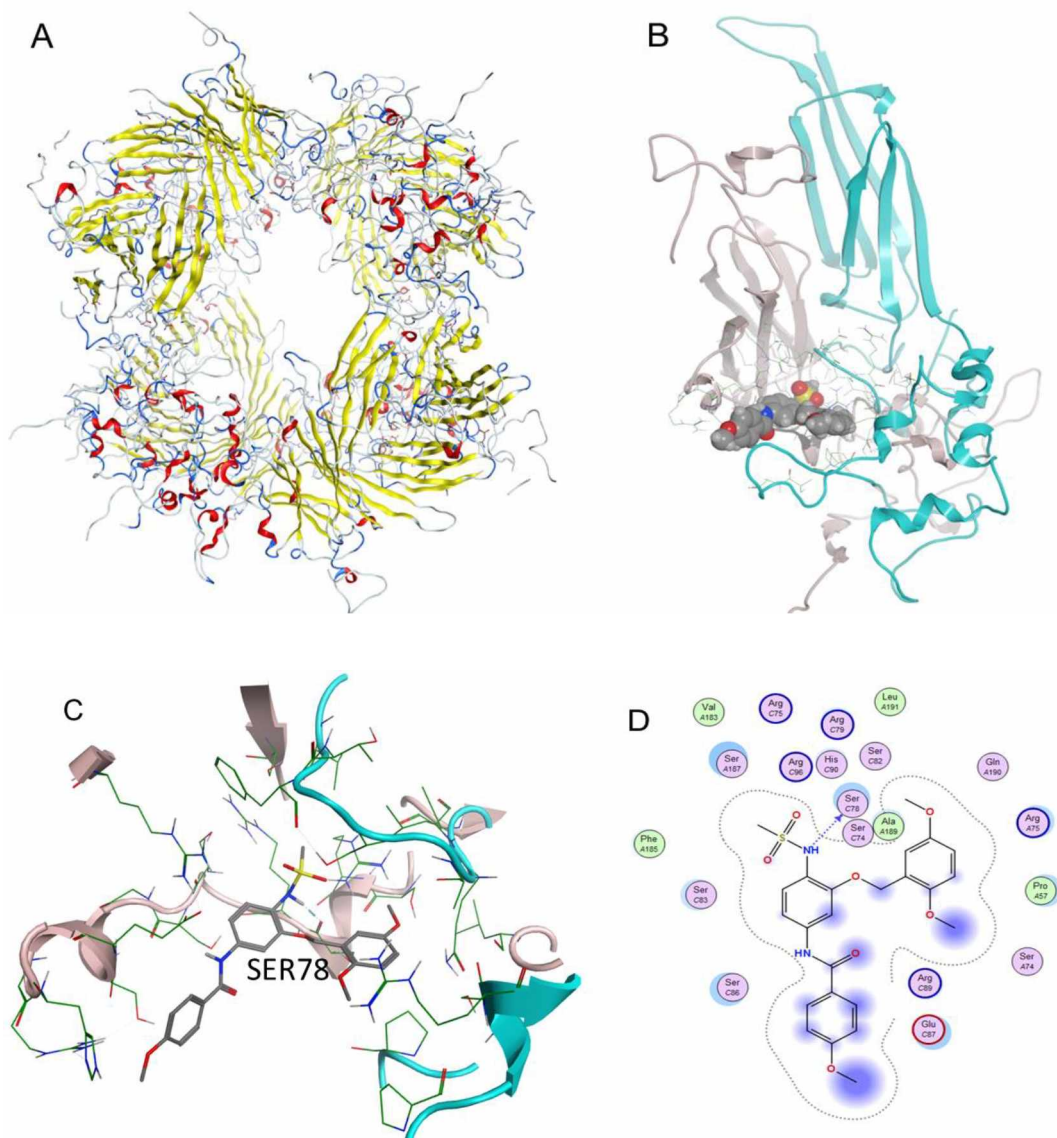


Figure 7. Binding of compound I with HSP27. **A)** Multimer HSP27 protein crystal in ribbon structure (6DV5.pdb. **B)** Binding pocket between two monomers with compound shown in space fill; **C)** Compound I binding to the HSP27 phosphorylation site, showing SER78 is blocked from phosphorylation; **D)** 2D ligand interaction diagram of compound I docked to HSP27 pocket.

3.3.5. Compound I dose dependently decreases AR and mutated AR protein levels in GBM cells

AR is a well-studied client protein of HSP27, and inhibition of HSP27 with siRNA induced AR degradation, which has been reported in prostate cancer²⁸. Herein we initiate the HSP27 inhibition strategy with small molecule due to the potential BBB crossing activity, which is critical for GBM treatment. The results exhibit that compound I could down regulate AR protein levels in GBM cells dose dependently (**Figure 8**). Compound I at 25, 50 and 100 nM all significantly induces degradation of AR compared to control in two GBM cell lines including T98G and U87. Furthermore, the mutated AR in T98G cells could be down regulated by compound I dose dependently as well. The results demonstrate the great superior of the strategy to targeting AR compared to the AR antagonists, since both wild type and mutated AR could all be abolished by the compound. The AR downregulation activity of the compound is also consistent to the selectivity of the compound to AR overexpressed cells in the cell proliferation study (**Table 1**). Regardless of the status of AR in glioblastoma cells, wild type or mutated, small molecule HSP27 inhibitor could all downregulate the AR protein level and inhibit the cell proliferation. So far, we demonstrate that compound I inhibits HSP27 chaperone function and down regulates AR in GBM cells. However, whether the two activities are correlated to each other in GBM just like in prostate cancer still needs to be confirmed.

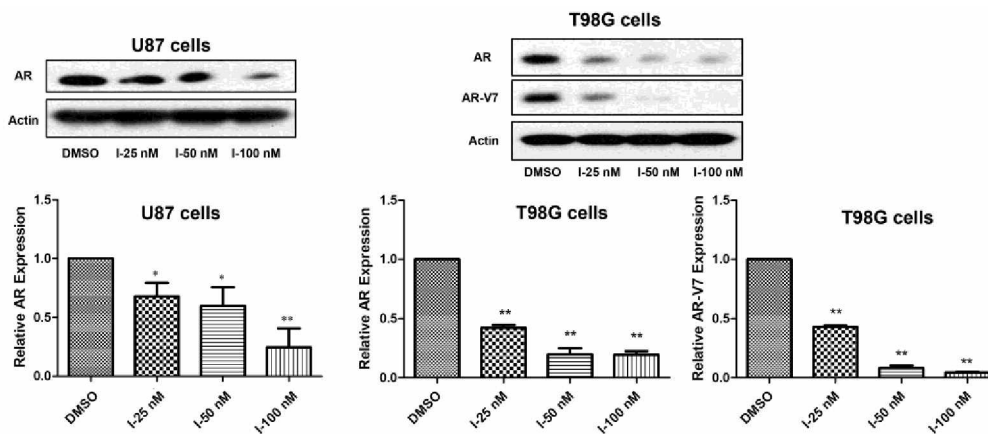


Figure 8. Compound I abolishes AR/mutated AR in GBM. AR and AR-V7 expression was analyzed by western blot after the compound treatment. The experiment was repeated three times independently and the representative image and quantification are shown. Data are expressed as Means \pm SD (n=3). * p < 0.05, ** p < 0.01 compared to DMSO treatment group by unpaired t test.

3.3.6. MG132 reverses the effect of compound I on AR in both U87 and T98G cells

AR is stabilized by HSP27, and without the protection of HSP27, AR will be degraded by proteasome, which has been reported in prostate cancer^{28,46}. We would like to determine if it is the same case in glioblastoma cells that when HSP27 is inhibited by compound I, more AR could be degraded by proteasomes. This is based on the assumption that compound I affects HSP27 activity and thus to accelerate AR degradation via ubiquitin-proteasome pathway⁵⁶. MG132 is a proteasome inhibitor that can block proteasome mediated protein degradation⁵⁷. We use MG132 as a tool to investigate whether compound I downregulate AR via proteasome pathway in T98G and U87 cells. The expression level of AR in these cells was determined by western blotting assay with the treatment of compound I at the absence or presence of MG132, and the results are shown in **Figure 9**. Compound I could significantly decrease AR expression at 50 nM and 100 nM in U87 cells (p < 0.01, treatment vs control), whereas with the

presence of MG132, AR downregulation effect is significantly attenuated ($p < 0.05$, with MG132 vs. without MG132). MG132 does not affect AR when used alone. The same results are observed in T98G cells with wild type of AR and mutated AR as well. Interestingly, it seems that MG132 does not fully rescued AR protein level in the combination, particularly in U87 cells. It is possible that the compound could down regulate AR with other mechanism besides proteasome pathway. In this case, even proteasome is blocked, AR might be decreased by compound I with some other unknown pathways. Regardless, the MG132 rescue effect further connects HSP27 with AR in GBM, and inhibiting HSP27 will lead to AR degradation via proteasome pathway.

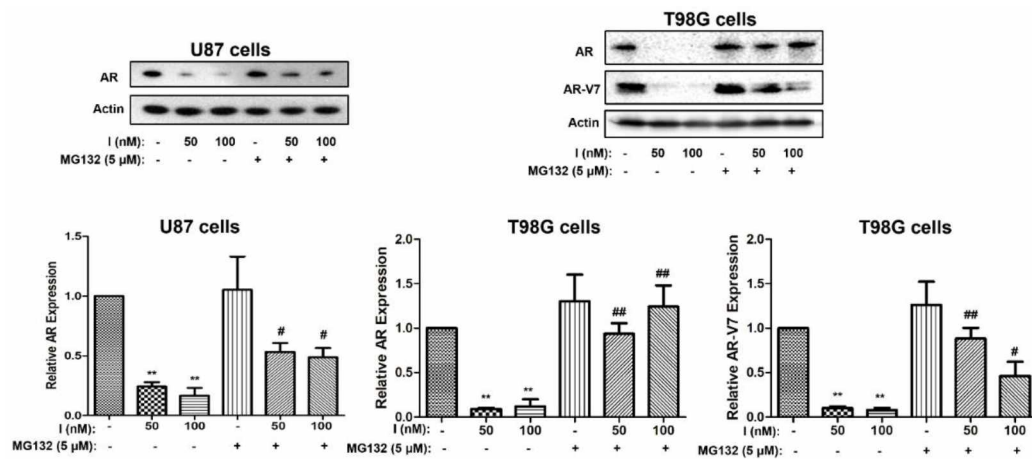


Figure 9. The downregulation of AR by compound I is through the proteasome pathway. AR or mutated AR (AR-V7) expression was analyzed by western blot after treatment by compound I with MG132 or without. The experiment was repeated three times independently and the representative image and quantification are shown. Data are expressed as Means \pm SD (n=3). ** $p < 0.01$ compared to DMSO treatment by unpaired t test. # $p < 0.05$, ## $p < 0.01$ combination compared to only compound I treatment by unpaired t test.

3.3.7. Compound I also suppresses AR transcription in GBM cells

We demonstrate that inhibiting HSP27 could downregulate AR through proteasome pathway to accelerate the protein degradation directly. The results from the combination

of compound **I** and MG132 suggest that AR might be regulated in multiple mechanisms by compound **I**, since MG132 could not fully reverse the effect of compound **I**. Therefore, we examined the mRNA of AR and the AR downstream gene PSA and NKX3.1 as well (**Figure 10**). The results listed here indicate that AR downstream gene PSA and NKX3.1 are significantly suppressed by compound **I** at 25 nM, which is consistent to the low AR protein level. Lower level of AR could not effectively activate the androgen response element (ARE) and initiate the transcription. Interestingly, AR is also suppressed via transcriptional regulation by compound **I**, and AR mRNA is down regulated significantly at 25 nM. The lower level of AR mRNA after the treatment of compound **I** is a new phenomenon, which has not been reported with HSP27 inhibition. It is possible that the downregulation of AR transcription is not the targeting effect of HSP27 inhibition. It is common that small molecule has off target effect. In this case, compound **I** might affect other pathways to decrease AR transcription, which needs further investigation in the future.

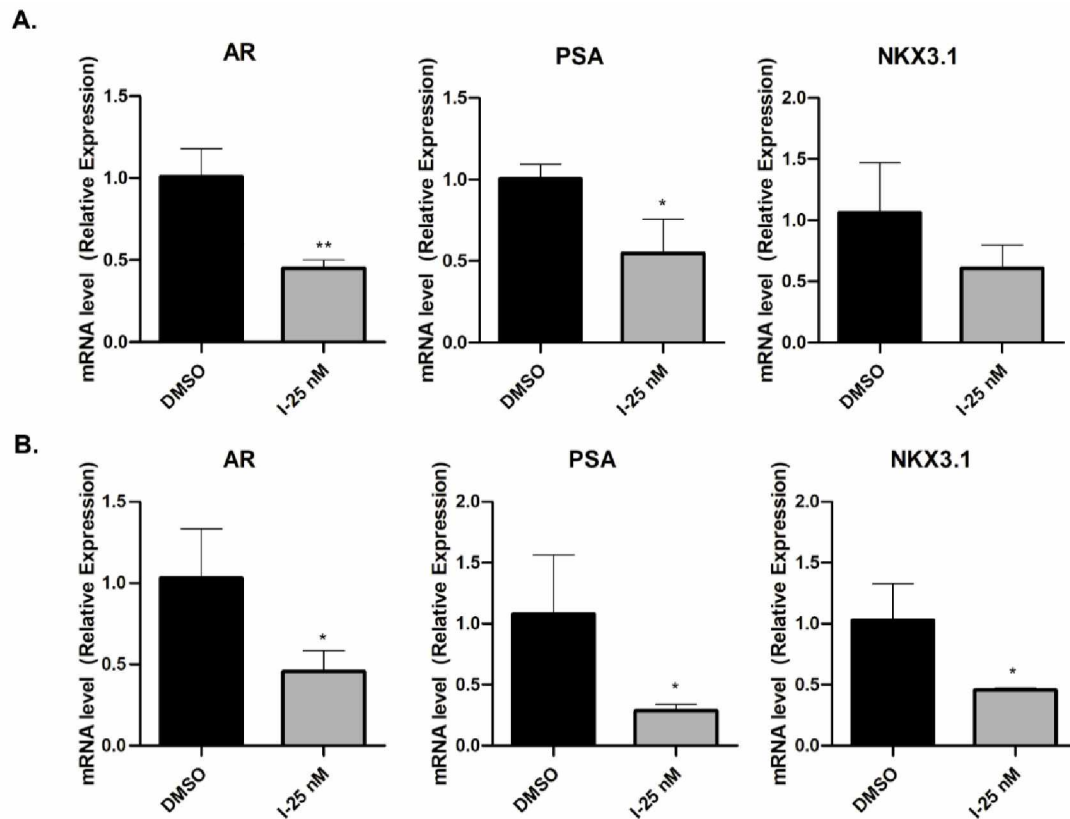


Figure 10. Transcriptional regulation of AR related gene expression. The cells were treated with compound **I** for 12 h and the RNA was extracted. AR, PSA, NKX3.1 gene expression was examined with real time PCR. The results in T98G cells (**A**) and U87 cells (**B**) are shown with the quantification results. Data are expressed as Means \pm SD (n=3). * $p < 0.05$, ** $p < 0.01$ compared to DMSO treatment group by unpaired t test.

3.3.8. Dihydrotestosterone (DHT) dissociates AR from HSP27 and decreases compound **I** induced AR degradation

AR initiates its biological function via testosterone binding and then translocates into nucleus to activate ARE. When AR is in the nucleus, the HSP27-AR complex is broken, and AR degradation could only resume when AR is out of the nucleus. To examine if HSP27-AR cooperation exists as we hypothesized in GBM, we used DHT to force AR translocating into the nucleus, which is a well-used method to initiate AR

transcription activity. By this approach, HSP27-AR complex will be temporarily broken, since HSP27 will not enter nucleus to continue stabilizing AR. Immunofluorescence staining method could be used to examine the interaction of HSP27 and AR. We observe that in T98G cells, AR is distributed in both the nucleus and cytosol in control group (**Figure 11**), which is due to the androgen residual in the cell culture medium. Part of the AR could be shuttled into the nucleus by the low level of androgens. HSP27 is distributed around the nucleus in the cytosol. When compound **I** is applied, AR level is significantly lower compared to the control group. This is consistent to the results of the western blotting assay, and compound **I** induces AR degradation via HSP27 inhibition. When DHT is applied, all the AR is concentrated in the nucleus and there is no distribution of AR in the cytosol anymore. The results suggest that the AR in GBM is sensitive to ligand DHT and responds to androgen stimulation very well. The high level of AR condensed in the nucleus disrupts HSP27-AR complex, because HSP27 does not distribute in nucleus. When DHT and compound **I** are combined, it is observed that the AR level in the nucleus is similar to only DHT treatment, suggesting that the HSP27-AR complex disruption eliminates the AR degradation induced by compound **I**. The results further demonstrate that compound **I** induce AR degradation through HSP27-AR axis. The same phenomenon could be observed in U87 cells as well.

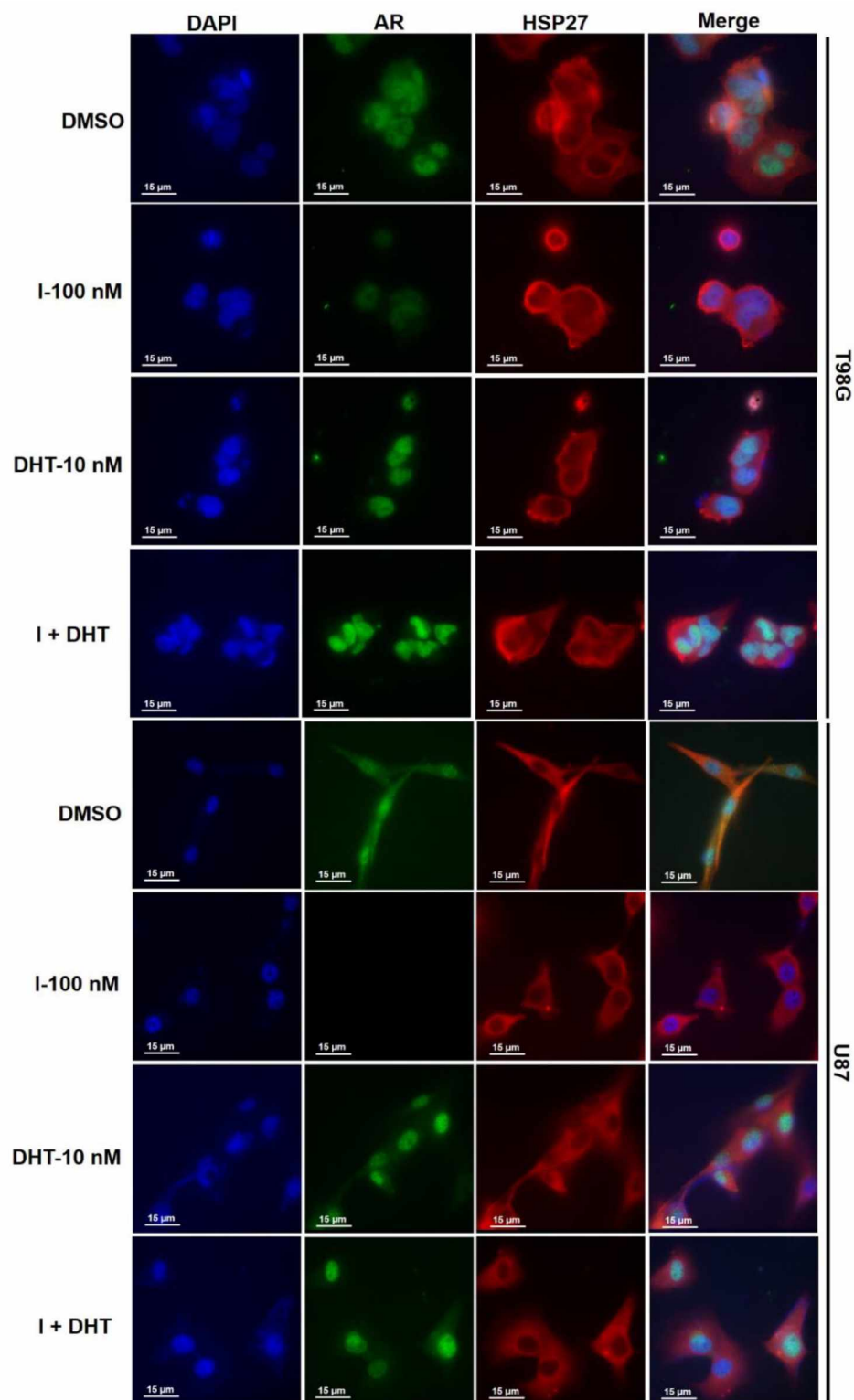


Figure 11. The expression and location of AR and HSP27 after T98G and U87 cells treated with compound I or DHT or combination, then the cells were analyzed by immunofluorescence assay.

3.3.9. Compound I inhibits tubulin polymerization via interfere with colchicine binding domain

This group of compounds were initially found binding to both HSP27 and tubulin ⁴⁷. We observed that compound I inhibits HSP27 and induces AR degradation, and it shows selectivity to AR overexpressed GBM cells (**Table 1**). However, compound I also inhibits the proliferation of GBM cells without AR expression, suggesting that the compound has general activity against GBM cells. This broad cell growth inhibition activity is unlikely to be correlated to the AR degradation. A more general target of compound I might be responsible for the general cell growth inhibition. Herein, we examine the tubulin polymerization inhibition activity of compound I (**Figure 12**). The results exhibit that compound I dose-dependently inhibits tubulin polymerization in the *in vitro* enzyme assay. The result is consistent to our previous studies that the compound I is a dual inhibitor to HSP27 and tubulin ^{48,49}, although it is more selective to AR overexpressed T98G cells due to the AR downregulation activity via HSP27 inhibition. In terms of potency for the inhibition of tubulin polymerization, compound I at 1 μ M is much more active than the positive control nocodazole, suggesting that compound I is also a potent tubulin inhibitor as a cancer therapeutic agent.

A docking study reveals that compound I is able to occupy the binding pocket of colchicine binding domain of tubulin. As can be seen from **Figure 13**, compound I binds to the colchicine binding site in tubulin (1SA0.pdb) ⁵⁸. Major hydrogen bond interactions can be seen between the sulfonamide moiety and ALA316, and LYS352. Also, a hydrogen bond is seen between a nitrogen and SER178. The binding model supports the

ability of compound **I** to destabilize normal tubulin function, and the ability of compound **I** to act as a possible chemotherapeutic agent.

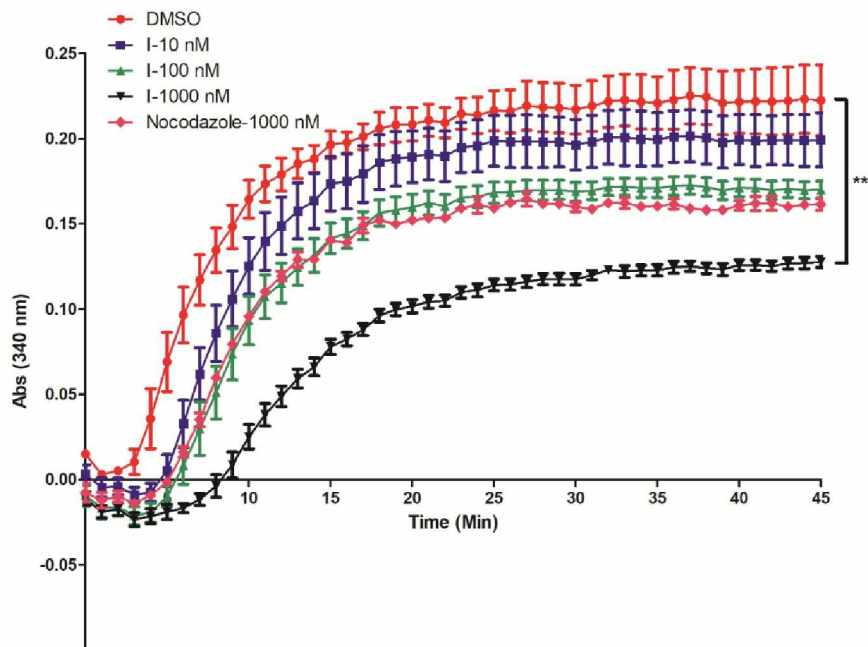
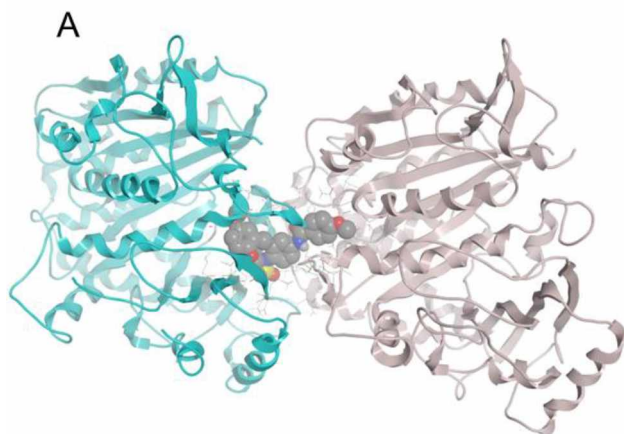


Figure 12. Tubulin polymerization in the presence of different concentrations of compound **I** and positive control nocodazole. DMSO is used as a negative control. The results are representative of three independent experiments and the mean value was used to generate the curve. The statistical analysis was performed with the end reading of the curve with unpaired *t* test, $**p < 0.01$ with compound **I** vs. control.



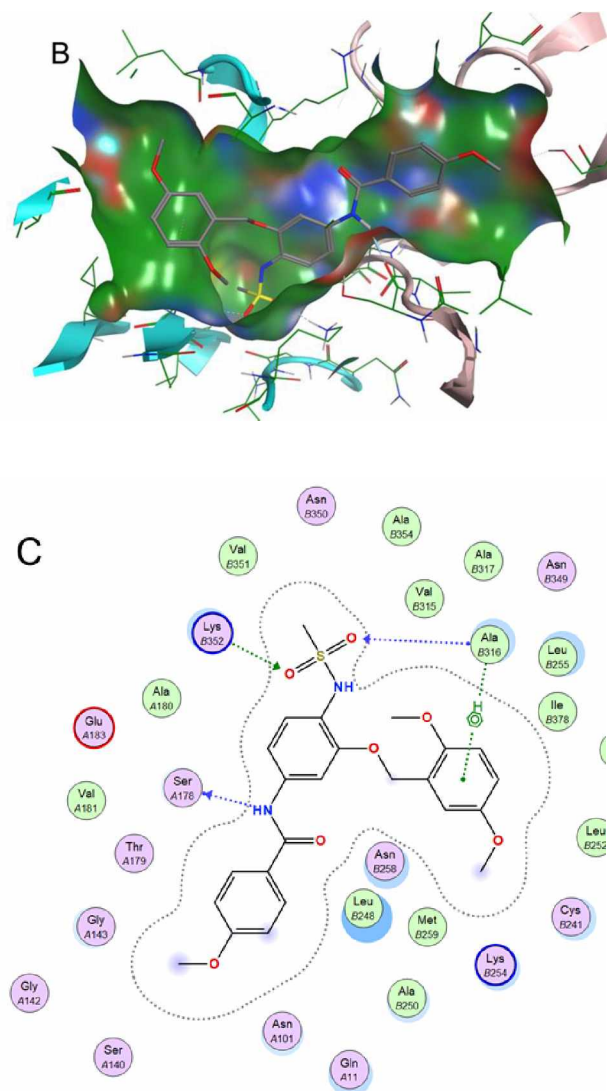


Figure 13. Interaction of compound **I** with tubulin at the colchicine binding pocket (1SA0.pdb). **A)** Dimer of tubulin shown as blue and pink, with compound **I** shown as space fill; **B)** binding pocket of compound **I** with solvent accessible surface shown; **C)** 2D ligand interaction plot with key amino acids contributing to the hydrogen bonding interactions.

3.3.10. Compound **I** does not inhibit cyclooxygenase 2 (COX-2)

Compound **I** is a promising drug candidate for potential treatment of AR overexpressed GBM. From the drug design point of view, we removed the initial N-methyl group of compound **I**, which actually was introduced to eliminate the COX-2

inhibition function of the very original lead compound nimesulide²⁶. the ionization of the sulfonamide moiety of nimesulide is critical for the COX-2 inhibition. With a Pka of 5.93, the majority of nimesulide is ionized to form the negative charge, which is a key factor for COX-2 binding. Introducing N-methyl group blocks the ionization and eliminate the COX-2 inhibition, which has been demonstrated in our previous study²⁶. However, the current investigation reveals that removing the methyl group could reduce *in vivo* toxicity and also improve solubility. There is a concern that whether removing this methyl group could bring COX-2 inhibition back. To clarify this potential problem, we measured the COX-2 inhibition of the compound using prostaglandin E₂ production assay (**Figure 14**). U87 cells were treated with compound **I** and nimesulide for 12 h. The cell culture medium was collected to determine the prostaglandin E₂ level. The results show that prostaglandin E₂ levels are significantly decreased compared to DMSO (33.03 ±6.03 pg/mL) with nimesulide (7.66 ± 1.18 pg/mL) as indicated in **Figure 14**, while there is no significant difference for compound **I** to control (35.33 ± 7.95 pg/mL). The results suggest that removing of the methyl group does not affect the COX-2 inhibition of compound **I**. It is speculated that the nitro group of nimesulide is critical to the COX-2 inhibition as well. In compound **I**, the nitro moiety is reduced to amino and formed a new benzamide moiety, and this changing leads to the change of the Pka of compound **I** to 8.65. at physiological pH condition, compound **I** will not form negative charge anymore, which could eliminate the COX-2 inhibition as well. Therefore, the methyl group of the sulfonamide moiety is not critical for COX-2 inhibition anymore.

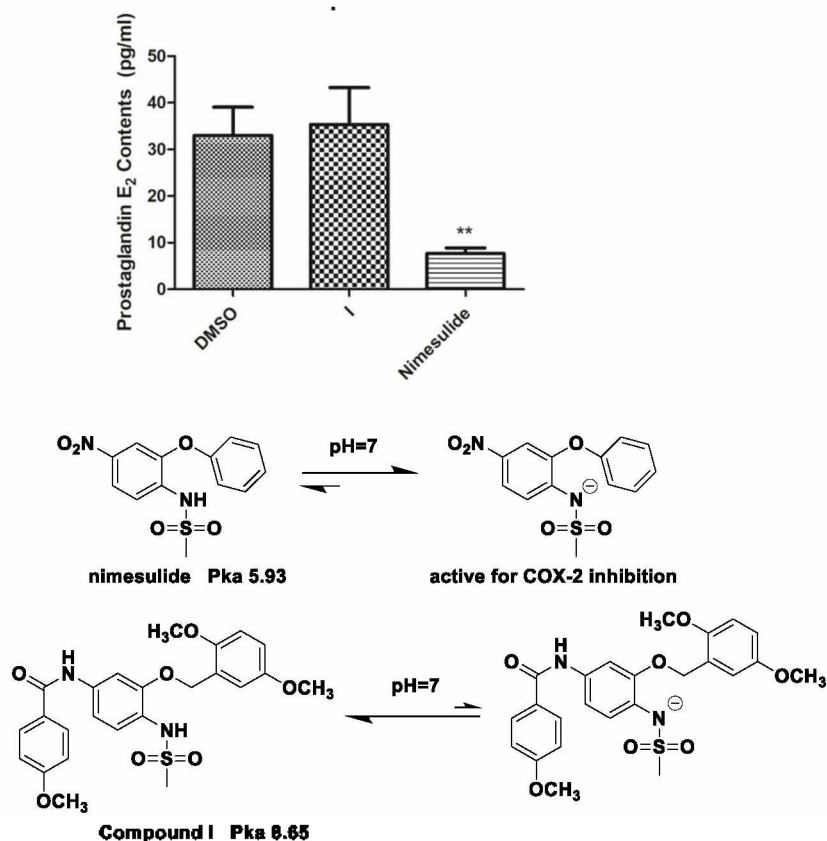


Figure 14. Compound I does not change Prostaglandin E₂ (PGE₂) production. U87 cells were treated with nimesulide (10 μ M) and compound I (10 nM) for 12 h, the medium was collected and the PGE₂ level was examined with ELISA. Data are expressed as Means \pm SD (n=3). ** $p < 0.01$ compared to DMSO treatment group.

3.3.11. Compound I significantly reduces the growth of human GBM and AR level in the xenograft tumor model

As a potential drug candidate, it is critical to determine the *in vivo* activity of compound I with the GBM model. In order to investigate the compound, the xenograft tumor mouse model was established by subcutaneously injecting U87 cells into the left and right flank of nude mice. Unfortunately, we did not successfully form a xenograft model with T98G cells with the same procedure. After U87 tumor reached 200 mm³, compound I was administrated into mice via intraperitoneal injection (IP) and oral every

other day for 2 weeks and tumor volume and mice weight were measured. As shown in **Figure 15 A**, mice body weight is not affected by the compound **I** treatment either with IP or oral administration, which is consistent to the toxicity study (**Figure 5**). The tumor size of compound **I** with both IP and oral administration is significantly ($p<0.05$) decreased compared with the DMSO group (**Figure 15 B**), and the tumor weight of compound **I** with IP injection is significant decreased compared with the DMSO group (**Figure 15 C**). Unfortunately, due to the variability of the tumor with oral administration, the tumor weight does not reach statistical significance compared to control. To confirm that tumor inhibition effect is correlated with AR protein, AR expression level in tumor was examined via western blotting (**Figure 15 D**). AR expression in both IP and oral administration groups for the compound **I** treatment is significantly ($p<0.01$) decreased compared with the DMSO group. The results demonstrate the great *in vivo* activity of compound **I** in the animals and provide strong evidence that compound **I** is a promising new drug candidate to treat AR overexpressed GBM.

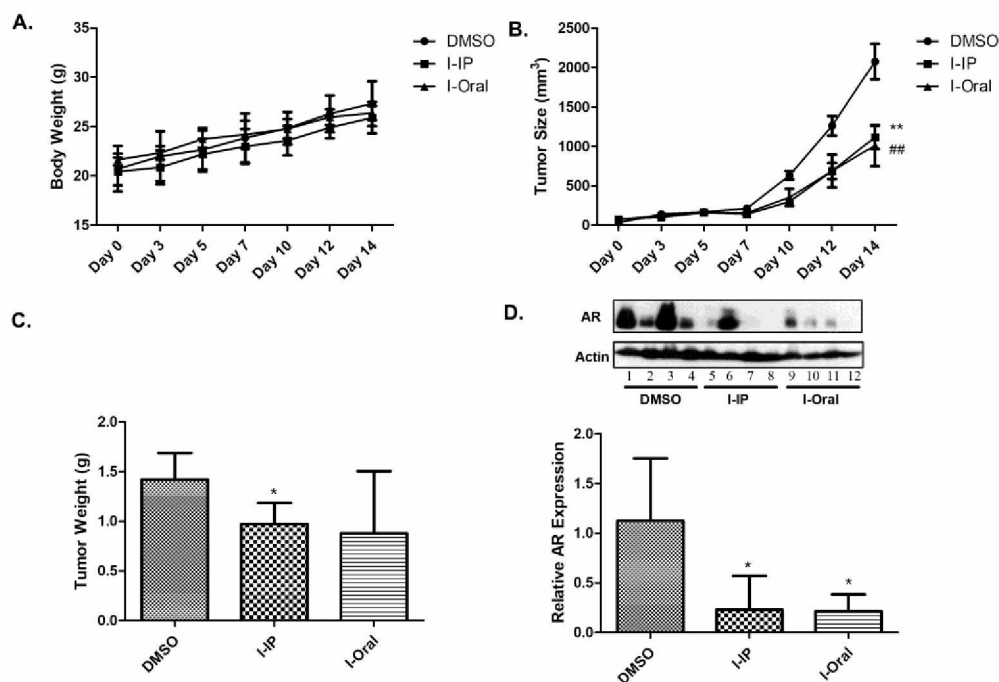


Figure 15. *In vivo* efficacy of compound **I** in human glioblastoma. A total of 5×10^6 U87 cells were inoculated subcutaneously into nude mice, which were randomly assigned to DMSO and compound **I** treated group. Nude mice were treated with compound **I** at 20 mg/kg with IP injection and oral administration. Body weight (**A**, $n=4$); tumor size (**B**, $n=8$, data are expressed as Means \pm SD. Oral $^{##}p < 0.01$, IP $^{**}p < 0.01$ compared to DMSO treatment group); tumor weight (**C**, $n=8$, data are expressed as Means \pm SD. $^*p < 0.05$ compared to DMSO treatment group) were measured and recorded; AR expression in tumor was analyzed by western blot, shown by representative images and by quantification (**D**, $n=4$, data are expressed as Means \pm SD. $^*p < 0.05$ compared to DMSO treatment group).

3.4. Conclusion

GBM is the most aggressive and malignant primary human brain cancer with high mortality rate ⁵⁹. It is reported that a higher incidence rate happens in men compared to women (3:2) ^{33,34,36}, indicating that there is a sex disparity of the disease, which may be correlated with different sex hormone pathways ⁶⁰. Further studies reveal that AR overexpression and mutation of AR are frequently observed in human GBM and suppressing AR expression could induce GBM cells death *in vitro* and *in vivo* ^{59,61}. AR plays an important role in GBM progression. It is well known HSP27 is a chaperone

protein that could stabilize AR. Targeting HSP27 to downregulate AR becomes a novel approach for the treatment of AR overexpressed GBM. We aim to develop small molecule HSP27 inhibitor as potential drug candidates to abolish AR in GBM, and mutated AR could be eliminated in this strategy as well, which makes this approach superior to other anti-androgen compounds. Compound **I** shows great potency and selectivity to inhibit AR overexpressed GBM cells. It inhibits HSP27 chaperone function, and induces AR degradation, which is correlated to the selectivity to AR overexpressed cells. The compound also inhibits tubulin polymerization, therefore shows general activity to inhibit cell proliferation. Compared to a similar analog with an extra N-methyl group, compound **I** shows lower toxicity to mice. The removal of N-methyl group does not bring the COX-2 inhibition back to the compound, suggesting that after the reduction of the nitro group in the very lead compound nimesulide, the COX-2 inhibition is eliminated in this scaffold. In addition to the HSP27 and tubulin inhibition, compound **I** also affects AR transcription with an unknown mechanism, since the mRNA of AR is also decreased after the treatment. It seems that the compound suppresses AR in GBM with multiple mechanisms. The *in vivo* study reveals that compound **I** inhibits U87 xenograft and abolishes the AR in the tumor samples as well after the treatment. All the *in vitro* and *in vivo* activity demonstrate that compound **I** is a promising drug candidate for AR overexpressed GBM.

CHAPTER IV

PHARMACOKINETIC AND BRAIN DISTRIBUTION STUDY OF AN ANTI- GLIOBLASTOMA AGENT IN MICE BY HPLC-MS/MS

4.1. Introduction

GBM is a common brain cancer and is considered the most aggressive malignant brain cancer in adults. The prognosis of GBM remains poor even when the combination treatment of chemotherapy and radiotherapy were performed after surgical removal of the tumor ⁴. The median survival rate of the patients is about 15 months with the treatment because of the high recurrence rate and resistance to therapeutics ². TMZ, an oral alkylating chemotherapy prodrug, is often used after surgical resection in the current treatment ⁵. However, the recurrence usually occurred months after the TMZ treatment. Therefore, there is an urgency to develop a new therapeutic approach for defending GBM.

Ever since the AR was first detected in astrocytoma in 1996 ⁶², many studies indicated that AR could be a potential target for the treatment of GBM. Testosterone could stimulate the progression of GBM by promoting proliferation, migration and

invasion via activating AR functions⁵⁹. Also, Zalzman et al revealed that siRNA induced AR gene silencing induced GBM cell death, while enzalutamide (AR antagonist) reduced the GBM tumor growth in nude mice²⁷. However, the AR mutation (AR-V7), which commonly occurred in GBM, causes the AR antagonist agents to be less effective⁶³. HSP27 is a well-documented chaperone protein to stabilize AR^{60,64,65}, and inhibition of HSP27 results in AR degradation regardless of the mutation¹⁰. Thus, HSP27 suppression could be a novel approach for AR overexpressed GBM treatment.

Compound **I** (Figure 16), a HSP27 inhibitor, has been identified to abolish AR in GBM²⁹. Compound **I** could significantly downregulate AR and AR-V7 at 50 nM, and the IC₅₀s to inhibit GBM cell growth could reach 5 nM. Moreover, compound **I** could inhibit GBM tumor growth in the mice xenograft model, and does not cause toxicity to animals even at much higher doses. Compound **I** could be the potential drug candidate treat GBM. However, whether compound **I** could cross BBB is a critical factor to consider for the treatment of GBM. Thus, a pre-clinical pharmacokinetic investigation and brain tissue detection of compound **I** is urgently needed to determine the pharmacokinetic profiles of compound **I**. In the present study, a sensitive and reliable HPLC-MS/MS method was established and validated for the determination of the concentrations of compound **I** in mice plasma and brain tissue. The method was successfully applied to the pharmacokinetic study of compound **I** in mice after intraperitoneal injection.

4.2. Materials and methods

4.2.1. Chemicals and reagents

Compound I and internal standard (IS) compound **14** (**Figure 16**) were prepared and characterized according to published methods ⁴⁸. MS-grade acetonitrile and ACS-grade methanol were purchased from Sigma-Aldrich (St. Louis, MO, USA), and LC/MS-grade formic acid was purchased from Fisher Scientific (Waltham, MA, USA). Double-Deionized water was prepared by Barnstead Nanopure[®] water purification system from Thermo Scientific (Waltham, MA, USA).

4.2.2. Animals

C57BL/6 mouse (36 males, 20-25 g) bred from the animal facility of Cleveland State University were used for the study. All the mice were given free access to water, a standard laboratory diet, and maintained under standard conditions (25°C±2°C, 12 h dark-light cycle, 50%±10 % humidity) in accordance with the institutional guidelines for Animal Research Facilities. All mice fasted overnight but were allowed free access to water before the drug injection.

4.2.3. Instrumentations and HPLC-MS/MS conditions

The HPLC-MS/MS method was performed with a Shimadzu UPLC system (Columbia, MD) which consisted of a Prominence DGU-20A_{3R} inline degasser, two LC-30 AD pumps, a SIL-30 AC autosampler and a CBM-20A controller. The chromatographic separation was performed on a Kinetex C₁₈ column (50 mm × 2.1 mm, 1.3 μm) with a mobile phase consisting of acetonitrile-0.1% formic acid and water (50:50,

v/v) at a flow rate of 0.3 mL/min. The temperature of the column was maintained at 36°C. The injection volume was 5.0 µL.

Mass spectrometric detection was operated on an AB Sciex Qtrap 5500 mass spectrometer (Toronto, Canada) with negative electrospray ionization mode. The multiple reaction monitoring (MRM) function was used for quantification with the transitions of compound **I** and IS compound **14**, which were detected at m/z 485.1→256.1 and m/z 499.2→268.2, respectively. The proposed fragmentation pathways of compound **I** and compound **14** are shown in **Figure 16**. The optimized ion source parameters were set as follows: ion spray voltage, -4200 V; temperature e, 450°C; heating gas, nebulization gas, curtain gas, 40 psi. Compound parameters were as follows: declustering potential, -100 V; entrance potential, -10V; collision energy, -35V for compound **I**, -40 V for compound **14**; collision exit potential, -15 V for compound **I**, -20 V for compound **14**. Data acquisition and quantification were performed using analyst software (version 1.6.2).

4.2.4. Preparation of standards and samples

4.2.4.1. Preparation of stock and working solution

The stock solutions were prepared by dissolving compound **I** and compound **14** in methanol at 1.0 mg/mL. Then, the stock solution of compound **I** was serially diluted with methanol into a concentration gradient: 1.0, 2.0, 5.0, 10, 20, 50, 100, 200, 500, 1000 ng/mL. Also, a 250 ng/mL working solution of compound **14** (IS) was prepared in methanol from the stock solution of compound **14**. All the solutions were stored at 4°C in the dark.

4.2.4.2. Preparation of calibration standards and quality control

The calibration standards were prepared as follows: After spiking with 100 μL of the corresponding standards solutions, 40 μL of compound **14** working solution, 100 μL of blank mouse plasma (collected and mixed from 6 mice) or brain homogenates (0.4 g of 6 blank brain tissues mixed with 2 mL PBS), and 800 μL of methanol were transferred into a 1.5 mL tube, the mixture was then vortexed and centrifuged at 12,000 g for 10 mins. The supernatant was collected and transferred into a new 1.5 mL tube. After being dried with nitrogen, the residue was stored at -80°C and dissolved with 50% acetonitrile before analysis. Also, the quality control (QC) samples were independently prepared with same blank mouse plasma or brain homogenates. The preparation method was the same as the calibration standards. The QC samples were prepared at concentrations of 2 ng/mL (low), 50 ng/mL (medium) and 200 ng/mL (high) and were then divided into aliquots and stored in the freezer at -80°C before analysis.

4.2.4.3. Preparation of samples

A simple protein precipitation method was applied to extract compound **I** from mouse plasma or brain homogenate (0.4 g brain tissue mix with 2 mL PBS). Briefly, 100 μL of each sample, 40 μL of compound **14** (IS, 250 ng/mL), and 800 μL of methanol were combined in a 1.5 mL tube. Then, it was vortexed and centrifuged at 12,000 g for 5 min. The supernatant was collected and then transferred into a new 1.5 mL tube. The liquid was dried by a nitrogen blowing instrument. The residue was stored at -80°C and dissolved with 100 μL 50% acetonitrile before analysis.

4.2.5. Method validation

In accordance with the FDA bioanalytical method validation guidance, the HPLC-MS/MS method was validated in terms of selectivity, linearity and sensitivity, precision and accuracy, matrix effect, and recovery and stability ⁶⁶.

4.2.5.1. Selectivity

The selectivity was determined by testing the blank plasma from six mice or blank brain tissue homogenate, blank matrices spiked with IS only, and plasma and brain samples obtained from mice dosed with compound I.

4.2.5.2. Linearity and sensitivity

The linearity of this method was examined via analysis of the standard curve containing ten different concentrations (1-1000 ng/mL). The standard curve was obtained by plotting the peak area ratios (compound I/compound 14, *Y*-axis) versus the concentrations (*X*-axis) of compound I and assessed by weighted least-squares linear regression using $1/x^2$ as the weighting factor. The lowest concentration (1.0 ng/mL) was considered as the lower limit of quantification (LLOQ).

4.2.5.3. Precision and accuracy

The precision and accuracy were investigated with the QC samples in 5 replicates, which were prepared and analyzed on three continuous days. The intra and inter-day precision was represented as the RSD and the accuracy was expressed as RE.

4.2.5.4. Extraction recovery and matrix effect

Extraction recovery was measured by calculating the ratio of the responses of QC samples spiked with analytes prior to extraction and the responses of those spiked with protein precipitated blank plasma or brain homogenates. The matrix effect was evaluated

by measuring the ratio of the responses in blank plasma or brain homogenates and those dissolved with 50% acetonitrile (v/v) at the same concentration. Generally, the extraction recovery should be over 85% and the matrix effects should be less than 15% according to FDA guidance for methodology development.

4.2.5.5. Stability

The stability was evaluated by testing five replicates of the samples at three QC levels under different conditions (24 h storage at room temperature, three freeze/thaw cycles and storage at -80°C for 30 days). The samples are considered stable if the average percentage concentration deviation is within 15% of the actual value.

4.2.6. Pharmacokinetic study

A dosing solution (5 mg/mL) of compound I was prepared in preclinical formulation vehicle [5% Cremophor EL (CrEL) with PBS]. The mouse received a 100 mg/kg dose of compound I by intraperitoneal (IP) administration. 400 µL mouse blood samples and the whole brain tissue were collected at each time point by euthanizing the treatment group of mice at 0.083 h, 0.25 h, 0.5 h, 1.0 h, 2.0 h, 4.0 h, 6.0 h, 12 h, 24 h, respectively. The blood was directly collected from heart, then followed by perfusion with PBS and brain tissue was collected consequently. The blood samples were centrifuged immediately at 3,000 g for 10 min at 4°C, and the supernatant plasma were collected, and immediately stored at -80°C until analysis. The brain tissue was weighted out and mixed with PBS (1:5, m/v) in Dounce Tissue Grinders (DWK Life Sciences), homogenized on ice. Then, aliquots of the homogenates were immediately frozen and stored at -80°C until analysis.

4.2.7. Data analysis

The plasma and brain homogenates samples were subjected to HPLC-MS/MS analysis as above and the concentrations of compound **I** were calculated according to the calibration curve. Microsoft Excel 2020 (Microsoft Co., USA) was used to calculate the pharmacokinetic parameters. GraphPad Prism 5.0 (GraphPad Software, USA) was used to plot the concentration-time curve. All the results were expressed as Mean \pm SD.

4.3. Results and discussion

4.3.1. Optimization of chromatography conditions and MS conditions

The chromatographic condition was optimized to improve peak shape, increase signal response of analytes, and shorten retention time. In the current chromatographic separation, a Kinetex C₁₈ column was used to separate the analytes. The composition of the mobile phase, especially the organic phase, was optimized in order to acquire good chromatographic separation. Compared with methanol-water, it was found that acetonitrile-water obtained higher peak shape. The signal response was significantly improved with 0.1% formic acid added into the water phase. Eventually, acetonitrile-0.1% formic acid and water (50:50, v/v) was adopted as the mobile phase at a flow rate of 0.3 mL/min. Under the optimized condition, sharp peaks of analyte and internal standard are acquired with the consistent separation. The retention time was 1.51 min for compound **I**, 1.88 min for compound **14**, respectively.

In order to optimize the mass spectrometer parameters, 200 ng/mL of compound **I** and 100 ng/mL of compound **14** in acetonitrile-0.1% formic acid and water (50:50, v/v) were injected into the mass spectrometer through direct infusion at 10 μ L/min. Negative modes of ESI was assessed for compound **I** and compound **14** (**Figure 16**). ESI (-) was

used for the study. The results showed that the predominant deprotonated molecular ions $[M-H]^-$ were m/z 485.1 (compound **I**) and m/z 499.2 (compound **14**). The multiple reaction monitoring (MRM) function was used for quantification of the transitions of compound **I** and internal standard compound **14**, which were detected at m/z 485.1 \rightarrow 256.1 and m/z 499.2 \rightarrow 268.2, respectively.

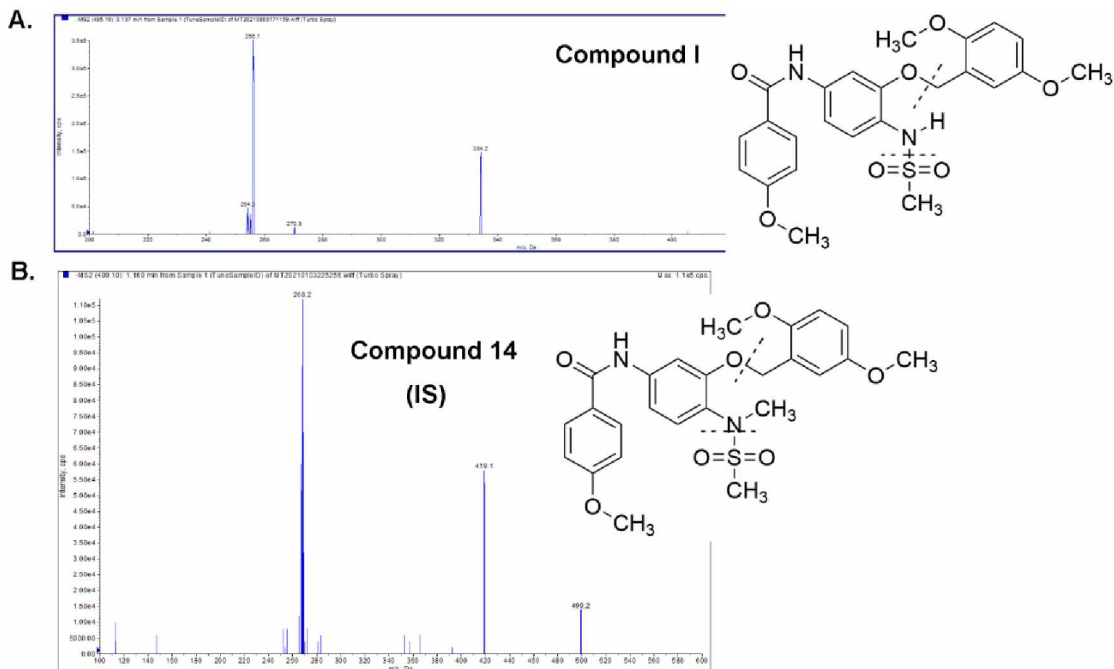


Figure 16. Full-scan product ion spectrum and proposed fragmentation pathways of (A) compound **I** and (B) compound **14** (IS).

4.3.2. Method validation

4.3.2.1. Selectivity

Selectivity was used to evaluate the potential interference of endogenous substances to the detection of analytes. In this present study, the retention time was 1.51 min for compound **I**, 1.88 min for compound **14**, respectively. Both of the analyte and internal standard showed well-separated peaks with no significant interference from

endogenous substances observed at their corresponding retention times under current detection condition. Typical chromatograms of blank mouse plasma or brain, blank plasma or brain homogenates spiked with IS (compound **14**, 100 ng/mL) and plasma and brain samples from mice with IP administration of compound **I** in 5% CrEL at 0.5 h shown in **Figure 17**.

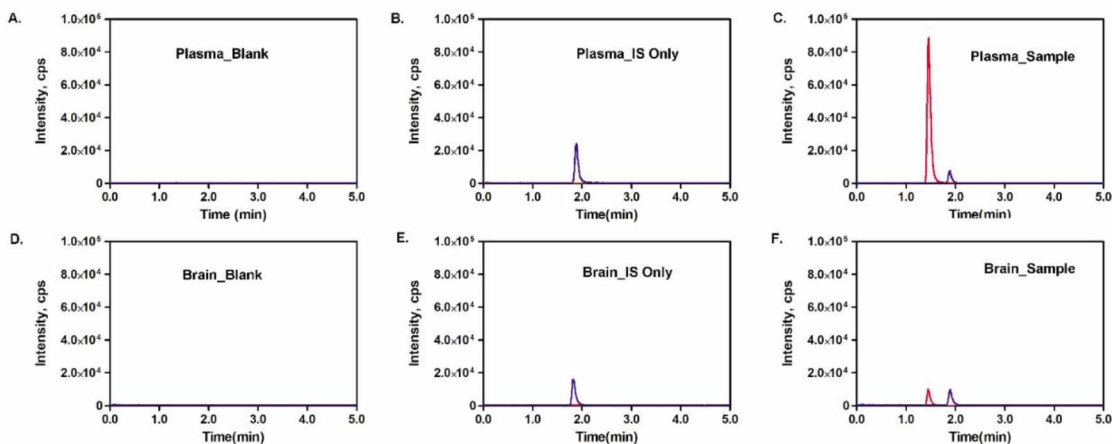


Figure 17. Typical chromatograms of different samples (**A**) blank mouse plasma, (**B**) mouse plasma spiked with IS (compound **14**, 100 ng/mL) only, (**C**) plasma samples from mice with IP administration of compound **I** in 5% CrEL at 1.0 h, (**D**) blank brain homogenates, (**E**) brain homogenates spiked with IS (compound **14**, 100 ng/mL) only, and (**F**) samples from mice with IP administration of compound **I** in 5% CrEL at 1.0 h.

4.3.2.2. Linearity and sensitivity

The calibration curve of the ratio of analyte/IS peak area (Y) to the concentration (X) was plotted via $1/x^2$ weighted linear least-square regression model. The calibration curve of compound **I** in mouse plasma was $Y=0.1234X+0.7208$, which exhibited good linearity ($r = 0.990$). The calibration curve of compound **I** in brain tissue was $Y=0.1460X+0.4691$, which exhibited good linearity ($r = 0.996$). The LLOQ for compound **I** was determined to be 1.0 ng/mL in all different mouse plasma and brain tissue samples.

4.3.2.3. Precision and accuracy

The precision was demonstrated as the RSD of the QC samples at three concentration levels (2, 50 and 500 ng/mL) while the accuracy was expressed as RE. The precision of intra- and inter-day accuracy are shown in **Table 3**. The RSD of Intra-day and Inter-day for precision are less than 3.85% and 8.29%, respectively. The RE for accuracy was within $\pm 7.33\%$. The results showed that the method was acceptable for precision and accuracy.

Table 3. Intra- and inter-assay precision, accuracy for the determining compound **I** in mouse plasma and brain tissue (n = 3 days, 5 replicates per day).

Samples	Analyte concentration (ng/mL)	Intra-day (RSD %)	Inter-day (RSD %)	Accuracy (RE%)
Plasma	2	1.80	8.29	-5.88
	50	2.05	4.41	-6.16
	200	2.77	4.50	3.12
Brain	2	1.81	4.85	6.21
	50	1.24	4.55	-5.54
	200	3.85	7.77	-7.33

4.3.2.4. Extraction recovery and matrix effects

Extraction recovery and matrix effects of QC samples from mouse plasma and brain tissue at three different concentrations (2, 50 and 200 ng/mL) were evaluated. The results are listed in **Table 4**. The results showed that the extraction recoveries were over 93.16% for three different levels of QC samples. The results indicated that this extraction method was qualified for the requirement of quantification of compound **I** plasma and brain sample drug concentration determination. The matrix effects at three concentrations were within 92.24-111.24%, indicating minor matrix effects.

Table 4. Extraction recovery and matrix effect of compound I in mouse plasma and brain tissue (n=5).

Samples	Analyte concentrations (ng/mL)	Extraction recovery (%)	RSD (%)	Matrix effect (%)	RSD (%)
Plasma	2	93.16±12.86	13.80	96.23±6.30	6.55
	50	105.30±2.57	2.44	104.22±5.42	5.20
	200	95.02±4.46	9.74	92.37±10.43	11.29
Brain	2	110.54±12.95	11.71	92.24±7.23	7.84
	50	110.15±8.88	8.06	99.38±9.11	9.17
	200	117.45±13.54	11.53	111.24±10.42	9.37

4.3.2.5. Stability

The stability of compound I in mouse plasma and brain homogenates was investigated by measuring the concentration of compound I in QC samples with three different storage conditions, including three freeze-thaw cycles, maintenance at room temperature for 24 h (short term) and at -80°C for 30 days (Long term). The results are shown in **Table 5**. The RE of compound I in mouse plasma and brain homogenate at three different level QC samples were both less than 8.7%. Compound I was found to be stable in mouse plasma and brain homogenate after three freeze-thaw cycles and after storing at room temperature for 24 h and -80 °C for 30 days.

Table 5. Stability of compound I in mouse plasma and brain tissue (n=5)

Samples	Analyte concentration (ng/mL)	Three freeze-thaw cycles		Room temperature for 24 h		Long term (30 days, -80°C)	
		RSD %	RE %	RSD %	RE %	RSD %	RE %
Plasma	2	11.59	-8.7	9.56	6.1	12.44	7.5
	50	9.97	5.8	10.21	-2.7	8.63	-6.4
	200	8.66	-3.5	6.64	6.5	6.76	5.6
Brain	2	8.45	5.7	8.14	-3.8	4.87	5.9
	50	8.58	7.2	10.51	-4.4	12.42	7.8
	200	8.51	4.5	5.71	-5.5	9.52	7.1

4.3.3. Pharmacokinetic study and brain tissue determination

The validated HPLC-MS/MS method was successfully used to evaluate the concentration of compound I in mouse plasma and brain tissue after IP dose (100 mg/kg). The mouse plasma and brain tissue concentrations of compound I at different dosing times are exhibited in **Figure 18**. The pharmacokinetic parameters are listed as Mean \pm SD in **Table 6**. The results showed that compound I was rapidly absorbed and distributed and the C_{max} was achieved within 1.0 h. The apparent elimination half-life ($t_{1/2}$) was 4.06 h, indicating compound I could be cleared fast from the mouse plasma. Also, C_{max} of compound I in mouse plasma reached to 68.97 $\mu\text{g/mL}$. Moreover, the compound I was detected in brain tissue after IP administration, the C_{max} of compound I in brain tissue is 0.88 $\mu\text{g/g}$ (1%-2% of the concentration in blood), indicating that part of compound I in the blood circulation was able to pass the blood-brain barrier (BBB) and accumulate in the brain tissue (**Figure 18 C & D**).

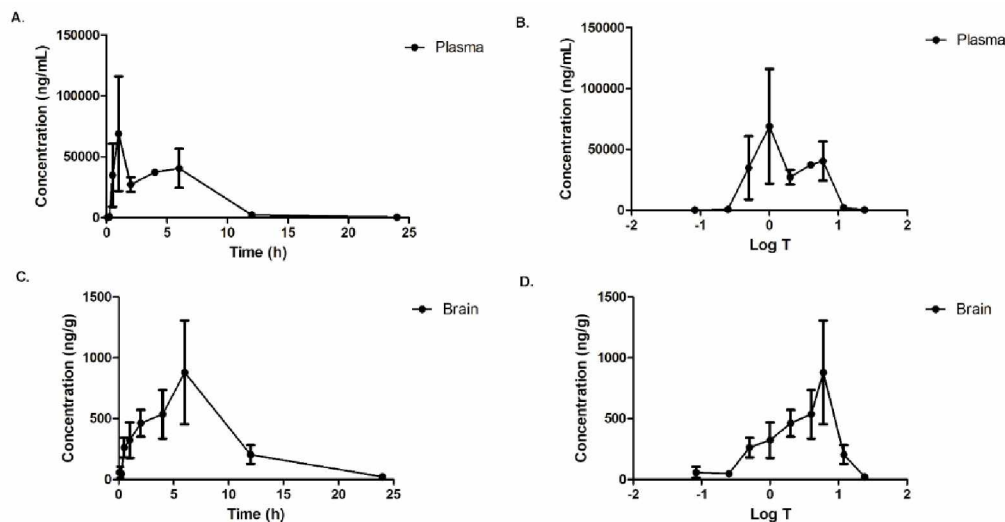


Figure 18. Plasma (A and B) and brain (C and D) tissue concentration-time profiles of compound I with IP administration in mice. (Mean \pm SD, n=4)

Table 6. Non-compartmental pharmacokinetic parameters of compound I in mouse after IP administration (n=4, Mean \pm SD).

Pharmacokinetic parameters	Value	
	Plasma	Brain
$t_{1/2}$	4.06 \pm 1.65 (h)	3.24 \pm 0.62 (h)
C_{max}	68.97 \pm 6.66 (μ g/mL)	0.88 \pm 0.85 (μ g/g)
AUC_{0-24h}	65.44 \pm 37.35 (μ g.h/mL)	1.54 \pm 0.81 (μ g.h/g)
$AUC_{0-\infty h}$	77.96 \pm 20.42 (μ g.h/mL)	1.66 \pm 0.78 (μ g.h/g)

4.4. Conclusions

A reliable and sensitive HPLC-MS/MS method for the quantification of compound I in mouse plasma and brain tissue was developed. The method was accurate, efficient, reliable, and successfully applied for evaluation of the pharmacokinetics of compound I in the *in vivo* study. The results indicated that compound I was rapidly distributed.

Moreover, compound **I** could cross the BBB, which indicates the compound could be delivered to the central nervous system. The pharmacokinetic profile summarized in the study provides valuable information for the further investigation of compound **I** as a potential anti-glioblastoma agent.

CHAPTER V
SYNTHESIS AND ANTI-GLIOBLASTOMA EFFECT EVALUATION OF HSP27
INHIBITORS

5.1. Introduction

GBM is the most common and aggressive brain tumor, with about 12,000 cases diagnosed in the United States annually ^{1,2}. The prognosis of GBM remains poor, despite with the advanced new surgical techniques combined with radiotherapy and chemotherapy ⁴. The median length of survival after a diagnosis is 15-18 months ². The current mainstay of treatment for GBM patients is surgery, followed by radiation therapy with temozolomide (TMZ, an oral alkylating chemotherapy medicine) ³¹. However, GBM usually reoccurs within couple months after the surgery. Identification of new molecular targets to develop more effective drugs for GBM treatment is very urgent, the current treatment protocol caused the low median survival rate for GBM patients.

The epidemiological survey has demonstrated that the incidence of GBM in men is 1.6 folds higher than that in women, indicating that sex related diversity ^{24,33}. Also, many recent researchers indicated that androgen plays an important role in the development of

GBM³⁶. It has been well established that androgen plays a vital role in the development of male phenotype, also exert the biological functions via association with androgen receptor (AR)⁶⁷. Recently, many studies claimed that AR is overexpressed in GBM and androgens contribute to the GBM progression^{27,29,39}. Thus, targeting AR might be a potential approach in GBM treatment. Androgen does promote GBM proliferation, migration and invasion via AR activation⁵⁹. Seviteronel, as a nonsteroidal antiandrogenic agent, has been investigated in clinical trials for AR-overexpressed GBM patients⁶⁸. AR antagonists, Enzalutamide and Bicalutamide, could inhibit the proliferation of GBM cells *in vitro* and *in vivo*^{27,69}. However, mutated AR (AR-V7), which lacks the binding domain becomes resistant, and was identified in about 30% of GBM surgical specimens, among to the wild-type AR⁶³, which suggests that the activity of AR targeting agents was restricted in the GBM treatment. It is urgent to develop an alternative approach to suppress AR activity in GBM.

Heat shock proteins play an important role in the folding, activation and regulation of transcriptional activity of steroid hormone receptors⁶⁰. Over expression HSP27 enhance the stability of its client proteins and prevent cell death from a variety of stress⁴¹. It is well known that AR is one of the client proteins of HSP27 and HSP27 escorts AR translocation into the nucleus to trigger androgen response elements (ARE) gene regulation^{28,41}. HSP27 is responsible for AR stability and seems to be a good direct target for HSP27-AR pathway in GBM. Currently, the most effective approach to target HSP27 is antisense oligonucleotides (ASO) or short interfering RNA (siRNA), which could decrease HSP27 expression in *in vitro* and *in vivo*^{70,71}. However, ASO and siRNA are not applicable to GBM because of the poor BBB permeability. Thus, small-molecule

HSP27 inhibitors could be a promising strategy to induce AR degradation in GBM, since small molecules have strong potential to pass BBB.

Previously, we identified compound **I** as a dual HSP27 and tubulin inhibitor, it exhibited significant activity to inhibit GBM growth *in vitro* and *in vivo*²⁹. The IC₅₀s of compound **I** against the proliferation of the four glioblastoma cell lines (T98G, U87, A172, U251) were less than 10 nM. Also, the tumor size was significantly shrunk and AR level in tumor was also decreased with compound **I** treatment in xenograft model²⁹. The previous results demonstrated that compound **I** is a promising new drug candidate to treat AR-overexpressed GBM. However, the previous pharmacokinetic study results showed that area under concentration-time curve (AUC) of compound **I** in brain tissue was only 2% of AUC in plasma⁷². This result indicated that compound **I** could cross the blood-brain barrier, but with very limited permeability. In this study we set out to identify a HSP27 inhibitor with higher activity to treat AR overexpressed GBM with higher permeability to brain tissue, 42 derivatives (5 dimers included) were synthesized based on compound **I** as the lead compound. Among the new candidates their HSP27 inhibition activity increased as well as an improved BBB penetration and potent *in vivo* activity.

5.2. Materials and Methods

5.2.1. Reagents

Thiazolyl Blue tetrazolium bromide, 98% (Alfa Aesar, P31B064). Insulin (Sigma Aldrich, 91077C). α -crystallin (Sigma Aldrich, C4163). Dithiothreitol (DTT) (Amresco, EC# 222-468-7). DMEM (Corning, 10-013-CV). RPMI 1640 (Corning, 10-040-CV). FBS (Atlanta Biologicals, S11150). Pen/Strep solution (Cleveland Clinic, 725-100p).

Anti- β -actin antibody (Cell Signaling Technology, 4967S). Bovine serum albumin (Millipore Sigma, 2905-OP). RIPA (Thermo Scientific, Prod# 89900). Protease inhibitor cocktail (Thermo Scientific, Prod# 1861278). BCA Protein Assay kit (Biovision, Prod# K813-2500-1). Anti-HSP27 antibody (Cell Signaling Technology, 2402S). Anti-Androgen Receptor antibody (Cell Signaling Technology, 5153S). Anti-AR-V7 antibody (Cell Signaling Technology, 68492S). Anti-Rabbit IgG (Cell Signaling Technology, 7074S). Anti-Rabbit Alexa Fluor 488 secondary antibody (Thermo Scientific, A-21206). Anti-Mouse Alexa Fluor 594 secondary antibody (Thermo Scientific, SA5-10168). Non-Fat dry milk (Rockland, B51-0500). Chemiluminescent Substrate (Thermo Scientific, 34577). Hematoxylin solution (Harris, VWR International, 95057-844). Eosin solution (VWR International, 95057-848). All the other chemicals are analytical grade.

5.2.2. Chemistry

Chemicals were commercially available and used as received without further purification unless otherwise noted. Thin layer chromatography (TLC) was performed on silica gel TLC plates with a fluorescence indicator at 254 nm (Analytikjena). Mass spectra were obtained on a Shimadzu Single Quad Mass spectrometer at Cleveland State University MS Facility Center. All NMR spectra were recorded on a Bruker 400 MHz spectrometer using DMSO- d_6 as the solvent.

Reversed phase HPLC analysis of compounds was conducted on a Beckman HPLC system with an Auto Sampler. The chromatographic separation was performed on a Kinetex C₁₈ column (50 mm \times 2.1 mm, 1.3 μ m) with a mobile phase consisting of acetonitrile-0.1% formic acid and water (80:20, v/v) at a flow rate of 0.3 mL/min. The

temperature of the column was maintained at 36°C. The injection volume was 5.0 μ L. The reaction procedure is illustrated in Scheme 1. The final step of the reaction and the product characterization are listed below.

N-(3-((2,5-dimethoxybenzyl)oxy)-4-(methylsulfonamido)phenyl)-3,5-bis(trifluoromethyl)benzamide (**1**). Yield 32%, White Powder. ^1H NMR (400 MHz, $\text{DMSO-}d^6$) δ_{H} 10.60 (s, 1H), 9.06 (s, 1H), 8.62 (s, 2H), 8.40 (s, 1H), 7.66 (s, 1H), 7.44 (d, $J= 8.6$ Hz, 1H), 7.30 (m, 2H), 6.98 (d, $J= 8.9$ Hz, 1H), 6.88 (d, $J= 3.9$ Hz, 1H), 5.11 (s, 2H), 3.79 (s, 3H), 3.74 (s, 3H), 2.90 (s, 3H); ^{13}C NMR (100 MHz, $\text{DMSO-}d^6$) δ_{C} 163.00, 153.68, 153.01, 150.97, 138.22, 137.48, 131.47, 131.14, 130.80, 129.04, 128.35, 125.73, 124.95, 122.23, 115.20, 113.79, 113.33, 112.08, 106.04, 65.52, 56.24, 55.91. ESI-MS calculated for ($\text{C}_{25}\text{H}_{22}\text{F}_6\text{N}_2\text{O}_6\text{S}$) [M-H]: m/z 591; Molecular Weight (calculated from structure): 592.51. HPLC mobile phase: 80% ACN with 0.1% formic acid, retention time 0.85 min, purity: >95%.

4-cyano-N-(3-((2,5-dimethoxybenzyl)oxy)-4-(methylsulfonamido)phenyl)benzamide (**2**). Yield 14%, Pale Yellow Powder. ^1H NMR (400 MHz, $\text{DMSO-}d^6$) δ_{H} 10.52 (s, 1H), 9.00 (s, 1H), 8.12 (m, 2H), 8.05 (m, 2H), 7.69 (s, 1H), 7.43 (d, $J= 8.5$ Hz, 1H), 7.41 (s, 1H), 7.26 (d, 1H), 6.99 (d, $J= 8.9$ Hz, 1H), 6.90 (d, $J= 8.9$ Hz, 1H), 5.10 (s, 2H), 3.79 (s, 3H), 3.74 (s, 3H), 2.90 (s, 3H); ^{13}C NMR (100 MHz, $\text{DMSO-}d^6$) δ_{C} 164.58, 153.67, 153.03, 150.96, 139.28, 138.60, 132.95, 128.98, 128.46, 125.76, 121.88, 118.77, 115.20, 114.40, 113.77, 113.03, 112.06, 105.79. ESI-MS calculated for ($\text{C}_{24}\text{H}_{23}\text{N}_3\text{O}_6\text{S}$) [M-H]: m/z 480; Molecular Weight (calculated from structure): 481.52. HPLC mobile phase: 80% ACN with 0.1% formic acid, retention time 0.67 min, purity: >95%.

4-chloro-N-(3-((2,5-dimethoxybenzyl)oxy)-4-(methylsulfonamido)phenyl)-3-nitrobenzamide (**3**). Yield 41%, Pale Yellow Powder. ^1H NMR (400 MHz, $\text{DMSO-}d^6$) δ_{H} 10.58 (s, 1H), 9.04 (s, 1H), 8.64 (s, 1H), 8.28 (d, $J= 8.4$ Hz, 1H), 8.00 (d, $J= 8.4$ Hz, 1H), 7.65 (s, 1H), 7.43 (d, $J= 8.6$ Hz, 1H), 7.41 (s, 1H), 7.28 (d, $J= 8.6$ Hz, 1H), 6.99 (d, $J= 8.9$ Hz, 1H), 6.81 (m, 1H), 5.10 (s, 2H), 3.79 (s, 3H), 3.73 (s, 3H), 2.89 (s, 3H); ^{13}C NMR (100 MHz, $\text{DMSO-}d^6$) δ_{C} 162.89, 153.68, 153.02, 150.95, 135.24, 133.30, 132.45, 128.60, 125.75, 125.30, 115.18, 113.77, 112.06, 105.86, 56.25, 55.92. ESI-MS calculated for $(\text{C}_{24}\text{H}_{24}\text{N}_2\text{O}_8\text{S})$ $[\text{M-H}]^-$: m/z 534; Molecular Weight (calculated from structure): 535.95. HPLC mobile phase: 80% ACN with 0.1% formic acid, retention time 0.70 min, purity: >95%.

N-(3-((2,5-dimethoxybenzyl)oxy)-4-(methylsulfonamido)phenyl)benzo[d][1,3]dioxole-5-carboxamide (**4**). Yield 39%, Gray Powder. ^1H NMR (400 MHz, $\text{DMSO-}d^6$) δ_{H} 10.10 (s, 1H), 8.95 (s, 1H), 7.69 (s, 1H), 7.59 (d, $J= 8.0$ Hz, 1H), 7.52 (s, 1H), 7.41 (d, $J= 8.9$ Hz, 1H), 7.28 (s, 1H), 7.22 (d, $J= 8.8$ Hz, 1H), 7.07 (d, $J= 8.0$ Hz, 1H), 6.99 (d, $J= 8.8$ Hz, 1H), 6.90 (d, $J= 8.9$ Hz, 1H), 5.10 (s, 2H), 3.79 (s, 3H), 3.73 (s, 3H), 2.89 (s, 3H); ^{13}C NMR (100 MHz, $\text{DMSO-}d^6$) δ_{C} 164.94, 153.70, 153.07, 151.01, 125.86, 123.33, 115.25, 113.83, 112.88, 112.11, 108.42, 108.15, 105.72, 102.31, 65.44, 56.27, 55.94. ESI-MS calculated for $(\text{C}_{24}\text{H}_{24}\text{N}_2\text{O}_8\text{S})$ $[\text{M-H}]^-$: m/z 499; Molecular Weight (calculated from structure): 500.52. HPLC mobile phase: 80% ACN with 0.1% formic acid, retention time 0.70 min, purity: >95%.

3,5-dichloro-N-(3-((2,5-dimethoxybenzyl)oxy)-4-(methylsulfonamido)phenyl)benzamide (**5**). Yield 39%, Pale Yellow Powder. ^1H NMR (400 MHz, $\text{DMSO-}d^6$) δ_{H} 10.45 (s, 1H), 9.02 (s, 1H), 7.99 (s, 2H), 7.89 (s, 1H), 7.65 (s, 1H), 7.42 (d, $J= 8.6$ Hz, 1H), 7.24 (m,

2H), 6.98 (d, $J= 8.8$ Hz, 1H), 6.90 (d, $J= 6.8$ Hz, 1H), 5.09 (s, 2H), 3.79 (s, 3H), 3.73 (s, 3H), 2.88 (s, 3H); ^{13}C NMR (100 MHz, DMSO- d^6) δ_{C} 163.13, 153.68, 153.01, 150.98, 138.43, 134.81, 131.48, 128.38, 126.95, 125.75, 121.98, 115.21, 113.80, 113.09, 112.09, 105.86, 65.47, 56.26, 55.92. ESI-MS calculated for (C₂₃H₂₂Cl₂N₂O₆S) [M-H]⁻: m/z 523; Molecular Weight (calculated from structure): 525.40. HPLC mobile phase: 80% ACN with 0.1% formic acid, retention time 0.67 min, purity: >95%.

N-(3-((2,5-dimethoxybenzyl)oxy)-4-(methylsulfonamido)phenyl)-3-iodobenzamide (6). Yield 25%, Yellow Powder. ^1H NMR (400 MHz, DMSO- d^6) δ_{H} 10.34 (s, 1H), 8.99 (s, 1H), 8.30 (s, 1H), 7.98 (d, $J= 7.8$ Hz, 2H), 7.65 (s, 1H), 7.40 (dd, $J= 2, 8.5$ Hz, 1H), 7.39 (d, $J= 2.6$ Hz, 1H), 7.28 (d, $J= 8.6$ Hz, 1H), 6.99 (d, 1H), 6.90 (d, $J= 8.9$ Hz, 1H), 5.08 (s, 2H), 3.79 (s, 3H), 3.73 (s, 3H), 2.86 (s, 3H); ^{13}C NMR (100 MHz, DMSO- d^6) δ_{C} 164.34, 153.68, 152.93, 150.96, 140.61, 137.30, 136.36, 131.06, 127.63, 115.20, 113.74, 113.08, 112.06, 95.16, 65.46, 56.25, 55.92. ESI-MS calculated for (C₂₃H₂₃IN₂O₆S) [M-H]⁻: m/z 581; Molecular Weight (calculated from structure): 582.41. HPLC mobile phase: 80% ACN with 0.1% formic acid, retention time 0.67 min, purity: >95%.

N-(3-((2,5-dimethoxybenzyl)oxy)-4-(methylsulfonamido)phenyl)-3-fluoro-4-(trifluoromethyl)benzamide (7). Yield 23%, Pale Yellow Powder. ^1H NMR (400 MHz, DMSO- d^6) δ_{H} 10.62 (s, 1H), 9.01 (s, 1H), 8.01 (m, 2H), 7.55 (m, 2H), 7.29 (d, 3H), 6.99 (d, $J= 9.0$ Hz, 1H), 6.86 (m, 1H), 5.08 (s, 2H), 3.78 (s, 3H), 3.73 (s, 3H), 2.84 (s, 3H); ^{13}C NMR (100 MHz, DMSO- d^6) δ_{C} 161.62, 153.67, 152.79, 150.97, 136.11, 129.62, 127.23, 126.03, 125.67, 115.17, 113.70, 112.64, 112.05, 105.65, 65.48, 26.25, 55.90. ESI-MS calculated for (C₂₄H₂₂F₄N₂O₆S) [M-H]⁻: m/z 541; Molecular Weight (calculated from

structure): 542.50. HPLC mobile phase: 80% ACN with 0.1% formic acid, retention time 0.70 min, purity: >95%.

N-(3-((2,5-dimethoxybenzyl)oxy)-4-(methylsulfonamido)phenyl)-4-iodobenzamide (**8**).

Yield 45%, Gray Powder. ^1H NMR (400 MHz, $\text{DMSO-}d^6$) δ_{H} 10.34 (s, 1H), 9.00 (s, 1H), 7.95 (d, $J= 8.4$ Hz, 2H), 7.77 (d, $J= 8.5$ Hz, 2H), 7.68 (s, 1H), 7.42 (d, $J= 8.6$ Hz, 1H), 7.40 (s, 1H), 7.27 (d, $J= 8.6$ Hz, 1H), 6.99 (d, $J= 8.9$ Hz, 1H), 6.87 (m, 1H), 5.08 (s, 2H), 3.79 (s, 3H), 3.73 (s, 3H), 2.87 (s, 3H); ^{13}C NMR (100 MHz, $\text{DMSO-}d^6$) δ_{C} 165.22, 153.67, 153.03, 150.96, 138.74, 137.75, 134.62, 130.05, 128.38, 125.83, 121.82, 115.19, 113.75, 112.97, 112.05, 105.78, 99.86, 65.43, 56.24, 55.91. ESI-MS calculated for ($\text{C}_{23}\text{H}_{23}\text{IN}_2\text{O}_6\text{S}$) [M-H]: m/z 581; Molecular Weight (calculated from structure): 582.41. HPLC mobile phase: 80% ACN with 0.1% formic acid, retention time 0.67 min, purity: >95%.

N-(3-((2,5-dimethoxybenzyl)oxy)-4-(methylsulfonamido)phenyl)-4-ethylbenzamide (**9**).

Yield 30%, Pale Gray Powder. ^1H NMR (400 MHz, $\text{DMSO-}d^6$) δ_{H} 10.34 (s, 1H), 8.98 (s, 1H), 7.91 (d, $J= 8.1$ Hz, 2H), 7.72 (s, 1H), 7.44 (d, $J= 8.1$ Hz, 1H), 7.42 (d, $J= 8.6$ Hz, 2H), 7.29 (s, 1H), 7.28 (d, $J= 8.6$ Hz, 1H), 6.99 (d, $J= 8.9$ Hz, 1H), 6.89 (m, 1H), 5.09 (s, 2H), 3.79 (s, 3H), 3.74 (s, 3H), 3.30 (d, 2H), 2.87 (s, 3H), 2.70 (t, 3H); ^{13}C NMR (100 MHz, $\text{DMSO-}d^6$) δ_{C} 165.22, 153.67, 153.03, 150.96, 138.74, 137.75, 134.62, 130.05, 128.38, 125.83, 121.82, 115.19, 113.75, 112.97, 112.05, 105.78, 99.86, 65.43, 56.24, 55.91. ESI-MS calculated for ($\text{C}_{25}\text{H}_{28}\text{N}_2\text{O}_6\text{S}$) [M-H]: m/z 483; Molecular Weight (calculated from structure): 484.57. HPLC mobile phase: 80% ACN with 0.1% formic acid, retention time 0.67 min, purity: >95%.

N-(3-((2,5-dimethoxybenzyl)oxy)-4-(methylsulfonamido)phenyl)-4-(dimethylamino)benzamide (**10**). Yield 20%, Gray Powder. ^1H NMR (400 MHz, DMSO- d^6) δ_{H} 10.34 (s, 1H), 8.95 (s, 1H), 7.89 (d, J = 8.9 Hz, 2H), 7.73 (s, 1H), 7.40 (m, 1H), 7.29 (s, 1H), 7.18 (d, J = 8.6 Hz, 1H), 7.00 (d, J = 8.9 Hz, 1H), 6.90 (m, 1H), 6.78 (d, J = 8.9 Hz, 2H), 5.08 (s, 2H), 3.79 (s, 3H), 3.74 (s, 3H), 3.01 (s, 6H), 2.86 (s, 3H); ^{13}C NMR (100 MHz, DMSO- d^6) δ_{C} 165.65, 153.67, 153.16, 152.92, 150.96, 139.83, 129.60, 128.66, 125.89, 121.33, 120.65, 115.21, 113.74, 112.65, 112.03, 111.24, 105.43, 65.35, 56.23, 55.91. ESI-MS calculated for (C₂₅H₂₉N₃O₆S) [M-H]⁻: m/z 498; Molecular Weight (calculated from structure): 499.58. HPLC mobile phase: 80% ACN with 0.1% formic acid, retention time 0.67 min, purity: >95%.

N-(3-((2,5-dimethoxybenzyl)oxy)-4-(methylsulfonamido)phenyl)-3,4-dimethoxybenzamide (**11**). Yield 27%, Pale Yellow Powder. ^1H NMR (400 MHz, DMSO- d^6) δ_{H} 10.34 (s, 1H), 8.99 (s, 1H), 7.71 (s, 1H), 7.65 (d, J = 8.4 Hz, 1H), 7.54 (s, 1H), 7.40 (d, J = 10.6 Hz, 1H), 7.38 (s, 1H), 7.29 (d, J = 8.6 Hz, 1H), 7.11 (d, J = 8.5 Hz, 1H), 6.99 (d, J = 8.9 Hz, 1H), 6.87 (d, 1H), 5.08 (s, 2H), 3.85 (s, 6H), 3.79 (s, 3H), 3.74 (s, 3H), 2.87 (s, 3H); ^{13}C NMR (100 MHz, DMSO- d^6) δ_{C} 165.37, 153.67, 153.11, 152.21, 150.96, 148.82, 139.29, 128.56, 127.30, 125.83, 121.47, 121.19, 115.23, 113.76, 112.96, 112.05, 111.59, 111.38, 105.73, 65.40, 56.23, 56.18, 56.13, 55.92. ESI-MS calculated for (C₂₅H₂₈N₂O₈S) [M-H]⁻: m/z 515; Molecular Weight (calculated from structure): 516.57. HPLC mobile phase: 80% ACN with 0.1% formic acid, retention time 0.67 min, purity: >95%.

4-chloro-N-(3-((2,5-dimethoxybenzyl)oxy)-4-(methylsulfonamido)phenyl)benzamide (**12**). Yield 55%, Pale Gray Powder. ^1H NMR (400 MHz, DMSO- d^6) δ_{H} 10.36 (s, 1H),

9.00 (s, 1H), 8.00 (d, $J= 8.5$ Hz, 2H), 7.69 (s, 1H), 7.42 (d, $J= 8.7$ Hz, 2H), 7.40 (s, 1H), 7.22 (d, $J= 8.6$ Hz, 2H), 6.99 (d, $J= 8.9$ Hz, 1H), 6.88 (m, 1H), 5.09 (s, 2H), 3.79 (s, 3H), 3.73 (s, 3H), 2.88 (s, 3H); ^{13}C NMR (100 MHz, $\text{DMSO-}d^6$) δ_{C} 164.86, 153.67, 153.07, 150.96, 138.88, 136.97, 133.96, 130.08, 128.96, 128.51, 125.80, 121.59, 115.19, 113.76, 112.96, 112.05, 105.74, 65.42, 56.24, 55.91. ESI-MS calculated for $(\text{C}_{23}\text{H}_{23}\text{ClN}_2\text{O}_6\text{S})$ $[\text{M-H}]^-$: m/z 489; Molecular Weight (calculated from structure): 490.96. HPLC mobile phase: 80% ACN with 0.1% formic acid, retention time 0.67 min, purity: >95%.

N-(3-((2,5-dimethoxybenzyl)oxy)-4-(methylsulfonamido)phenyl)-4-nitrobenzamide (**13**). Yield 42%, Yellow Powder. ^1H NMR (400 MHz, $\text{DMSO-}d^6$) δ_{H} 10.36 (s, 1H), 9.04 (s, 1H), 8.40 (d, $J= 8.8$ Hz, 2H), 8.20 (d, $J= 8.7$ Hz, 2H), 7.69 (s, 1H), 7.45 (d, $J= 10.4$ Hz, 1H), 7.42 (s, 1H), 7.28 (d, $J= 12.8$ Hz, 1H), 6.99 (d, $J= 8.9$ Hz, 1H), 6.88 (m, 1H), 5.10 (s, 2H), 3.79 (s, 3H), 3.73 (s, 3H), 2.89 (s, 3H); ^{13}C NMR (100 MHz, $\text{DMSO-}d^6$) δ_{C} 164.31, 153.67, 153.02, 150.96, 149.68, 140.92, 138.52, 138.52, 129.67, 128.42, 125.76, 124.04, 122.01, 115.19, 113.76, 113.08, 112.05, 105.84, 65.47, 56.25, 55.91. ESI-MS calculated for $(\text{C}_{23}\text{H}_{23}\text{N}_3\text{O}_8\text{S})$ $[\text{M-H}]^-$: m/z 500; Molecular Weight (calculated from structure): 501.51. HPLC mobile phase: 80% ACN with 0.1% formic acid, retention time 0.67 min, purity: >95%.

3-cyano-N-(3-((2,5-dimethoxybenzyl)oxy)-4-(methylsulfonamido)phenyl)benzamide (**14**). Yield 44%, Pale Yellow Powder. ^1H NMR (400 MHz, $\text{DMSO-}d^6$) δ_{H} 10.36 (s, 1H), 9.04 (s, 1H), 8.27 (s, 1H), 8.24 (d, $J= 8.0$ Hz, 1H), 8.09 (d, $J= 7.7$ Hz, 1H), 7.79 (dd, $J= 2, 7.8$ Hz, 1H), 7.67 (s, 1H), 7.43 (d, $J= 10.4$ Hz, 1H), 7.29 (d, $J= 16.1$ Hz, 1H), 7.28 (s, 1H), 6.99 (d, $J= 8.9$ Hz, 1H), 6.87 (m, 1H), 5.10 (s, 2H), 3.79 (s, 3H), 3.73 (s, 3H), 2.88 (s, 3H); ^{13}C NMR (100 MHz, $\text{DMSO-}d^6$) δ_{C} 164.07, 153.69, 153.05, 150.96, 138.60, 136.27,

135.53, 132.98, 131.72, 130.33, 128.47, 125.77, 121.89, 118.78, 115.18, 113.76, 112.98, 112.05, 112.01, 105.74, 65.46, 56.25, 55.92. ESI-MS calculated for (C₂₄H₂₃N₃O₆S) [M-H]⁻: *m/z* 480; Molecular Weight (calculated from structure): 481.52. HPLC mobile phase: 80% ACN with 0.1% formic acid, retention time 0.67 min, purity: >95%.

3-bromo-N-(3-((2,5-dimethoxybenzyl)oxy)-4-(methylsulfonamido)phenyl)benzamide

(15). Yield 24%, Pale Gray Powder. ¹H NMR (400 MHz, DMSO-*d*⁶) δ_H 10.36 (s, 1H), 9.04 (s, 1H), 8.15 (s, 1H), 7.97 (d, *J* = 7.9 Hz, 1H), 7.80 (d, *J* = 8.0 Hz, 1H), 7.67 (s, 1H), 7.52 (dd, *J* = 3, 7.9 Hz 1H), 7.29 (s, 1H), 7.25 (d, *J* = 8.5 Hz, 1H), 7.00 (d, *J* = 8.9 Hz, 1H), 6.87 (m, 1H), 5.09 (s, 2H), 3.79 (s, 3H), 3.73 (s, 3H), 2.88 (s, 3H); ¹³C NMR (100 MHz, DMSO-*d*⁶) δ_C 164.38, 153.67, 153.03, 150.97, 138.67, 137.42, 134.84, 131.15, 130.67, 128.39, 127.33, 125.81, 122.15, 121.84, 115.21, 113.77, 113.01, 112.06, 105.81, 65.45, 56.24, 55.92. ESI-MS calculated for (C₂₃H₂₃BrN₂O₆S) [M-H]⁻: *m/z* 535; Molecular Weight (calculated from structure): 535.41. HPLC mobile phase: 80% ACN with 0.1% formic acid, retention time 0.67 min, purity: >95%.

N-(3-((2,5-dimethoxybenzyl)oxy)-4-(methylsulfonamido)phenyl)-3-nitrobenzamide (16).

Yield 47%, Pale Yellow Powder. ¹H NMR (400 MHz, DMSO-*d*⁶) δ_H 10.63 (s, 1H), 9.04 (s, 1H), 8.80 (s, 1H), 8.46 (m, 2H), 7.86 (t, 1H), 7.68 (s, 1H), 7.45 (d, *J* = 6.6 Hz, 1H), 7.28 (m, 2H), 7.00 (d, *J* = 8.9 Hz, 1H), 6.87 (m, 1H), 5.09 (s, 2H), 3.79 (s, 3H), 3.73 (s, 3H), 2.88 (s, 3H); ¹³C NMR (100 MHz, DMSO-*d*⁶) δ_C 163.78, 153.68, 150.97, 148.25, 138.50, 136.63, 134.65, 130.70, 128.41, 126.72, 125.78, 122.85, 122.00, 115.21, 113.78, 113.17, 112.07, 105.94, 65.49, 56.25, 55.92. ESI-MS calculated for (C₂₃H₂₃N₃O₈S) [M-H]⁻: *m/z* 500; Molecular Weight (calculated from structure): 501.51. HPLC mobile phase: 80% ACN with 0.1% formic acid, retention time 0.68 min, purity: >95%.

4-bromo-N-(3-((2,5-dimethoxybenzyl)oxy)-4-(methylsulfonamido)phenyl)benzamide

(17). Yield 40%, Pale Gray Powder. ^1H NMR (400 MHz, $\text{DMSO-}d^6$) δ_{H} 10.37 (s, 1H), 9.01 (s, 1H), 7.91 (d, $J= 8.5$ Hz, 2H), 7.76 (d, $J= 8.5$ Hz, 2H), 7.68(s, 1H), 7.42 (d, $J= 10.7$ Hz, 1H), 7.27 (s, 1H), 7.22 (d, $J= 8.6$ Hz, 1H), 7.00 (d, $J= 8.9$ Hz, 1H), 6.87 (m, 1H), 5.09 (s, 2H), 3.79 (s, 3H), 3.73 (s, 3H), 2.88 (s, 3H); ^{13}C NMR (100 MHz, $\text{DMSO-}d^6$) δ_{C} 164.98, 153.67, 153.06, 150.96, 138.87, 134.32, 131.90, 130.25, 128.51, 125.91, 125.79, 121.61, 115.19, 113.75, 112.96, 112.04, 105.74, 65.43, 56.24, 55.91. ESI-MS calculated for ($\text{C}_{23}\text{H}_{23}\text{BrN}_2\text{O}_6\text{S}$) $[\text{M-H}]^-$: m/z 535; Molecular Weight (calculated from structure): 535.41. HPLC mobile phase: 80% ACN with 0.1% formic acid, retention time 0.68 min, purity: >95%.

N-(3-((2,5-dimethoxybenzyl)oxy)-4-(methylsulfonamido)phenyl)-2,4-

bis(trifluoromethyl)benzamide (18). Yield 31%, Pale Gray Powder. ^1H NMR (400 MHz, $\text{DMSO-}d^6$) δ_{H} 10.75 (s, 1H), 9.01 (s, 1H), 8.24 (m, 2H), 7.99 (d, $J= 7.8$ Hz, 1H), 7.67 (s, 1H), 7.57 (s, 1H), 7.26 (m, 3H), 6.99 (d, $J= 8.9$ Hz, 1H), 6.87 (m, 1H), 5.09 (s, 2H), 3.78 (s, 3H), 3.73 (s, 3H), 2.89 (s, 3H); ^{13}C NMR (100 MHz, $\text{DMSO-}d^6$) δ_{C} 164.65, 153.66, 153.18, 151.04, 140.14, 138.33, 131.10, 130.77, 130.57, 130.31, 128.66, 127.58, 127.26, 125.68, 124.96, 124.75, 123.94, 122.24, 122.10, 115.30, 113.89, 112.35, 112.08, 105.13, 65.47, 56.23, 55.91. ESI-MS calculated for ($\text{C}_{25}\text{H}_{22}\text{F}_6\text{N}_2\text{O}_6\text{S}$) $[\text{M-H}]^-$: m/z 591; Molecular Weight (calculated from structure): 592.51. HPLC mobile phase: 80% ACN with 0.1% formic acid, retention time 0.68 min, purity: >95%.

N-(3-((2,5-dimethoxybenzyl)oxy)-4-(methylsulfonamido)phenyl)-4-

(methylthio)benzamide (19). Yield 60%, Pale Gray Powder. ^1H NMR (400 MHz, $\text{DMSO-}d^6$) δ_{H} 10.23 (s, 1H), 9.00 (s, 1H), 7.92 (d, $J= 8.5$ Hz, 2H), 7.70 (s, 1H), 7.41 (m,

3H), 7.29 (s, 1H), 7.23 (d, $J=8.6$ Hz, 1H), 7.00 (d, $J=8.9$ Hz, 1H), 6.87 (m, 1H), 5.09 (s, 2H), 3.80 (s, 3H), 3.73 (s, 3H), 2.87 (s, 3H), 2.55 (s, 3H); ^{13}C NMR (100 MHz, $\text{DMSO-}d^6$) δ_{C} 165.33, 153.67, 153.10, 150.96, 143.72, 139.17, 131.10, 128.62, 128.56, 125.82, 125.37, 121.31, 115.20, 113.75, 112.89, 112.03, 105.67, 65.40, 56.23, 55.91, 14.60. ESI-MS calculated for $(\text{C}_{24}\text{H}_{26}\text{N}_2\text{O}_6\text{S}_2)$ $[\text{M-H}]^-$: m/z 501; Molecular Weight (calculated from structure): 502.60. HPLC mobile phase: 80% ACN with 0.1% formic acid, retention time 0.70 min, purity: >95%.

N-(3-((2,5-dimethoxybenzyl)oxy)-4-(methylsulfonamido)phenyl)-3-ethoxybenzamide
(20). Yield 30%, White Powder. ^1H NMR (400 MHz, $\text{DMSO-}d^6$) δ_{H} 10.26 (s, 1H), 9.00 (s, 1H), 7.72 (s, 1H), 7.44 (m, 4H), 7.82 (s, 1H), 7.24 (d, $J=8.6$ Hz, 1H), 7.15 (d, $J=8.1$ Hz, 1H), 7.00 (d, $J=8.9$ Hz, 1H), 6.87 (m, 1H), 5.08 (s, 2H), 4.12 (m, 2H), 3.79 (s, 3H), 3.73 (s, 3H), 2.87 (s, 3H), 1.37 (t, 3H); ^{13}C NMR (100 MHz, $\text{DMSO-}d^6$) δ_{C} 165.67, 158.93, 153.67, 150.98, 139.06, 136.60, 130.05, 128.51, 125.82, 120.22, 118.13, 115.23, 113.97, 113.77, 112.94, 112.05, 105.73, 65.41, 63.79, 56.24, 55.92, 15.08. ESI-MS calculated for $(\text{C}_{25}\text{H}_{28}\text{N}_2\text{O}_7\text{S})$ $[\text{M-H}]^-$: m/z 499; Molecular Weight (calculated from structure): 500.57. HPLC mobile phase: 80% ACN with 0.1% formic acid, retention time 0.68 min, purity: >95%.

N-(3-((2,5-dimethoxybenzyl)oxy)-4-(methylsulfonamido)phenyl)-3-methoxybenzamide
(21). Yield 29%, Pale Gray Powder. ^1H NMR (400 MHz, $\text{DMSO-}d^6$) δ_{H} 10.27 (s, 1H), 9.00 (s, 1H), 7.70 (s, 1H), 7.54 (d, $J=8.4$ Hz, 1H), 7.44 (m, 3H), 7.29 (d, $J=2.9$ Hz, 1H), 7.21 (d, $J=8.6$ Hz, 1H), 7.18 (d, $J=8.1$ Hz, 1H), 7.00 (d, $J=8.9$ Hz, 1H), 6.87 (m, 1H), 5.08 (s, 2H), 3.85 (s, 3H), 3.79 (s, 3H), 3.73 (s, 3H), 2.87 (s, 3H); ^{13}C NMR (100 MHz, $\text{DMSO-}d^6$) δ_{C} 165.69, 159.68, 153.67, 153.08, 150.97, 139.06, 136.66, 130.04, 128.53,

125.81, 121.43, 120.29, 117.81, 115.23, 113.76, 113.45, 112.96, 112.04, 105.74, 65.41, 56.23, 55.91, 55.83. ESI-MS calculated for (C₂₄H₂₆N₂O₇S) [M-H]⁻: *m/z* 485; Molecular Weight (calculated from structure): 486.54. HPLC mobile phase: 80% ACN with 0.1% formic acid, retention time 0.68 min, purity: >95%.

3-chloro-N-(3-((2,5-dimethoxybenzyl)oxy)-4-(methylsulfonamido)phenyl)benzamide

(22). Yield 20%, Gray Powder. ¹H NMR (400 MHz, DMSO-*d*⁶) δ_H 10.25 (s, 1H), 8.99 (s, 1H), 7.49 (m, 4H), 7.28 (d, *J* = 2.9 Hz, 1H), 7.23 (d, *J* = 8.6 Hz, 1H), 7.16 (m, 1H), 7.00 (d, *J* = 8.9 Hz, 1H), 6.87 (m, 1H), 5.09 (s, 2H), 3.79 (s, 3H), 3.73 (s, 3H), 2.88 (s, 3H); ¹³C NMR (100 MHz, DMSO-*d*⁶) δ_C 164.47, 153.67, 153.03, 150.96, 137.23, 133.69, 131.95, 130.91, 128.41, 127.83, 126.96, 125.81, 115.19, 113.75, 113.00, 112.05, 105.79, 65.43, 56.24, 55.91. ESI-MS calculated for (C₂₃H₂₃ClN₂O₆S) [M-H]⁻: *m/z* 489; Molecular Weight (calculated from structure): 490.96. HPLC mobile phase: 80% ACN with 0.1% formic acid, retention time 0.68 min, purity: >95%.

N-(3-((2,5-dimethoxybenzyl)oxy)-4-(methylsulfonamido)phenyl)-4-methyl-3-

nitrobenzamide (23). Yield 20%, Gray Powder. ¹H NMR (400 MHz, DMSO-*d*⁶) δ_H 10.51 (s, 1H), 9.03 (s, 1H), 8.58 (s, 1H), 8.22 (d, *J* = 8.0 Hz, 1H), 7.70 (m, 2H), 7.44 (d, *J* = 8.0 Hz, 1H), 7.28 (m, 2H), 7.00 (d, *J* = 8.9 Hz, 1H), 6.87 (m, 1H), 5.09 (s, 2H), 3.79 (s, 3H), 3.73 (s, 3H), 2.88 (s, 3H), 2.61 (s, 3H); ¹³C NMR (100 MHz, DMSO-*d*⁶) δ_C 163.62, 153.68, 153.03, 150.96, 136.85, 134.13, 133.58, 132.59, 125.79, 123.99, 115.19, 113.77, 113.11, 112.06, 105.88, 65.46, 56.24, 55.92, 20.02. ESI-MS calculated for (C₂₄H₂₅N₃O₈S) [M-H]⁻: *m/z* 514; Molecular Weight (calculated from structure): 515.54. HPLC mobile phase: 80% ACN with 0.1% formic acid, retention time 0.70 min, purity: >95%.

N-(3-((2,5-dimethoxybenzyl)oxy)-4-(methylsulfonamido)phenyl)-4-(trifluoromethyl)benzamide (**24**). Yield 39%, Pale Gray Powder. ¹H NMR (400 MHz, DMSO-*d*⁶) δ_H 10.41 (s, 1H), 9.01 (s, 1H), 8.09 (d, *J*= 8.8 Hz, 1H), 7.68 (s, 1H), 7.54 (d, *J*= 8.2 Hz, 1H), 7.42 (d, *J*= 8.6 Hz, 1H), 7.27 (m, 2H), 7.00 (d, *J*= 8.9 Hz, 1H), 6.87 (m, 1H), 5.09 (s, 2H), 3.79 (s, 3H), 3.73 (s, 3H), 2.88 (s, 3H); ¹³C NMR (100 MHz, DMSO-*d*⁶) δ_C 164.79, 153.68, 153.06, 150.99, 138.85, 134.41, 130.51, 128.45, 125.79, 121.65, 121.17, 115.22, 113.81, 112.96, 112.09, 105.76, 65.46, 56.26, 55.92. ESI-MS calculated for (C₂₄H₂₃F₃N₂O₆S) [M-H]⁻: *m/z* 539; Molecular Weight (calculated from structure): 524.51. HPLC mobile phase: 80% ACN with 0.1% formic acid, retention time 0.72 min, purity: >95%.

N-(3-((2,5-dimethoxybenzyl)oxy)-4-(methylsulfonamido)phenyl)-3-(trifluoromethyl)benzamide (**25**). Yield 37%, White Powder. ¹H NMR (400 MHz, DMSO-*d*⁶) δ_H 10.51 (s, 1H), 9.03 (s, 1H), 8.28 (m, 2H), 7.98 (d, *J*= 7.7 Hz, 1H), 7.80 (m, 1H), 7.566 (s, 1H), 7.43 (d, *J*= 8.6 Hz, 1H), 7.28 (m, 2H), 7.00 (d, *J*= 8.9 Hz, 1H), 6.87 (m, 1H), 5.09 (s, 2H), 3.79 (s, 3H), 3.73 (s, 3H), 2.88 (s, 3H); ¹³C NMR (100 MHz, DMSO-*d*⁶) δ_C 164.46, 153.68, 152.96, 150.97, 136.15, 132.29, 130.23, 129.83, 129.51, 128.67, 128.21, 125.83, 124.70, 124.66, 115.21, 113.78, 113.18, 112.07, 105.99, 65.48, 56.25, 55.92. ESI-MS calculated for (C₂₄H₂₃F₃N₂O₆S) [M-H]⁻: *m/z* 523; Molecular Weight (calculated from structure): 524.51. HPLC mobile phase: 80% ACN with 0.1% formic acid, retention time 0.71 min, purity: >95%.

N-(3-((2,5-dimethoxybenzyl)oxy)-4-(methylsulfonamido)phenyl)-2-naphthamide (**26**). Yield 36%, Gray Powder. ¹H NMR (400 MHz, DMSO-*d*⁶) δ_H 10.50 (s, 1H), 9.02 (s, 1H), 8.59 (s, 1H), 8.09 (m, 4H), 7.75 (s, 1H), 7.65 (m, 2H), 7.50 (dd, *J*= 3, 6.6 Hz 1H), 7.29

(m, 2H), 7.00 (d, $J=8.9$ Hz, 1H), 6.87 (m, 1H), 5.11 (s, 2H), 3.80 (s, 3H), 3.74 (s, 3H), 2.89 (s, 3H); ^{13}C NMR (100 MHz, $\text{DMSO-}d^6$) δ_{C} 166.04, 153.68, 153.13, 150.99, 139.17, 134.78, 132.57, 132.54, 129.43, 128.52, 128.44, 128.37, 128.16, 127.37, 125.84, 124.68, 121.46, 115.23, 113.78, 112.94, 112.08, 105.73, 65.46, 56.26, 55.93. ESI-MS calculated for ($\text{C}_{27}\text{H}_{26}\text{N}_2\text{O}_6\text{S}$) $[\text{M-H}]^-$: m/z 505; Molecular Weight (calculated from structure): 506.57. HPLC mobile phase: 80% ACN with 0.1% formic acid, retention time 0.68 min, purity: >95%.

N-(3-((2,5-dimethoxybenzyl)oxy)-4-(methylsulfonamido)phenyl)-3,4,5-trimethoxybenzamide (**27**). Yield 55%, White Powder. ^1H NMR (400 MHz, $\text{DMSO-}d^6$) δ_{H} 10.17 (s, 1H), 8.97 (s, 1H), 7.68 (s, 1H), 7.35 (d, $J=8.2$ Hz, 1H), 7.25 (m, 4H), 7.00 (d, $J=8.9$ Hz, 1H), 6.87 (m, 1H), 5.09 (s, 2H), 3.89 (s, 6H), 3.79 (s, 3H), 3.73 (s, 6H), 2.88 (s, 3H); ^{13}C NMR (100 MHz, $\text{DMSO-}d^6$) δ_{C} 165.43, 153.65, 153.10, 151.02, 140.91, 138.91, 130.32, 128.36, 125.77, 121.55, 115.30, 113.85, 113.24, 112.11, 105.99, 105.83, 65.47, 60.63, 56.63, 56.25, 55.91. ESI-MS calculated for ($\text{C}_{26}\text{H}_{30}\text{N}_2\text{O}_9\text{S}$) $[\text{M-H}]^-$: m/z 545; Molecular Weight (calculated from structure): 546.59. HPLC mobile phase: 80% ACN with 0.1% formic acid, retention time 0.70 min, purity: >95%.

3,4-dichloro-N-(3-((2,5-dimethoxybenzyl)oxy)-4-(methylsulfonamido)phenyl)benzamide (**28**). Yield 33%, Pale Gray Powder. ^1H NMR (400 MHz, $\text{DMSO-}d^6$) δ_{H} 10.44 (s, 1H), 9.03 (s, 1H), 8.22 (d, $J=2.0$ Hz, 1H), 7.96 (m, 1H), 7.85 (d, $J=8.4$ Hz, 1H), 7.56 (d, $J=1.8$ Hz, 1H), 7.40 (m, 1H), 7.25 (m, 2H), 7.00 (d, $J=8.9$ Hz, 1H), 6.87 (m, 1H), 5.09 (s, 2H), 3.79 (s, 3H), 3.73 (s, 3H), 2.88 (s, 3H); ^{13}C NMR (100 MHz, $\text{DMSO-}d^6$) δ_{C} 163.62, 153.67, 153.02, 150.98, 138.57, 135.52, 134.94, 131.79, 131.26, 130.03, 128.50, 128.41, 125.75, 121.83, 115.21, 113.80, 112.09, 105.84, 65.47, 56.25, 55.92. ESI-MS calculated

for (C₂₃H₂₂Cl₂N₂O₆S) [M-H]⁻: *m/z* 523; Molecular Weight (calculated from structure): 525.40. HPLC mobile phase: 80% ACN with 0.1% formic acid, retention time 0.71 min, purity: >95%.

N-(3-((2,5-dimethoxybenzyl)oxy)-4-(methylsulfonamido)phenyl)-4-methylbenzamide (29). Yield 22%, Gray Powder. ¹H NMR (400 MHz, DMSO-*d*⁶) δ_H 10.22 (s, 1H), 8.99 (s, 1H), 7.88 (d, *J*= 8.1 Hz, 2H), 7.71 (s, 1H), 7.43 (d, *J*= 8.6 Hz, 1H), 7.35 (d, *J*= 8.0 Hz, 2H), 7.28 (d, *J*= 3.0 Hz, 1H), 7.21 (d, *J*= 8.6 Hz, 1H), 7.00 (d, *J*= 8.9 Hz, 1H), 6.87 (m, 1H), 5.08 (s, 2H), 3.79 (s, 3H), 3.73 (s, 3H), 2.87 (s, 3H), 2.40 (s, 3H); ¹³C NMR (100 MHz, DMSO-*d*⁶) δ_C 165.81, 153.67, 153.08, 151.00, 142.18, 139.19, 132.36, 129.40, 128.48, 128.13, 125.83, 121.31, 115.24, 113.81, 112.90, 112.09, 105.72, 65.43, 56.25, 55.92, 21.48. ESI-MS calculated for (C₂₄H₂₆N₂O₆S) [M-H]⁻: *m/z* 469; Molecular Weight (calculated from structure): 470.54. HPLC mobile phase: 80% ACN with 0.1% formic acid, retention time 0.72 min, purity: >95%.

N-(3-((2,5-dimethoxybenzyl)oxy)-4-(methylsulfonamido)phenyl)hexanamide (30). Yield 55%, Yellow Powder. ¹H NMR (400 MHz, DMSO-*d*⁶) δ_H 9.94 (s, 1H), 8.93 (s, 1H), 7.53 (s, 1H), 7.25 (d, *J*=2.8 Hz, 1H), 7.15 (s, 2H), 6.99 (d, *J*= 8.9 Hz, 1H), 6.87 (m, 1H), 5.04 (s, 2H), 3.79 (s, 3H), 3.73 (s, 3H), 2.84 (s, 3H), 2.29 (t, 2H), 1.59 (m, 2H), 1.29 (m, 4H), 0.88 (m, 3H); ¹³C NMR (100 MHz, DMSO-*d*⁶) δ_C 171.86, 153.66, 153.26, 150.98, 139.38, 128.82, 125.82, 120.66, 115.19, 113.78, 112.07, 111.61, 104.43, 65.35, 56.25, 55.91, 36.88, 31.34, 25.22, 22.35, 14.31. ESI-MS calculated for (C₂₂H₃₀N₂O₆S) [M-H]⁻: *m/z* 449; Molecular Weight (calculated from structure): 450.55. HPLC mobile phase: 80% ACN with 0.1% formic acid, retention time 0.68 min, purity: >95%.

N-(3-((2,5-dimethoxybenzyl)oxy)-4-(methylsulfonamido)phenyl)-[1,1'-biphenyl]-4-carboxamide (**31**). Yield 36%, Gray Powder. ^1H NMR (400 MHz, $\text{DMSO-}d^6$) δ_{H} 10.35 (s, 1H), 9.00 (s, 1H), 8.06 (d, $J= 8.3$ Hz, 2H), 7.86 (d, $J= 8.3$ Hz, 2H), 7.76 (m, 3H), 7.53 (m, 2H), 7.45 (m, 2H), 7.00 (d, $J= 8.9$ Hz, 1H), 6.87 (m, 1H), 5.10 (s, 2H), 3.80 (s, 3H), 3.74 (s, 3H), 2.88 (s, 3H); ^{13}C NMR (100 MHz, $\text{DMSO-}d^6$) δ_{C} 165.59, 153.69, 153.10, 151.00, 143.68, 139.56, 139.13, 134.01, 129.55, 128.82, 128.65, 128.50, 127.40, 127.07, 125.84, 115.24, 113.80, 112.92, 112.09, 105.73, 65.45, 56.26, 55.93. ESI-MS calculated for ($\text{C}_{29}\text{H}_{28}\text{N}_2\text{O}_6\text{S}$) $[\text{M-H}]^-$: m/z 531; Molecular Weight (calculated from structure): 532.61. HPLC mobile phase: 80% ACN with 0.1% formic acid, retention time 0.69 min, purity: >95%.

N-(3-((2,5-dimethoxybenzyl)oxy)-4-(methylsulfonamido)phenyl)-3-methylbenzamide (**32**). Yield 46%, Pale Gray Powder. ^1H NMR (400 MHz, $\text{DMSO-}d^6$) δ_{H} 10.26 (s, 1H), 8.98 (s, 1H), 7.76 (m, 3H), 7.42 (m, 3H), 7.28 (s, 1H), 7.22 (d, $J= 8.8$ Hz, 1H), 6.99 (d, $J= 8.9$ Hz, 1H), 6.87 (m, 1H), 5.09 (s, 2H), 3.79 (s, 3H), 3.73 (s, 3H), 2.88 (s, 3H); ^{13}C NMR (100 MHz, $\text{DMSO-}d^6$) δ_{C} 166.74, 153.46, 152.85, 151.21, 138.62, 138.54, 134.83, 132.98, 128.98, 128.35, 127.97, 125.55, 125.08, 121.53, 115.49, 114.12, 113.29, 112.34, 106.14, 65.54, 56.26, 55.85, 21.29. ESI-MS calculated for ($\text{C}_{24}\text{H}_{26}\text{N}_2\text{O}_6\text{S}$) $[\text{M-H}]^-$: m/z 469; Molecular Weight (calculated from structure): 470.54. HPLC mobile phase: 80% ACN with 0.1% formic acid, retention time 0.71 min, purity: >95%.

N-(3-((2,5-dimethoxybenzyl)oxy)-4-(methylsulfonamido)phenyl)-4-(trifluoromethoxy)benzamide (**33**). Yield 38%, Pale Gray Powder. ^1H NMR (400 MHz, $\text{DMSO-}d^6$) δ_{H} 10.40 (s, 1H), 8.99 (s, 1H), 8.08 (d, $J= 8.4$ Hz, 2H), 7.69 (s, 1H), 7.55 (d, $J= 8.2$ Hz, 2H), 7.40 (d, $J= 8.7$ Hz, 1H), 7.27 (m, 2H), 7.00 (d, $J= 8.9$ Hz, 1H), 6.87 (m, 1H), 5.09 (s, 2H), 3.79

(s, 3H), 3.73 (s, 3H), 2.88 (s, 3H); ^{13}C NMR (100 MHz, $\text{DMSO-}d^6$) δ_{C} 164.79, 153.68, 153.05, 150.99, 138.80, 134.41, 130.50, 128.41, 125.80, 121.72, 121.17, 119.18, 115.22, 113.81, 112.97, 112.09, 105.77, 65.46, 56.26, 55.92. ESI-MS calculated for $(\text{C}_{24}\text{H}_{23}\text{F}_3\text{N}_2\text{O}_7\text{S})$ $[\text{M-H}]^-$: m/z 539; Molecular Weight (calculated from structure): 540.51. HPLC mobile phase: 80% ACN with 0.1% formic acid, retention time 0.77 min, purity: >95%.

N-(3-((2,5-dimethoxybenzyl)oxy)-4-(methylsulfonamido)phenyl)-2-methylbenzamide (34). Yield 23%, Gray Powder. ^1H NMR (400 MHz, $\text{DMSO-}d^6$) δ_{H} 10.31 (s, 1H), 8.93 (s, 1H), 7.68 (s, 1H), 7.44 (m, 2H), 7.30 (m, 3H), 7.20 (d, $J=7.9$ Hz, 1H), 7.00 (d, $J=8.6$ Hz, 1H), 6.87 (m, 1H), 5.09 (s, 2H), 3.79 (s, 3H), 3.73 (s, 3H), 2.88 (s, 3H); ^{13}C NMR (100 MHz, $\text{DMSO-}d^6$) δ_{C} 168.30, 153.66, 153.13, 151.04, 137.56, 135.69, 131.00, 128.43, 127.65, 126.09, 125.86, 115.31, 113.83, 112.30, 112.08, 105.19, 65.43, 56.25, 55.92, 19.77. ESI-MS calculated for $(\text{C}_{24}\text{H}_{26}\text{N}_2\text{O}_6\text{S})$ $[\text{M-H}]^-$: m/z 469; Molecular Weight (calculated from structure): 470.54. HPLC mobile phase: 80% ACN with 0.1% formic acid, retention time 0.73 min, purity: >95%.

N-(3-((2,5-dimethoxybenzyl)oxy)-4-(methylsulfonamido)phenyl)thiophene-2-carboxamide (35). Yield 53%, Gray Powder. ^1H NMR (400 MHz, $\text{DMSO-}d^6$) δ_{H} 10.27 (s, 1H), 8.98 (s, 1H), 8.02 (s, 1H), 7.88 (d, $J=4.6$ Hz, 1H), 7.64 (s, 1H), 7.37 (d, $J=8.6$ Hz, 1H), 7.25 (m, 3H), 7.00 (d, $J=8.9$ Hz, 1H), 6.87 (m, 1H), 5.09 (s, 2H), 3.80 (s, 3H), 3.74 (s, 3H), 2.88 (s, 3H); ^{13}C NMR (100 MHz, $\text{DMSO-}d^6$) δ_{C} 160.34, 153.68, 150.98, 140.38, 138.52, 132.48, 129.63, 128.54, 128.40, 125.83, 121.74, 115.23, 113.80, 112.92, 112.06, 105.73, 65.45, 56.25, 55.92. ESI-MS calculated for $(\text{C}_{21}\text{H}_{22}\text{N}_2\text{O}_6\text{S}_2)$ $[\text{M-H}]^-$: m/z 461;

Molecular Weight (calculated from structure): 462.54. HPLC mobile phase: 80% ACN with 0.1% formic acid, retention time 0.72 min, purity: >95%.

N-(3-((2,5-dimethoxybenzyl)oxy)-4-(methylsulfonamido)phenyl)isoxazole-5-carboxamide (**36**). Yield 48%, Yellow Powder. ^1H NMR (400 MHz, DMSO- d^6) δ_{H} 10.79 (s, 1H), 9.03 (s, 1H), 8.82 (s, 1H), 7.65 (s, 1H), 7.42 (d, $J= 8.6$ Hz, 1H), 7.26 (m, 3H), 7.00 (d, $J= 8.6$ Hz, 1H), 6.87 (m, 1H), 5.09 (s, 2H), 3.79 (s, 3H), 3.73 (s, 3H), 2.88 (s, 3H); ^{13}C NMR (100 MHz, DMSO- d^6) δ_{C} 162.90, 154.52, 153.64, 152.91, 152.33, 151.04, 137.40, 128.18, 125.65, 122.46, 115.28, 113.88, 113.38, 112.15, 107.32, 106.21, 65.55, 56.27, 55.90. ESI-MS calculated for (C₂₀H₂₁N₃O₇S) [M-H]⁻: m/z 446; Molecular Weight (calculated from structure): 447.46. HPLC mobile phase: 80% ACN with 0.1% formic acid, retention time 0.67 min, purity: >95%.

N1,N5-bis(3-((2,5-dimethoxybenzyl)oxy)-4-(methylsulfonamido)phenyl)glutaramide (**37**). Yield 25%, Gray Powder. ^1H NMR (400 MHz, DMSO- d^6) δ_{H} 9.97 (s, 2H), 8.89 (s, 2H), 7.55 (s, 1H), 7.25 (s, 2H), 7.17 (s, 4H), 7.00 (d, $J= 8.8$ Hz, 2H), 6.89 (d, $J= 8.6$ Hz, 2H), 5.04 (s, 4H), 3.78 (s, 6H), 3.73 (s, 6H), 2.85 (s, 6H), 2.38 (m, 4), 1.91 (m, 2); ^{13}C NMR (100 MHz, DMSO- d^6) δ_{C} 171.37, 153.66, 153.25, 150.97, 139.33, 128.79, 125.81, 120.73, 115.19, 113.78, 112.07, 111.66, 104.47, 65.37, 56.25, 55.91, 36.06, 21.31. ESI-MS calculated for (C₃₇H₄₄N₄O₁₂S₂) [M-H]⁻: m/z 799; Molecular Weight (calculated from structure): 800.90. HPLC mobile phase: 80% ACN with 0.1% formic acid, retention time 0.70 min, purity: >95%.

2,2'-oxybis(N-(3-((2,5-dimethoxybenzyl)oxy)-4-(methylsulfonamido)phenyl)acetamide) (**38**). Yield 18%, Gray Powder. ^1H NMR (400 MHz, DMSO- d^6) δ_{H} 9.77 (s, 2H), 8.84 (s, 2H), 7.39 (s, 2H), 7.23 (s, 2H), 7.14 (s, 2H), 7.00 (m, 4H), 6.88 (s, 2H), 5.04 (s, 4H), 3.78

(s, 6H), 3.72 (s, 6H), 3.67 (s, 4H), 3.59 (s, 4H), 2.85 (s, 3H); ^{13}C NMR (100 MHz, DMSO- d_6) δ_{C} 168.55, 153.64, 153.11, 150.96, 125.76, 115.19, 113.76, 112.31, 112.03, 71.28, 65.40, 56.22, 55.89. ESI-MS calculated for ($\text{C}_{36}\text{H}_{42}\text{N}_4\text{O}_{13}\text{S}_2$) $[\text{M-H}]^-$: m/z 801; Molecular Weight (calculated from structure): 802.87. HPLC mobile phase: 80% ACN with 0.1% formic acid, retention time 0.68 min, purity: >95%.

ethane-1,2-diyl bis((3-((2,5-dimethoxybenzyl)oxy)-4-(methylsulfonamido)phenyl)carbamate) (**39**). Yield 24%, Pale Gray Powder. ^1H NMR (400 MHz, DMSO- d_6) δ_{H} 9.80 (s, 2H), 8.86 (s, 2H), 7.39 (s, 2H), 7.22 (s, 2H), 7.15 (d, $J=7.5$ Hz, 2H), 7.03 (m, 4H), 6.87 (s, 2H), 5.04 (s, 4H), 4.35 (s, 3H), 3.78 (s, 6H), 3.72 (s, 6H), 2.85 (s, 6H), 2.51 (s, 6H); ^{13}C NMR (100 MHz, DMSO- d_6) δ_{C} 153.73, 153.61, 153.46, 151.05, 139.05, 129.01, 125.71, 120.36, 115.31, 113.86, 112.09, 110.93, 103.81, 65.34, 63.20, 56.24, 55.89. ESI-MS calculated for ($\text{C}_{36}\text{H}_{42}\text{N}_4\text{O}_{14}\text{S}_2$) $[\text{M-H}]^-$: m/z 817; Molecular Weight (calculated from structure): 818.87. HPLC mobile phase: 80% ACN with 0.1% formic acid, retention time 0.65 min, purity: >95%.

(ethane-1,2-diylbis(oxy))bis(ethane-2,1-diyl)bis((3-((2,5-dimethoxybenzyl)oxy)-4-(methylsulfonamido)phenyl)carbamate) (**40**). Yield 19%, Pale Gray Powder. ^1H NMR (400 MHz, DMSO- d_6) δ_{H} 9.77 (s, 2H), 8.85 (s, 2H), 7.38 (s, 2H), 7.23 (s, 2H), 7.15 (d, $J=7.9$ Hz, 2H), 7.00 (m, 4H), 6.87 (m, 2H), 5.03 (s, 4H), 4.21 (s, 4H), 3.77 (s, 6H), 3.72 (s, 6H), 3.67 (s, 4H), 3.59 (s, 4H), 2.84 (s, 6H); ^{13}C NMR (100 MHz, DMSO- d_6) δ_{C} 153.87, 153.64, 153.49, 151.04, 139.20, 129.04, 125.76, 120.27, 115.31, 113.84, 112.08, 110.82, 103.71, 70.20, 69.16, 65.34, 64.07, 56.24, 55.90. ESI-MS calculated for ($\text{C}_{40}\text{H}_{50}\text{N}_4\text{O}_{16}\text{S}_2$) $[\text{M-H}]^-$: m/z 905; Molecular Weight (calculated from structure): 906.97. HPLC mobile phase: 80% ACN with 0.1% formic acid, retention time 0.68 min, purity: >95%.

4-amino-N-(3-((2,5-dimethoxybenzyl)oxy)-4-(methylsulfonamido)phenyl)benzamide

(41). Yield 60%, Pale Yellow Powder. ^1H NMR (400 MHz, DMSO- d^6) δ_{H} 9.82 (s, 1H), 8.92 (s, 1H), 7.72 (d, J = 8.7 Hz, 3H), 7.41 (d, J = 8.6 Hz, 1H), 7.29 (d, J = 2.8 Hz, 1H), 7.17 (d, J = 8.5 Hz, 1H), 6.99 (d, J = 8.9 Hz, 1H), 6.87 (m, 1H), 6.60 (d, J = 8.5 Hz, 2H), 5.78 (s, 2H), 5.07 (s, 2H), 3.79 (s, 3H), 3.73 (s, 3H), 2.86 (s, 3H); ^{13}C NMR (100 MHz, DMSO- d^6) δ_{C} 165.75, 153.67, 153.19, 152.72, 150.95, 139.94, 129.63, 128.70, 125.90, 121.37, 120.54, 115.21, 113.71, 113.03, 112.57, 112.01, 105.36, 65.35, 56.21, 55.90. ESI-MS calculated for (C₂₃H₂₅N₃O₆S) [M-H]⁻: m/z 470; Molecular Weight (calculated from structure): 471.53. HPLC mobile phase: 80% ACN with 0.1% formic acid, retention time 0.65 min, purity: >95%.

4,4'-((2,2'-oxybis(acetyl))bis(azanediy))bis(N-(3-((2,5-dimethoxybenzyl)oxy)-4-(methylsulfonamido)phenyl)benzamide) (42). Yield 60%, Gray Powder. ^1H NMR (400 MHz, DMSO- d^6) δ_{H} 10.36 (s, 1H), 10.20 (s, 1H), 8.98 (s, 2H), 7.99 (d, J = 8.6 Hz, 3H), 7.84 (d, J = 8.6 Hz, 3H), 7.70 (m, 2H), 7.42 (d, J = 8.8 Hz, 2H), 7.22 (d, J = 8.6 Hz, 2H), 7.00 (d, J = 8.9 Hz, 2H), 6.87 (m, 2H), 5.09 (s, 4H), 4.35 (s, 3H), 3.79 (s, 6H), 3.73 (s, 6H), 2.88 (s, 6H); ^{13}C NMR (100 MHz, DMSO- d^6) δ_{C} 169.07, 165.31, 153.68, 153.08, 150.98, 141.84, 130.06, 129.10, 125.86, 119.35, 115.23, 113.78, 112.90, 112.08, 105.73, 89.07, 71.35, 65.44, 56.25, 55.92. ESI-MS calculated for (C₅₀H₅₂N₆O₁₅S₂) [M-H]⁻: m/z 1039; Molecular Weight (calculated from structure): 1041.11. HPLC mobile phase: 80% ACN with 0.1% formic acid, retention time 0.65 min, purity: >95%.

5.2.3. Cell culture

T98G, A172, U87 and U251 cells were from ATCC. The cells were maintained in RPMI1640 or DMEM supplemented with 10% fetal bovine serum (FBS), 100 U/mL penicillin and 100 mg/mL streptomycin in a humidified incubator with 5% CO₂ at 37 °C.

5.2.4. Cell viability analysis

MTT assay was used to evaluate the effect of HSP27 inhibitors on the growth of T98G, A172, U87 and U251 cells in eight replications. 3000 cells per well were seeded with RPMI1640 or DMEM in 96-well flat-bottomed plates for 24 h and were then exposed to various concentrations of test compounds dissolved into DMSO (highest final concentration 0.1%) in the medium for 48 h. controls received DMSO at a same concentration as that in highest does drug-treated cells. Cells were incubated in 100 µL 1 mg/mL of MTT reagent diluted in fresh media at 37 °C for 2 h. Supernatants were removed from the wells, and the precipitated MTT dye was dissolved in 200 µL/well DMSO. Absorbance at 570 nm was determined on a SpectraMax Plus 384 spectrophotometer (Molecular Devices).

5.2.5. Experimental animals

Male C57BL/6 mice and nude mice were purchased from Taconic lab. Mice were housed in Plexiglas cages, kept on a 12/12 -h light-dark cycle, and received food and water ad libitum in a temperature- and humidity- controlled environment. All the experimental procedures involving animals were performed in accordance with the guide

for the Care and Use of The Cleveland State University (CSU) Institutional Animal Care and Use Committee (IACUC).

5.2.6. Maximum Tolerated Dose (MTD) study

12 C57BL/6 mice were randomly divided into three groups. Mice were injected with vehicle (DMSO) or compounds (100 mg/kg in PBS) by intraperitoneal injection (IP) daily. Mice would be euthanized after 10 days treatment. Body weights were determined at the start dosing day and the end dosing day.

Hematology analysis. Non-fasted blood samples were collected from the heart immediately for hematology analysis after the euthanizing. Hematology analysis was performed with a hematology analyzer—Element HT5 (Heska Corporation, USA).

Hematoxylin and eosin (H&E) staining. Five tissues (Heart, liver, spleen, lung, kidney) were collected. Then, the tissues are fixed in 10% neutral buffered formalin (10 mL of formalin per cm³ tissue). Tissues are cut and transferred into cassettes. Tissues were immersed into increasing concentration ethanol to remove the water and formalin (dehydration), then, using xylene was used to remove alcohol and allow infiltration with paraffin wax. Then, tissues were embedded into paraffin wax. Tissues were cut at 4 μm by microtome (sectioning). Generally, tissue slides are transparent when unstained. H&E staining would be thus used to provide contrast to tissue sections, leading tissue structures more visible and easier to evaluate. The protocol was slightly modified from Wang's method²⁸.

5.2.7. Western blotting

Cells were cultured in 6-well culture plates and incubated with DMSO or inhibitors and then lysed with RIPA supplemented with a protease inhibitor cocktail. After incubating the cells on ice for 10 min, lysates were collected into a 1.5 mL centrifuge tube, then, the supernatant would be collected after centrifuged at 10,000 g for 10 min. Protein concentrations were determined by the BCA Protein Assay kit. Fifty micrograms of total protein lysate for each sample were boiled with 1x loading buffer for 10 min. Samples were then separated on a 10% SDS-polyacrylamide gel and transferred to polyvinylidene fluoride (PVDF) membrane. The membrane was blocked for 2 h with 5% non-fat milk in 1x TBS-T (150 mM NaCl, 10 mM Tris, pH7.4, 0.1% Tween 20) at room temperature and then incubated with primary antibody at 4°C overnight. After the membrane was incubated with the primary antibody and washed three times with 1x TBS-T for 10 min each wash, it was incubated with the secondary antibody for 60 min at room temperature. The membrane was washed three times again for 10 min each time with 1x TBS-T. Eventually, the membranes were incubated with SuperSignal West Pico Chemiluminescent Substrate (Pierce) according to the protocol of the manufacturer.

5.2.8. HSP27 chaperone activity assay

24 μ L 1 mg/mL insulin stock solution was added to the single well of 384 well plate, 3 μ L 5 mg/mL α -crystallin (a segment of HSP27 responsible for the chaperone function of HSP27), 71 μ L PBS with three different concentrations (10, 100 and 1000 nM) of compounds dissolved inside were added as well. The mixture was thoroughly mixed and incubated at 37 °C for 5 min, then 2 μ L of 1 M DTT in water was added to

initiate the insulin aggregation. The mixture of insulin in the absence or presence of α -crystallin with 0.1% DMSO was used as control. The absorbance at 400 nm was monitored every three minutes continuously for 2 h using Molecular Devices SpectraMax Microplate reader.

5.2.9. Immunofluorescence assay

U87 and T98G cells were seeded in 6-well plates. Cover slips were placed into the wells and the cells could attach naturally. After 24 h, cells were treated with compounds **4** and **26** at 50 nM for 12 h, respectively. Then, cells were washed with PBS and fixed with 4% paraformaldehyde for 10 min, permeabilized with 0.1% Triton X-100 for 10 min, blocked with 1% bovine serum albumin for 30 min. Several washing steps with PBS occurred in between fixation, permeabilization and blocking. Then, incubation with the AR primary antibody for 1 h. Followed by washing with PBS then fluorescein-labeled secondary antibodies for 1 h. DAPI (1 μ g/mL) was incubated for 10 min to stain the nucleus. Images were visualized and analyzed using Echo Revolve Microscope.

5.2.10. *In vivo* xenograft study

U87 cells were re-suspended in sterile PBS (100 μ L) and injected (5×10^6 cells/injection) subcutaneously at the left and right flank of a male nude mouse (5-6 weeks, n = 4/group, 2 tumors per mouse and 8 tumors per group). Tumors and body weight were monitored with Vernier calipers three times weekly, and tumor volume was calculated by the following formula: $V = 2/3 d_1 \times d_2^2$, where d_1 is the larger diameter and d_2 is the smaller diameter. When the tumor volume reached approximately 50 mm³, mice

were injected with vehicle (DMSO) or compound **4** or **26** (20 mg/kg in PBS) by intraperitoneal injection (IP) three times weekly for 14 days, and the tumor size were monitored and measured at the same time. In the end, mice were euthanized by exposure to excess CO₂ and the tumors were removed, weighted. And every two tumors from every single one mouse was mixed and homogenized with RIPA buffer (Protein inhibitors and PMSF were added) to prepare the tumor lysates after tumor were weighted.

5.2.11. Determination of anti-glioblastoma agents in mouse plasma and brain

HPLC-MS/MS conditions: The HPLC-MS/MS method was performed with a Shimadzu UPLC system (Columbia, MD) which consisted of a Prominence DGU-20A_{3R} inline degasser, two LC-30 AD pumps, a SIL-30 AC autosampler and a CBM-20A controller. The chromatographic separation was performed on a Kinetex C₁₈ column (50 mm × 2.1 mm, 1.3 μm) with a mobile phase consisting of acetonitrile-0.1% formic acid and water (50:50, v/v) at a flow rate of 0.3 mL/min. The temperature of the column was maintained at 36°C. The injection volume was 5.0 μL. Mass spectrometric detection was operated on an AB Sciex Qtrap 5500 mass spectrometer (Toronto, Canada) with negative electrospray ionization mode. The multiple reaction monitoring (MRM) function was used for quantification with the transitions of compound **4**, **26** and IS compound **I**, which were detected at m/z 501.2→151.1, m/z 507.2→151.1 and m/z 487.1→151.1, respectively (product ion spectrums showed in supplemental material). The optimized ion source parameters were set as follows: ion spray voltage, 2000 V; ion source temperature, 550°C; nebulization gas 40 psi; auxiliary gas, 40 psi; curtain gas, 30 psi. Compound parameters were as follows: compound **4**: declustering potential, 40V; entrance potential, 5V;

collision energy, 23V; Collision entrance potential, 15V. compound 26: declustering potential, 40V; entrance potential, 5V; collision energy, 25V; Collision entrance potential, 15V. compound I (Internal standard): declustering potential, 35V; entrance potential, 5V; collision energy, 30V; Collision entrance potential, 15V. Preparation of standards and samples. The stock solutions were prepared by dissolving compound 4, 26 and compound I in methanol at 1.0 mg/mL. Then, the stock solution of compound 4 or 26 was serially diluted with methanol into a concentration gradient: 1.0, 2.0, 5.0, 10, 20, 50, 100, 200, 500, 1000 ng/mL. Also, a 500 ng/mL working solution of compound I (IS) was prepared in methanol from the stock solution. All the solutions were stored at 4°C in the dark. A simple protein precipitation method was applied to extract compound 4 or 26 from mouse plasma or brain homogenate (0.4 g brain tissue mix with 2 mL PBS). Briefly, 100 µL of each sample, 40 µL of compound I (IS, 500 ng/mL), and 800 µL of methanol were combined in a 1.5 mL tube. Then, it was vortexed and centrifuged at 12,000 g for 5 min. The supernatant was collected and then transferred into a new 1.5 mL tube. The liquid was dried by a nitrogen blowing instrument. The residue was stored at -80 °C and dissolved with 100 µL 50% acetonitrile before analysis.

5.2.12. Statistical analysis

Statistical and graphical information was determined using GraphPad Prism software (GraphPad Software Incorporated) and Microsoft Excel (Microsoft Corporation). Gray values from western blot were determined via Quantity One Software (Bio-Rad). The determination of IC₅₀s was performed using nonlinear regression analysis.

Statistically significant differences were calculated with the two-tailed unpaired Student's *t*-test and *p* values reported at 95% confidence intervals.

5.3. Results and discussions

5.3.1. Lead optimization and summarization of the structure-activity relationship (SAR)

Our previous study identified compound I (shown in **Figure 19**. N-(3-((2,5-dimethoxybenzyl)oxy)-4-(methylsulfonamido) phenyl)-4-methoxybenzamide), as a dual tubulin and HSP27 inhibitor, having potent anti-glioblastoma activity *in vitro* and *in vivo*²⁹. Compound I displayed potent antiproliferative activity against four different GBM cells in the range of 1-10 nM, also significantly shrunk the GBM tumor size in nude mice xenograft model at 20 mg/kg. In the current study, a total of 42 new derivatives and dimers based on compound I were synthesized by modifying the circled moiety in **Figure 19**. We have explored different structures at R₁ domain, including aromatic rings and aliphatic groups.

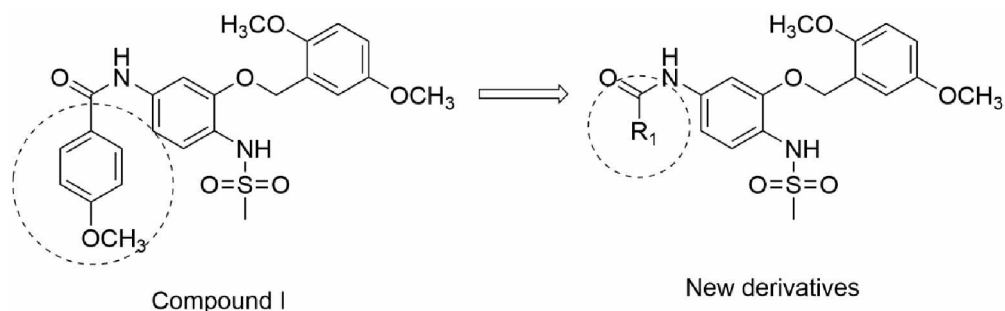
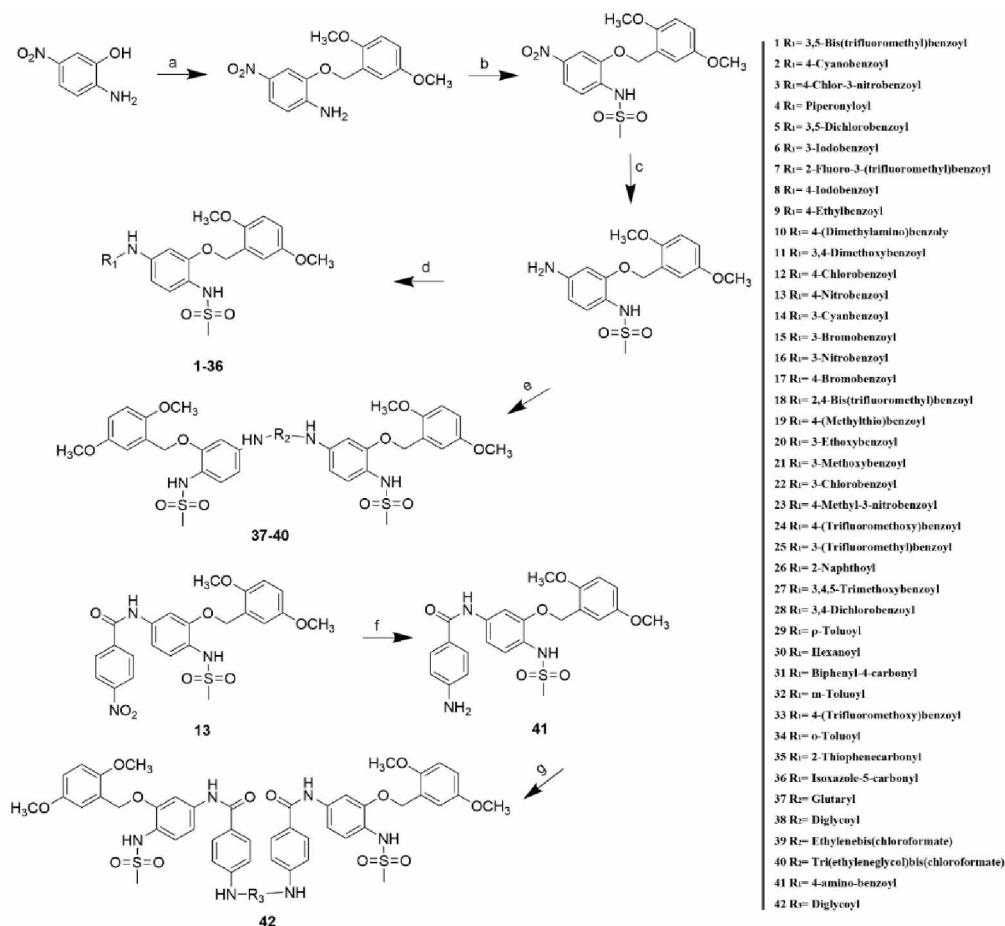


Figure 19. Core structure of the new derivatives.

In this project, 42 different new derivatives were synthesized. The synthesis is illustrated in **Scheme 1**.

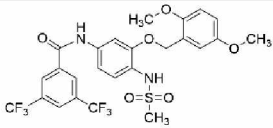
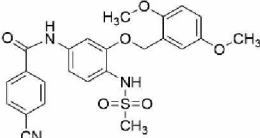
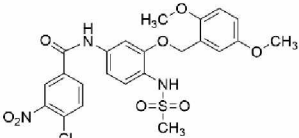
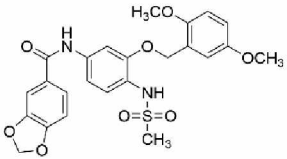
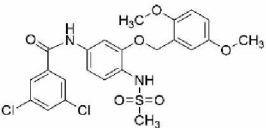


Scheme 1. Synthesis of compounds 1-42. Reagents and conditions: (a) 2, 5-dimethoxybenzyl chloride, DMF, K_2CO_3 ; (b) Methanesulfonyl chloride, NaH, DMF; (c) NH_4Cl , Zn, H_2O , THF; (d) R_1COCl , K_2CO_3 , DMF; (e) $R_2C_2O_2Cl_2$, DMF, K_2CO_3 ; (f) NH_4Cl , Zn, H_2O , THF; (g) $R_3C_2O_2Cl_2$, DMF, K_2CO_3 .

All of these new compounds were examined for potency on the growth inhibition of four different GBM cells including A172, U87, T98G and U251cells, and AR downregulation effect in T98G cells. The results are summarized in **Table 7** and **Figure 20**. In **Table 7**, the results showed that compounds **4**, **5**, **6**, **8**, **11**, **12**, **17**, **19**, **25**, **26** and **29** have the IC_{50} s lower than 1 μM in all the GBM cells. Meanwhile, compounds **4**, **13**, **15**, **19**, **26**, **33**, **34**, **35**, **36** and **37** showed significant AR downregulation activity at 100 nM

in T98G cells. To refine the screening results, compounds dose was decreased to 50 nM to determine AR downregulation activity in T98G cells. The results showed in **Figure 21**, indicated that compounds **4** and **26** have potent AR downregulation activity at 50 nM in T98G cells, similar to compound **I**. Also, the IC₅₀s of compounds **4**, **8**, **19** and **26** is lower than 0.1 μM in all the GBM cells. With the crosstalk of the IC₅₀s and AR downregulation activity of these new compounds, both compounds **4** and **26** have potent AR downregulation activity and low IC₅₀s in the GBMs. Thus, compounds **4** and **26** were identified, which have similar activity to compound **I**, potentially targeting HSP27 to induce AR degradation in GBM.

Table 7. Growth inhibitory effects of the new compounds in GBM cells.

No.	Compound Structure	IC ₅₀ s (μM)			
		A172	U87	T98G	U251
1		5.76±2.16	2.65±0.50	1.04±0.29	0.46±0.16
2		1.88±0.48	2.88±0.82	0.79±0.26	0.49±0.15
3		0.87±0.22	>10	0.57±0.17	0.33±0.11
4		0.056±0.015	0.12±0.045	0.035±0.011	0.013±0.00
5		0.17±0.049	0.15±0.074	0.097±0.036	0.137±0.06

No.	Compound Structure	A172	U87	T98G	U251
		IC50s (μM)			
6		0.15±0.042	0.21±0.096	0.13±0.044	0.12±0.05
7		0.59±0.23	1.5±0.55	4.77±2.85	0.50±0.22
8		0.029±0.093	0.046±0.022	0.048±0.018	0.03±0.01
9		0.75±0.33	1.87±0.83	3.85±2.18	0.19±0.09
10		>10	>10	1.91±0.95	2.17±1.00
11		0.63±0.017	0.22±0.11	0.09±0.03	0.07±0.03
12		0.107±0.0419	0.208±0.091	0.077±0.029	0.051±0.02
13		>10	>10	1.19±0.521	1.461±0.53
14		3.253±1.821	1.889±0.619	5.026±3.271	0.898±0.49

No.	Compound Structure	IC50s (μM)			
		A172	U87	T98G	U251
15		0.865±0.415	0.530±0.267	2.674±1.096	0.189±0.10
16		2.821±1.051	2.038±0.936	5.069±1.410	1.033±0.39
17		0.04±0.011	0.155±0.071	0.148±0.058	0.105±0.04
18		2.359±1.220	1.706±0.893	2.363±0.554	1.995±0.72
19		0.042±0.012	0.092±0.032	0.029±0.009	0.024±0.01
20		0.129±0.047	3.829±2.328	0.0384±0.012	0.019±0.01
21		0.633±0.280	8.313±4.629	0.220±0.099	0.357±0.16
22		0.279±0.074	>10	0.065±0.024	0.636±0.24
23		3.795±2.037	2.630±0.966	3.688±1.394	0.690±0.22

No.	Compound Structure	IC50s (μM)			
		A172	U87	T98G	U251
24		0.576±0.258	2.085±0.840	>10	0.131±0.05
25		0.386±0.119	0.998±0.440	0.423±0.151	0.244±0.09
26		0.028±0.0056	0.067±0.025	0.023±0.0007	0.015±0.00
27		0.180±0.056	3.367±1.685	0.218±0.079	0.180±0.06
28		0.410±0.121	0.476±0.231	2.382±0.846	0.535±0.23
29		0.598±0.188	0.091±0.036	0.213±0.094	0.059±0.02
30		0.754±0.199	2.043±0.921	1.186±0.413	1.826±0.89
31		1.930±0.738	6.907±5.179	0.455±0.189	1.181±0.27
32		1.285±0.418	>10	0.422±0.152	0.355±0.13

No.	Compound Structure	IC50s (μM)			
		A172	U87	T98G	U251
33		0.640±0.176	2.490±1.085	0.899±0.377	0.168±0.06
34		1.358±0.447	1.189±0.445	0.306±0.110	0.184±0.07
35		>10	>10	3.430±0.814	2.864±0.67
36		>10	>10	3.965±1.098	1.998±0.71
37		>10	>10	>10	>10
38		>10	>10	>10	>10
39		8.267±2.129	5.232±1.323	2.276±0.655	2.437±0.65
40		>10	>10	5.468±1.030	3.071±0.76
41		5.266±1.869	2.064±0.513	3.609±1.777	2.437±0.89

No.	Compound Structure	A172	U87	T98G	U251
		IC50s (μM)			
42		>10	>10	>10	>10

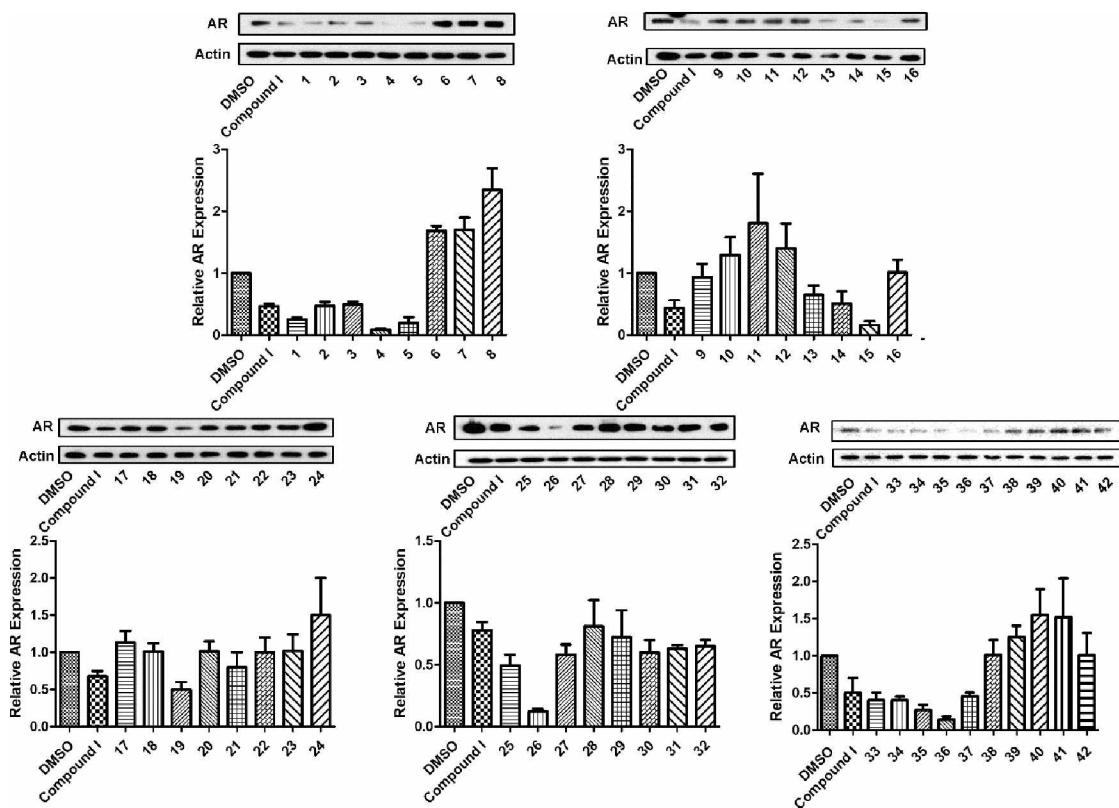


Figure 20. AR downregulation effect of compounds 1-42 at 100 nM for 12 h in T98G cells. The proteins were analyzed by western blotting with specific antibodies and the results are representative images and quantification. Data are expressed as Mean \pm SD (n=3).

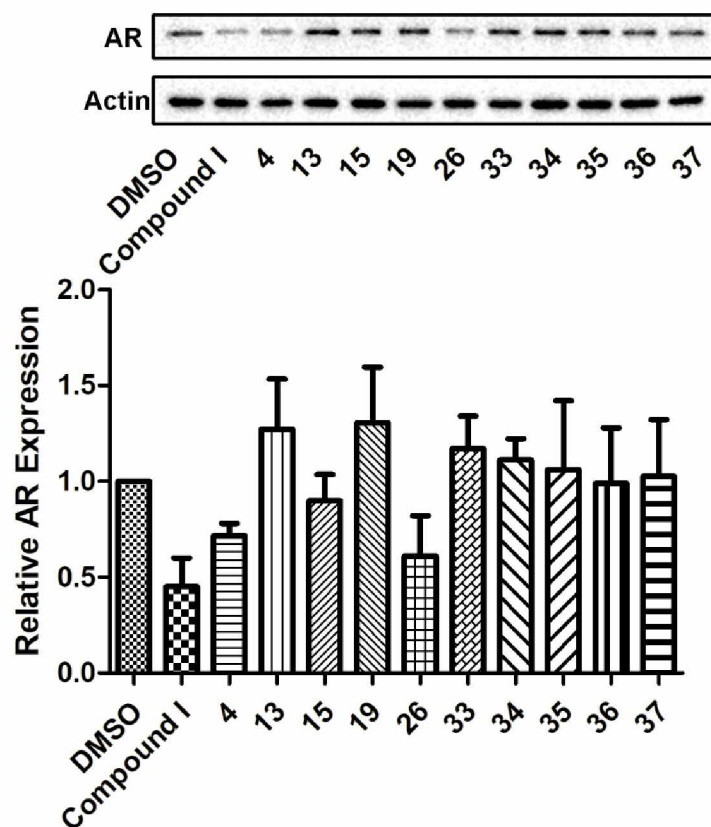


Figure 21. AR downregulation effect of promising compounds at 50 nM for 12 h in T98G cells. The proteins were analyzed by western blotting with specific antibodies and the results are representative images and quantification. Data are expressed as Mean \pm SD (n=3).

5.3.2. Compounds 4 and 26 inhibit the chaperone activity of HSP27

The lead compound, compound I was identified to bind to HSP27 from our previous study²⁹. Thus, the chaperone activity of HSP27 of the derivatives, compounds 4 and 26 was determined. It is well confirmed that HSP27 is critical for stabilizing its client proteins, including AR^{60,64,65}. The cellular protective function of HSP27 is regulated by the chaperone activity and preventing cell death from stress stimulation. To determine the *in vitro* chaperone activity, insulin is often used as a model substrate protein to mimic the

protein aggregation and HSP27 serves as the chaperone to prevent aggregation. In the current study, dithiothreitol (DTT) could denature insulin, which induces insulin B chain aggregation. α -crystalline is the chaperone function domain of HSP27, which was used in this study to perform the chaperone assay. In the presence of the chaperone protein, insulin aggregation level could be decreased, because the stable complex was formed by HSP27 and unfolded insulin B chain⁵⁴. The aggregated insulin could be determined by the absorbance at 400 nm. The capability of compounds **4** and **26** to modulate the *in vitro* chaperone activity of HSP27 was evaluated by monitoring the DTT induced insulin aggregation in the presence of α -crystalline with or without compounds **4** and **26**. The results showed in **Figure 22**, α -crystalline exhibits significant potency against DTT-induced insulin aggregation. Compounds **4** and **26** do not interfere with DTT-induced insulin aggregation, while the chaperone activity of α -crystalline was inhibited with the presence of compound **4** or **26**. The results indicated that the inhibitory activity of compounds **4** and **26** to the *in vitro* chaperone function of HSP27.

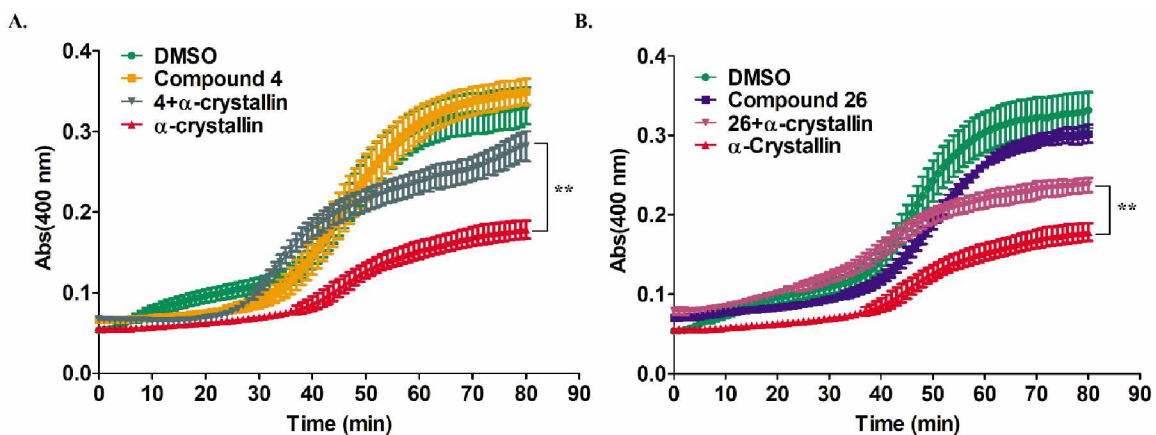


Figure 22. Inhibition of Compounds **4** and **26** chaperone function. α -crystallin lost the activity to prevent DTT-induced insulin B chain aggregation in the presence of compound **4** or **26**. The kinetics of the DTT-induced insulin B chain aggregation was monitored in the absence of a chaperone protein or in the presence of a chaperone protein with or without compound **4** or **26**. The mixture of insulin and DTT with or without other components with the assay buffer was incubated for 80 min at 37°C, and the absorbance

at 400 nm was measured. The compound at this concentration or below did not interfere with DTT and insulin interaction. The results are representative of three independent experiments, each curve was measured in triplicate, and the mean was used to generate the curve. The representative one of the three experiments is presented. The statistical analysis was performed for the end reading of the curve with the unpaired *t*-test, ***p*<0.01, with compound **4** or **26** versus without compound **4** or **26**.

5.3.3. Compounds 4 and 26 dose-dependently decrease AR and mutated AR protein levels in GBM cells

It is well established that AR is one of the most common client proteins of HSP27 and AR degradation induced by knocking down HSP27 has been reported in prostate cancer⁷³. Our hypothesis is eliminating AR via inhibiting HSP27 by a small molecule with potential to cross the BBB, which is vital for GBM treatment. The results showed in **Figure 23** showed that Compounds **4** and **26** downregulate AR protein level in GBM cells dose-dependently. Both compounds **4** and **26** could significantly downregulate AR protein level at 25, 50 and 100 nM in T98G and U87 cells. Moreover, compounds **4** and **26** also could downregulate mutated AR (AR-V7) in T98G cells, since AR-V7 was not detected in U87 cells. The results demonstrated that the advantage to targeting AR compared with AR antagonists, since both wild type and mutated AR could be down regulated by the compounds. So far, compounds **4** and **26**, as small-molecule HSP27 inhibitors, could inhibit GBM cell proliferation potently and downregulate AR protein level.

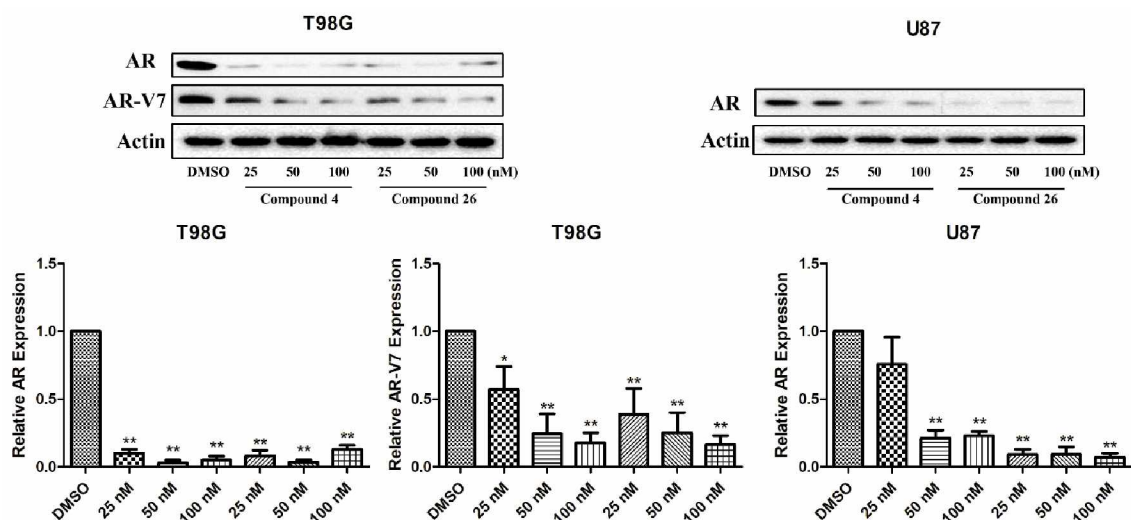


Figure 23. AR and or mutated AR (AR-V7) was abolished with compound 4 or 26 treatment in T98G cells and U87 cells. AR and AR-V7 expressions were analyzed by western blotting after the compound treatment. The experiment was repeated three times independently, and the representative image and quantification are shown. Data are expressed as Mean \pm SD (n=3). * p < 0.05, ** p < 0.01 compared to the DMSO treatment group by the unpaired t -test.

5.3.4. AR downregulation effect of compounds 4 and 26 was confirmed with immunofluorescence imaging

We also examined the AR distribution in U87 cells and T98G cells after the treatment with both compounds 4 and 26, respectively. Immunofluorescence imaging was used to visualize the AR protein in living cells. The results showed that the fluorescence intensities of AR were decreased with the treatment of compounds 4 and 26 in both cell lines compared to DMSO group (Figure 24), which is consistent to the western blotting results. Furthermore, AR was eliminated in nucleus in T98G cells with compounds 4 and 26 treatment, which indicating that HSP27 chaperone activity was suppressed to escort the client protein AR translocated into nucleus.

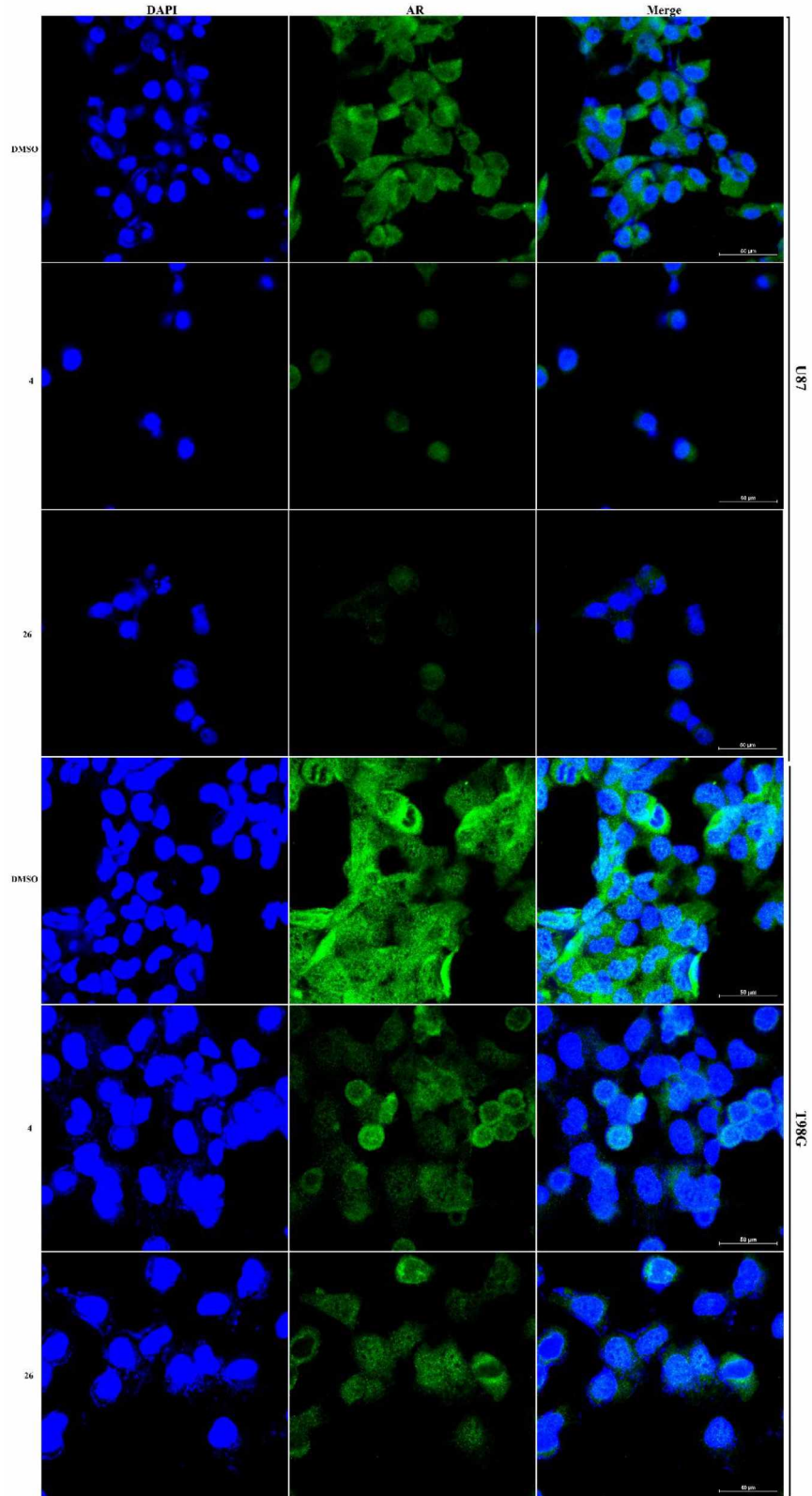


Figure 24. Expression and location of AR with DMSO or compounds treatment in T98G cells and U87 cells. The cells were analyzed by the immunofluorescence assay.

5.3.5. Compounds 4 and 26 significantly shrunk the GBM growth and AR level in the xenograft tumor model

The *in vivo* activity with GBM model test is necessary to be a potential drug candidate, compounds **4** and **26**, as HSP27 inhibitors, bear potent *in vitro* anti-GBM activities. In this study, the xenograft tumor model was developed by subcutaneously injecting U87 cells into the left and right flank of nude mice. Compounds **4** and **26** were administrated into the nude mice with intraperitoneal injection (IP) every two days for 2 weeks, once the tumor size reach to 150 mm³. The mice body weight and tumor size were measured and recorded. As shown in **Figure 25**, nude mice body weight was not affected with compound **4** or **26** administration. The results were consistent with the *in vivo* toxicity study (**Figure 25B**). The tumor images were lined up in **Figure 25 A**, the tumor size was subjectively considered decreased. The tumor size was also measured during treatment and the measurements showed significant decrease in tumor size in both compounds **4** and **26**, compared with DMSO group in **Figure 25C**. Tumor weight results showed in **Figure 25D**, showed compounds **4** and **26** group significantly decreased the tumor weight compared with DMSO group. To confirm that GBM tumor inhibition effect was from AR suppression. The AR expression level in tumor was examined via western blot (**Figure 25E**), AR protein level was decreased in both compounds **4** and **26** groups, compared with DMSO group. The results indicated that both compounds **4** and **26** exhibit potent *in vivo* activity, providing the solid evidence that compounds **4** and **26** could be promising new drug candidates to treat AR overexpressed GBM.

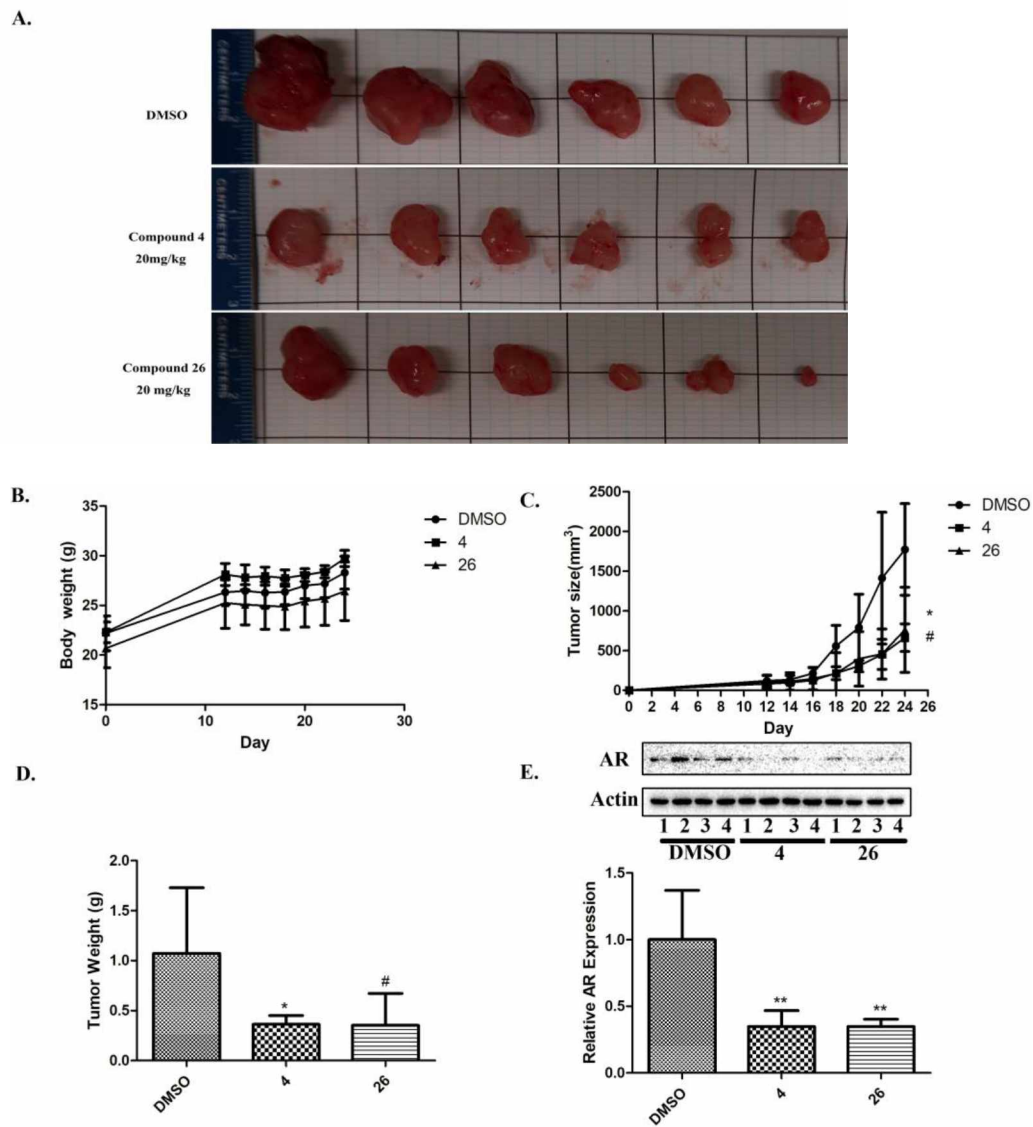


Figure 25. *In vivo* efficacy of compound **4** and **26** in human GBM. A total of 5×10^6 U87 cells were inoculated subcutaneously into nude mice, which were randomly assigned to DMSO and the compounds treated groups. Nude mice were treated with compound **4** or **26** at 20 mg/kg with IP injection. Tumor images (**A**, $n=8$); Body weight (**B**, $n=4$); Tumor size (**C**, $n=8$, data are expressed as Mean \pm SD, compound **4** * $p<0.05$, compound **26** # $p<0.05$ compared to DMSO group); tumor weight (**D**, $n=8$, data are expressed as Mean \pm SD, compound **4** * $p<0.05$, compound **26** # $p<0.05$ compared to DMSO group) and AR expression in tumor was analyzed by western blotting, as shown by representative images and by quantification (**E**, $n=4$, data are expressed as Mean \pm SD, compound **4** ** $p<0.01$, compound **26** ## $p<0.01$ compared to DMSO group)

5.3.6. Compounds 4 and 26 could cross blood brain barrier

Since compounds 4 and 26 could inhibit GBM tumor growth in mice xenograft model, and do not cause toxicity to mice, compounds 4 and 26 could be the potential drug candidates to treat GBM. However, whether the candidates could cross blood brain barrier is a critical factor to consider for the treatment of GBM. Thus, the determination of compounds 4 and 26 in mouse plasma and brain with HPLC-MS/MS was applied. The mouse plasma and brain concentrations of compounds 4 and 26 at different time are exhibited in **Figure 26**. The pharmacokinetic parameters are listed as Mean \pm SD in **Table 8**. The results showed that compounds 4 and 26 were rapidly absorbed and distributed. The apparent elimination half-life ($t_{1/2}$) of compounds 4 and 26 were 5.25 h and 6.28 h, respectively, indicating both of compounds 4 and 26 could be cleared fast from the mouse plasma. Moreover, AUC of compound 4 in mouse plasma reached to 32.13 $\mu\text{g}\cdot\text{h}/\text{mL}$. Moreover, the compound 4 was detected in brain tissue after IP administration, the AUC of compound 4 in brain tissue is 0.62 $\mu\text{g}\cdot\text{h}/\text{g}$ (2% of the concentration in blood), indicating that compound 4 in the blood circulation was able to pass the blood-brain barrier (BBB) and accumulate in the brain tissue (**Figure 26A & B**). AUC of compound 26 in mouse plasma reached to 80.84 $\mu\text{g}\cdot\text{h}/\text{mL}$. Moreover, the compound 26 was detected in brain tissue after IP administration, the AUC of compound 26 in brain tissue is 2.44 $\mu\text{g}\cdot\text{h}/\text{g}$ (3% of the concentration in blood), indicating that compound 26 in the blood circulation was able to pass the blood-brain barrier (BBB) and accumulate in the brain tissue (**Figure 26C & D**). compared with the lead compound, compound I from our previous study ⁷⁴, compounds 4 and 26 have slightly increased BBB permeability.

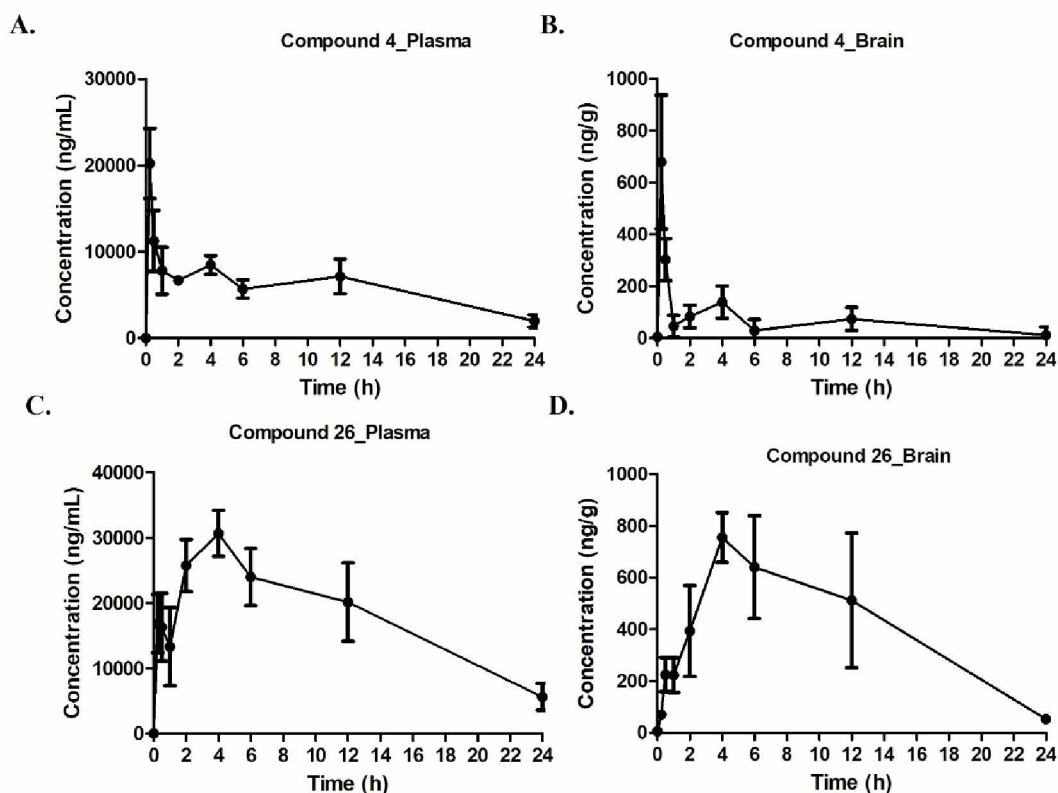


Figure 26. Plasma and brain tissue concentration-time profiles of compound 4 (A and B) and 26 (C and D) with IP administration in mice. (Mean \pm SD, n=4)

Table 8. Non-compartmental pharmacokinetic parameters of compounds 4 and 26 in mouse after IP administration (n=4, Mean \pm SD).

Pharmacokinetic parameters	Values	
	Plasma	Brain
Compound 4		
$t_{1/2}$	5.25 \pm 1.57 (h)	6.06 \pm 2.00 (h)
C_{max}	20.20 \pm 8.10 (μ g/mL)	0.68 \pm 0.25 (μ g/g)
AUC_{0-24h}	20.02 \pm 5.62 (μ g.h/mL)	0.31 \pm 0.05 (μ g.h/g)
$AUC_{0-\infty h}$	32.13 \pm 5.59 (μ g.h/mL)	0.62 \pm 0.24 (μ g.h/g)
Compound 26		
$t_{1/2}$	6.28 \pm 1.39 (h)	8.66 \pm 3.81 (h)
C_{max}	30.62 \pm 6.99 (μ g/mL)	0.76 \pm 0.19 (μ g/g)
AUC_{0-24h}	61.92 \pm 15.47 (μ g.h/mL)	1.34 \pm 0.31 (μ g.h/g)
$AUC_{0-\infty h}$	80.84 \pm 12.78 (μ g.h/mL)	2.44 \pm 0.53 (μ g.h/g)

5.3.7. Compounds 4 and 26 do not show *in vivo* toxicity with high dose exposure

To further confirm these two promising compounds 4 and 26 could be the drug candidates, the *in vivo* toxicity is necessary to determine. In this study, C57BL/6 mice were exposed to the compounds 4 and 26, respectively, at 100 mg/kg per day for 10 days to evaluate the toxicity. Mice condition observation, body weight, tissue staining and hematology in mice were determined to demonstrate the toxicity of compounds 4 and 26.

(1) Condition observation: all of the groups of mice did not show any syndromes of toxicity, such as dehydration, acute pain or distress. (2) Body weight: the mice body weight was monitored and recorded every day before dosing, the results showed in **Figure 27A**, there is no growth rate difference between compounds 4 and 26 groups with DMSO group in 10 days. (3) Hematology. The results showed in **Table 9**. There is no significant changed compared with DMSO group. (4) Tissue staining. At the end of the day, the mice were sacrificed, then the tissues (kidney, spleen, lung, liver and heart) were collected and rinsed with PBS, then, fixed with 4% formalin for 24 h at room temperature. After tissues were sliced and stained with Hematoxylin and Eosin. The images were taken from the microscope, the results showed in **Figure 27B**. The results showed that compared with DMSO group, there is no severe injuries observed in compounds 4 and 26 groups in kidney, spleen, lung, liver and heart tissues. In kidney, normal histology of the glomerulus and tubules was found and there is no necrosis and glomerular atrophy and other inflammatory changes in drug treatment groups; In spleen, it showed that intact and distinct spleen follicle with clear white pulp, red pulp and marginal zone in all the DMSO and drug treatment groups; In lung, there is no severe injury or fibrosis observed in all the groups; In liver, all these groups showed normal hepatic architecture with central vein

and surrounding hepatocytes, sinusoids and nucleus; In heart, there is no obvious infarcts, inflammatory cell infiltration, rupture or necrosis of myocardial cells. Overall, there is no abnormal physical condition observed in compounds **4** and **26** treatment group, the body weight growth rate in drug treatment groups also similar to DMSO group and there is no obvious tissue damage in various tissue pathology slides observed in both compounds **4** and **26** groups, which indicating compounds **4** and **26** do not cause acute toxicity in mice.

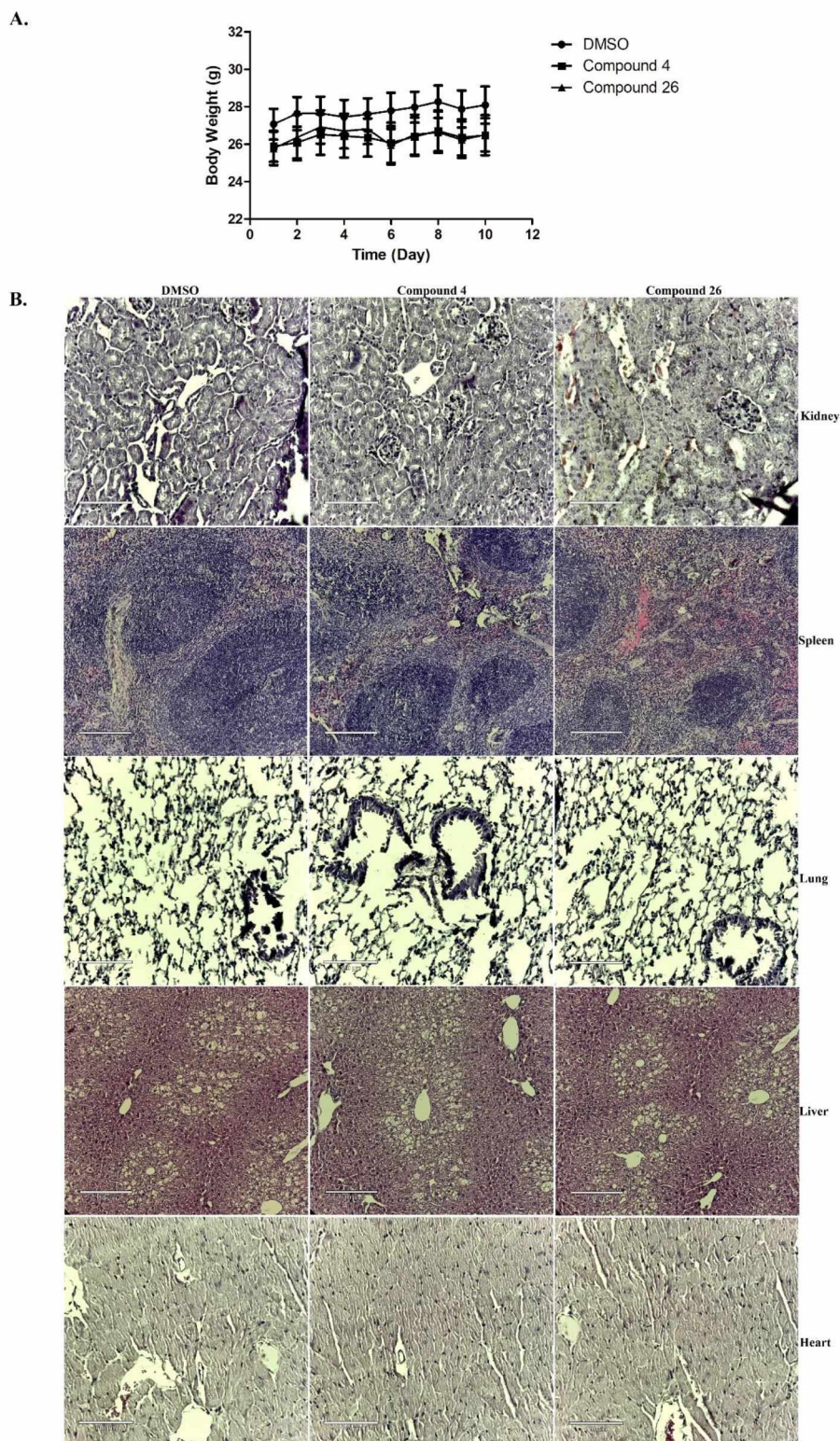


Figure 27. Body weight (**A**) and microscope images of the kidney, spleen, lung, liver and heart stained with H&E staining after compounds **4** or **26** treatment (**B**). Data expressed with Mean \pm SD (n=3).

Table 9. Comparative hematology (Mean \pm SD) between different groups.

Parameters	Groups			Reference Range
	DMSO	4	26	
WBC ($10^3/\mu\text{L}$)	9.69 \pm 1.48	10.83 \pm 1.58	11.18 \pm 2.07 \uparrow	0.80-10.6
Neu ($10^3/\mu\text{L}$)	1.24 \pm 0.40	2.40 \pm 0.76	2.57 \pm 0.77	0.23-3.60
Lym ($10^3/\mu\text{L}$)	7.63 \pm 1.06	7.68 \pm 0.97	7.84 \pm 1.20	0.60-8.90
Mon ($10^3/\mu\text{L}$)	0.62 \pm 0.45	0.55 \pm 0.24	0.56 \pm 0.20	0.04-1.40
Eos ($10^3/\mu\text{L}$)	0.12 \pm 0.07	0.14 \pm 0.12	0.12 \pm 0.03	0.00-0.51
Bas ($10^3/\mu\text{L}$)	0.09 \pm 0.06	0.06 \pm 0.02	0.09 \pm 0.04	0.00-0.12
Neu (%)	12.70 \pm 2.95	21.95 \pm 5.08	22.70 \pm 3.81	6.50-50.0
Lym (%)	79.14 \pm 7.36	71.33 \pm 6.89	70.60 \pm 4.65	40.0-92.0
Mon (%)	6.14 \pm 4.17	5.00 \pm 1.57	4.92 \pm 1.03	0.90-18.0
Eos (%)	1.14 \pm 0.55	1.23 \pm 0.88	1.04 \pm 0.21	0.00-7.50
Bas (%)	0.88 \pm 0.53	0.50 \pm 0.16	0.74 \pm 0.23	0.00-1.50
RBC ($10^6/\mu\text{L}$)	12.21 \pm 0.54 \uparrow	10.47 \pm 0.18	11.46 \pm 0.52	6.80-12.00
HGB (g/dL)	15.62 \pm 0.58	13.83 \pm 0.36	15.34 \pm 0.45	10.5-19.0
HCT (%)	59.36 \pm 1.28 \uparrow	52.03 \pm 0.73	55.16 \pm 2.15	37.2-58.0
MCV (fL)	48.68 \pm 1.28	49.73 \pm 0.34	48.20 \pm 2.48	42.6-55.6
MCH (pg)	12.78 \pm 0.16 \downarrow	13.23 \pm 0.17	13.40 \pm 0.42	13.0-19.8
MCHC (g/dL)	26.34 \pm 0.69	26.65 \pm 0.37	27.80 \pm 0.66	26.0-37.9
RDW-CV (%)	16.74 \pm 0.48	16.30 \pm 0.36	17.14 \pm 0.92	11.1-21.1
PLT ($10^3/\mu\text{L}$)	1510.6 \pm 451.2	1940.75 \pm 155.9	1461.8 \pm 425.5	565-1849
MPV (fL)	4.88 \pm 0.13	4.75 \pm 0.06	4.98 \pm 0.20	3.6-6.8

*Reference ranges obtained from Heska hematology analyzer based on the age, sex of species

“ \downarrow ” means the value is shortage of reference range;

“ \uparrow ” means the value is excess of reference range.

5.4. Conclusion

GBM is the most common and aggressive brain tumor, with very poor prognosis ². Recently studies indicated that AR is considered as a potential therapeutic target to treat GBM ^{38,63}. In our previous study, compound **I** was identified as a promising drug candidate for AR-overexpressed GBM, while it could suppress GBM *in vitro* and *in vivo* by abolishing ARs ²⁹.

Based on the structure of compound **I**, a series of potential anti-glioblastoma compounds were developed in this study. Both compounds **4** and **26** exhibited potent *in vitro* anti-glioblastoma activity, including nanomolar level IC_{50s} and AR downregulation effects in GBMs, indicating that the anti-glioblastoma activity is similar to the lead compound, compound **I**. As HSP27 inhibitors, both compounds **4** and **26** could inhibit α -crystallin effect on insulin B chain aggregation, exhibiting potent HSP27 chaperone activity inhibition capacity. It is well documented that HSP27 stabilizes AR and escorts it translocating into nucleus, triggering ARE regulation and cell proliferation⁷⁴. Our hypothesis is that both compounds **4** and **26** could induce AR downregulation via inhibiting HSP27 chaperone activity. Compounds **4** and **26** could down regulate AR and AR-V7 proteins in GBM cells, also the immunofluorescence assay results indicated that AR level was decreased in nucleus mainly with the presence of compounds **4** and **26**. This result just solidified our hypothesis that the compounds induce AR degradation, particularly abolishing AR translocation into the nucleus, by inhibiting HSP27 chaperone activity. The *in vivo* study revealed that compounds **4** and **26** inhibit the U87 xenograft and abolishes the AR in the tumor samples as well. Furthermore, the pharmacokinetic studies indicated that compounds **4** and **26** could be distributed rapidly and be able to cross blood brain barrier (BBB). Compared with compound **I**, these two compounds have slightly higher permeability from blood into brain tissue, indicating that piperonyloyl and 2-Naphthoyl moieties are more helpful to cross BBB compared with 4-methoxyl benzoyl moiety. Furthermore, these two moieties change from 4-methoxyl benzoyl moiety do not exhibit any *in vivo* toxicity. Overall, this study indicated that compounds **4** and **26** could be the promising drugs to treat AR over expressed GBM, also provided a meaningful

insight for the further structural modification to retain or improve the potency and BBB permeability.

CHAPTER VI

CONCLUSIONS AND FUTURE DIRECTIONS

GBM is the most common and malignant primary human brain cancer with poor prognosis and high mortality rate. It is reported that a higher incidence rate happens in men compared to women, indicating that there is a sex disparity of the disease, which may be correlated with different sex hormone pathways. Further studies revealed that AR overexpression and mutation of AR are frequently observed in human GBM and suppressing AR expression could induce GBM cells death *in vitro* and *in vivo*. It is well known HSP27 is a chaperone protein that could stabilize AR. Targeting HSP27 to downregulate AR becomes a novel approach for the treatment of AR overexpressed GBM. We aimed to develop small molecule HSP27 inhibitor as potential drug candidates to abolish AR in GBM, and mutated AR could be eliminated in this strategy as well, which makes this approach superior to other anti-androgen compounds. Compound **I** showed great potency and selectivity to inhibit AR overexpressed GBM cells. It inhibits HSP27 chaperone function, and induces AR degradation, which is correlated to the selectivity to AR overexpressed cells. The compound also inhibits tubulin polymerization, therefore shows general activity to inhibit cell proliferation. Compared to a similar analog

with an extra N-methyl group, compound **I** shows lower toxicity to mice. The removal of N-methyl group does not bring the COX-2 inhibition back to the compound, suggesting that after the reduction of the nitro group in the very lead compound nimesulide, the COX-2 inhibition is eliminated in this scaffold. In addition to the HSP27 and tubulin inhibition, compound **I** also affects AR transcription with an unknown mechanism, since the mRNA of AR is also decreased after the treatment. It seems that the compound suppresses AR in GBM with multiple mechanisms. The *in vivo* study reveals that compound **I** inhibits U87 xenograft and abolishes the AR in the tumor samples as well after the treatment. All the *in vitro* and *in vivo* activity demonstrate that compound **I** is a promising drug candidate for AR overexpressed GBM.

To verify if compound **I** could cross blood brain barrier (BBB), a reliable and sensitive HPLC-MS/MS method for the quantification of compound **I** in mouse plasma and brain tissue was developed. The method was accurate, efficient, reliable, and successfully applied for evaluation of the pharmacokinetics of compound **I** in the *in vivo* study. The results indicated that compound **I** was rapidly distributed. Moreover, compound **I** could cross the BBB, which indicates the compound could be delivered to the central nervous system. The pharmacokinetic profile summarized in the study provides valuable information for the further investigation of compound **I** as a potential anti-glioblastoma agent.

From the view of drug discovery, the structure of compound **I** was optimized, to improve the potency of anti-glioblastoma. Based on the structure of compound **I**, a total of 42 potential anti-glioblastoma analogues were synthesized in this study. Both compounds **4** and **26** exhibited potent *in vitro* anti-glioblastoma activity, including

nanomolar level IC_{50} s and AR downregulation effects in GBMs, indicating that the anti-glioblastoma activity is similar to the lead compound, compound **I**. As HSP27 inhibitors, both compounds **4** and **26** could inhibit α -crystallin effect on insulin B chain aggregation, exhibiting potent HSP27 chaperone activity inhibition capacity. It is well documented that HSP27 stabilizes AR and escorts it is translocating into nucleus, triggering ARE regulation and cell proliferation. Our hypothesis is that both compounds **4** and **26** could induce AR downregulation via inhibiting HSP27 chaperone activity. Compounds **4** and **26** could down regulate AR and AR-V7 proteins in GBM cells, also the immunofluorescence assay results indicated that AR level was decreased in nucleus mainly with the presence of compounds **4** and **26**. This result just solidified our hypothesis that the compounds induce AR degradation, particularly abolishing AR translocation into the nucleus, by inhibiting HSP27 chaperone activity. The *in vivo* study revealed that compounds **4** and **26** inhibit the U87 xenograft and abolishes the AR in the tumor samples as well. Furthermore, the pharmacokinetic studies indicated that compounds **4** and **26** could be distributed rapidly and be able to cross BBB. Compared with compound **I**, these two compounds have slightly higher permeability from blood into brain tissue, indicating that piperonyloyl and 2-Naphthoyl moieties are more helpful to cross BBB compared with 4-methoxyl benzoyl moiety. Furthermore, these two moieties change from 4-methoxyl benzoyl moiety do not exhibit any *in vivo* toxicity. Overall, this study indicated that compounds **4** and **26** could be the promising drugs to treat AR over expressed GBM, also provided a meaningful insight for the further structural modification to retain or improve the potency and BBB permeability.

However, the anti-GBM potency of compounds **4** and **26** is similar to the lead compound **I**, even compounds **4** and **26** have higher HSP27 chaperone activity inhibition effect. Furthermore, the new derivatives, compounds **4** and **26** have low BBB permeability, which is similar to compound **I**. In the future, more structural optimization is needed.

BIBLIOGRAPHY

- (1) Glioblastoma | MD Anderson Cancer Center.
- (2) Davis, M. E. Glioblastoma: Overview of Disease and Treatment. *Clin. J. Oncol. Nurs.* **2016**, *20* (5), S2.
- (3) Wirsching, H.-G.; Weller, M. Glioblastoma. *Malig. Brain Tumors* **2017**, 265–288.
- (4) Simon, T.; Jackson, E.; Giamas, G. Breaking through the Glioblastoma Micro-Environment via Extracellular Vesicles. *Oncogene* **2020**, *39* (23), 4477–4490.
- (5) Stupp, R.; Hegi, M. E.; Mason, W. P.; Van Den Bent, M. J.; Taphoorn, M. J. B.; Janzer, R. C.; Ludwin, S. K.; Allgeier, A.; Fisher, B.; Belanger, K. Effects of Radiotherapy with Concomitant and Adjuvant Temozolomide versus Radiotherapy Alone on Survival in Glioblastoma in a Randomised Phase III Study: 5-Year Analysis of the EORTC-NCIC Trial. *Lancet Oncol.* **2009**, *10* (5), 459–466.
- (6) Salzman, M. Surgical Resection of Malignant Brain Tumors: Who Benefits? *Oncol. (willist. Park. NY)* **1988**, *2* (8), 47–56.
- (7) Alifieris, C.; Trafalis, D. T. Glioblastoma Multiforme: Pathogenesis and Treatment. *Pharmacol. Ther.* **2015**, *152*, 63–82.
- (8) Walker, M. D.; Green, S. B.; Byar, D. P.; Alexander Jr, E.; Batzdorf, U.; Brooks, W. H.; Hunt, W. E.; MacCarty, C. S.; Mahaley Jr, M. S.; Mealey Jr, J. Randomized Comparisons of Radiotherapy and Nitrosoureas for the Treatment of Malignant Glioma after Surgery. *N. Engl. J. Med.* **1980**, *303* (23), 1323–1329.

- (9) Salazar, O. M.; Rubin, M. D. P.; Feldstein, M. L.; Pizzutiello, R. High Dose Radiation Therapy in the Treatment of Malignant Gliomas. *Int. J. Radiat. Oncol. Biol. Phys.* **1979**, *5* (10), 1733–1740.
- (10) Janjua, T. I.; Rewatkar, P.; Ahmed-Cox, A.; Saeed, I.; Mansfeld, F. M.; Kulshreshtha, R.; Kumeria, T.; Ziegler, D. S.; Kavallaris, M.; Mazziere, R. Frontiers in the Treatment of Glioblastoma: Past, Present and Emerging. *Adv. Drug Deliv. Rev.* **2021**, *171*, 108–138.
- (11) Mittal, S.; Klinger, N. V.; Michelhaugh, S. K.; Barger, G. R.; Pannullo, S. C.; Juhász, C. Alternating Electric Tumor Treating Fields for Treatment of Glioblastoma: Rationale, Preclinical, and Clinical Studies. *J. Neurosurg.* **2017**, *128* (2), 414–421.
- (12) Anton, K.; Baehring, J. M.; Mayer, T. Glioblastoma Multiforme: Overview of Current Treatment and Future Perspectives. *Hematol. Clin.* **2012**, *26* (4), 825–853.
- (13) Burris-Hiday, S. D.; Scott, E. E. Steroidogenic Cytochrome P450 17A1 Structure and Function. *Mol. Cell. Endocrinol.* **2021**, *528*, 111261.
- (14) Activity of Seviteronel in Patients With Androgen Receptor (AR)-Positive Glioblastoma - Full Text View - ClinicalTrials.Gov.
- (15) Di Filippo, L. D.; Duarte, J. L.; Luiz, M. T.; de Araújo, J. T. C.; Chorilli, M. Drug Delivery Nanosystems in Glioblastoma Multiforme Treatment: Current State of the Art. *Curr. Neuropharmacol.* **2021**, *19* (6), 787–812.
- (16) Lauko, A.; Lo, A.; Ahluwalia, M. S.; Lathia, J. D. Cancer Cell Heterogeneity &

Plasticity in Glioblastoma and Brain Tumors. In *Seminars in Cancer Biology*; Elsevier, 2021.

- (17) Lima, F. R. S.; Kahn, S. A.; Soletti, R. C.; Biasoli, D.; Alves, T.; da Fonseca, A. C. C.; Garcia, C.; Romão, L.; Brito, J.; Holanda-Afonso, R. Glioblastoma: Therapeutic Challenges, What Lies Ahead. *Biochim. Biophys. Acta (BBA)-Reviews Cancer* **2012**, *1826* (2), 338–349.
- (18) Ye, X.; Xu, S.; Xin, Y.; Yu, S.; Ping, Y.; Chen, L.; Xiao, H.; Wang, B.; Yi, L.; Wang, Q. Tumor-Associated Microglia/Macrophages Enhance the Invasion of Glioma Stem-like Cells via TGF- β 1 Signaling Pathway. *J. Immunol.* **2012**, *189* (1), 444–453.
- (19) Alyautdin, R.; Khalin, I.; Nafeeza, M. I.; Haron, M. H.; Kuznetsov, D. Nanoscale Drug Delivery Systems and the Blood–Brain Barrier. *Int. J. Nanomedicine* **2014**, *9*, 795.
- (20) Saraiva, C.; Praça, C.; Ferreira, R.; Santos, T.; Ferreira, L.; Bernardino, L. Nanoparticle-Mediated Brain Drug Delivery: Overcoming Blood–Brain Barrier to Treat Neurodegenerative Diseases. *J. Control. release* **2016**, *235*, 34–47.
- (21) Cardoso, F. L.; Brites, D.; Brito, M. A. Looking at the Blood–Brain Barrier: Molecular Anatomy and Possible Investigation Approaches. *Brain Res. Rev.* **2010**, *64* (2), 328–363.
- (22) Bouchoucha, M.; Béliveau, É.; Kleitz, F.; Calon, F.; Fortin, M.-A. Antibody-Conjugated Mesoporous Silica Nanoparticles for Brain Microvessel Endothelial Cell Targeting. *J. Mater. Chem. B* **2017**, *5* (37), 7721–7735.

- (23) Pardridge, W. M. The Blood-Brain Barrier: Bottleneck in Brain Drug Development. *NeuroRx* **2005**, *2* (1), 3–14.
- (24) Chen, B.; Chen, C.; Zhang, Y.; Xu, J. Recent Incidence Trend of Elderly Patients with Glioblastoma in the United States, 2000–2017. *BMC Cancer* **2021**, *21* (1), 1–10.
- (25) Aurilio, G.; Cimadamore, A.; Mazzucchelli, R.; Lopez-Beltran, A.; Verri, E.; Scarpelli, M.; Massari, F.; Cheng, L.; Santoni, M.; Montironi, R. Androgen Receptor Signaling Pathway in Prostate Cancer: From Genetics to Clinical Applications. *Cells* **2020**, *9* (12), 2653.
- (26) Yu, X.; Jiang, Y.; Wei, W.; Cong, P.; Ding, Y.; Xiang, L.; Wu, K. Androgen Receptor Signaling Regulates Growth of Glioblastoma Multiforme in Men. *Tumor Biol.* **2015**, *36* (2), 967–972.
- (27) Zalcman, N.; Canello, T.; Ovadia, H.; Charbit, H.; Zelikovitch, B.; Mordechai, A.; Fellig, Y.; Rabani, S.; Shahar, T.; Lossos, A. Androgen Receptor: A Potential Therapeutic Target for Glioblastoma. *Oncotarget* **2018**, *9* (28), 19980.
- (28) Zoubeidi, A.; Zardan, A.; Beraldi, E.; Fazli, L.; Sowery, R.; Rennie, P.; Nelson, C.; Gleave, M. Cooperative Interactions between Androgen Receptor (AR) and Heat-Shock Protein 27 Facilitate AR Transcriptional Activity. *Cancer Res.* **2007**, *67* (21), 10455–10465.
- (29) Li, Y.; Orahoske, C. M.; Geldenhuys, W. J.; Bhattarai, A.; Sabbagh, A.; Bobba, V.; Salem, F. M.; Zhang, W.; Shukla, G. C.; Lathia, J. D. Small-Molecule HSP27 Inhibitor Abolishes Androgen Receptors in Glioblastoma. *J. Med. Chem.* **2021**, *64*

- (3), 1570–1583.
- (30) Stupp, R.; Taillibert, S.; Kanner, A. A.; Kesari, S.; Steinberg, D. M.; Toms, S. A.; Taylor, L. P.; Lieberman, F.; Silvani, A.; Fink, K. L.; et al. Maintenance Therapy With Tumor-Treating Fields Plus Temozolomide vs Temozolomide Alone for Glioblastoma. *JAMA* **2015**, *314* (23), 2535.
<https://doi.org/10.1001/jama.2015.16669>.
- (31) Stupp, R.; Taillibert, S.; Kanner, A.; Read, W.; Steinberg, D. M.; Lhermitte, B.; Toms, S.; Idhah, A.; Ahluwalia, M. S.; Fink, K.; et al. Effect of Tumor-Treating Fields Plus Maintenance Temozolomide vs Maintenance Temozolomide Alone on Survival in Patients With Glioblastoma. *JAMA* **2017**, *318* (23), 2306.
<https://doi.org/10.1001/jama.2017.18718>.
- (32) Lee, S. Y. Temozolomide Resistance in Glioblastoma Multiforme. *Genes Dis.* **2016**, *3* (3), 198–210. <https://doi.org/10.1016/j.gendis.2016.04.007>.
- (33) Ostrom, Q. T.; Cote, D. J.; Ascha, M.; Kruchko, C.; Barnholtz-Sloan, J. S. Adult Glioma Incidence and Survival by Race or Ethnicity in the United States from 2000 to 2014. *JAMA Oncol.* **2018**, *4* (9), 1254–1262.
- (34) Ostrom, Q. T.; Rubin, J. B.; Lathia, J. D.; Berens, M. E.; Barnholtz-Sloan, J. S. Females Have the Survival Advantage in Glioblastoma. *Neuro. Oncol.* **2018**, *20* (4), 576–577. <https://doi.org/10.1093/neuonc/noy002>.
- (35) Bayik, D.; Zhou, Y.; Park, C.; Hong, C.; Vail, D.; Silver, D. J.; Lauko, A.; Roversi, G.; Watson, D. C.; Lo, A.; et al. Myeloid-Derived Suppressor Cell Subsets Drive Glioblastoma Growth in a Sex-Specific Manner. *Cancer Discov.* **2020**, *10* (8),

1210–1225. <https://doi.org/10.1158/2159-8290.CD-19-1355>.

- (36) Yang, W.; Warrington, N. M.; Taylor, S. J.; Whitmire, P.; Carrasco, E.; Singleton, K. W.; Wu, N.; Lathia, J. D.; Berens, M. E.; Kim, A. H. Sex Differences in GBM Revealed by Analysis of Patient Imaging, Transcriptome, and Survival Data. *Sci. Transl. Med.* **2019**, *11* (473), eaao5253.
- (37) Bao, D.; Cheng, C.; Lan, X.; Xing, R.; Chen, Z.; Zhao, H.; Sun, J.; Wang, Y.; Niu, C.; Zhang, B. Regulation of P53wt Glioma Cell Proliferation by Androgen Receptor-Mediated Inhibition of Small VCP/P97-Interacting Protein Expression. *Oncotarget* **2017**, *8* (14), 23142.
- (38) Zalsman, N.; Canello, T.; Ovadia, H.; Charbit, H.; Zelikovitch, B.; Mordechai, A.; Fellig, Y.; Rabani, S.; Shahar, T.; Lossos, A. CSIG-24. ANDROGEN RECEPTOR IS A POTENTIAL THERAPEUTIC TARGET IN GLIOBLASTOMA. *Neuro. Oncol.* **2017**, *19* (suppl_6), vi54–vi55.
- (39) Lavon, I.; Zalsman, N.; Canello, T.; Charbit, H.; Zelikovitch, B.; Mordechai, A.; Fellig, Y.; Rabani, S.; Shahar, T.; Lossos, A. CSIG-13. Androgen Receptor Is Involved in Glioblastoma and Presents a Potential Therapeutic Target. Oxford University Press US 2016.
- (40) H., S.; C., W.; J., D.; K., W.-R.; E., B.-B.; J., E.; T., L.; D., S.; C., S.; D., W. Abstracts from the 23rd Annual Scientific Meeting and Education Day of the Society for Neuro-Oncology November 15 – 18, 2018 New Orleans, Louisiana. *Neuro. Oncol.* **2018**, *20* (suppl_6), NP-NP. <https://doi.org/10.1093/neuonc/noy148>.
- (41) Gibert, B.; Eckel, B.; Fasquelle, L.; Moulin, M.; Bouhallier, F.; Gonin, V.; Mellier,

- G.; Simon, S.; Kretz-Remy, C.; Arrigo, A.-P. Knock down of Heat Shock Protein 27 (HspB1) Induces Degradation of Several Putative Client Proteins. *PLoS One* **2012**, *7* (1), e29719.
- (42) Lelj-Garolla, B.; Mauk, A. G. Roles of the N- and C-Terminal Sequences in Hsp27 Self-Association and Chaperone Activity. *Protein Sci.* **2012**, *21* (1), 122–133. <https://doi.org/10.1002/pro.761>.
- (43) McDonald, E. T.; Bortolus, M.; Koteiche, H. A.; Mchaourab, H. S. Sequence, Structure, and Dynamic Determinants of Hsp27 (HspB1) Equilibrium Dissociation Are Encoded by the N-Terminal Domain. *Biochemistry* **2012**, *51* (6), 1257–1268. <https://doi.org/10.1021/bi2017624>.
- (44) Neckers, L.; Workman, P. Hsp90 Molecular Chaperone Inhibitors: Are We There Yet? *Clin. Cancer Res.* **2012**, *18* (1), 64–76. <https://doi.org/10.1158/1078-0432.CCR-11-1000>.
- (45) Jakubowicz-Gil, J.; Langner, E.; Bądziul, D.; Wertel, I.; Rzeski, W. Silencing of Hsp27 and Hsp72 in Glioma Cells as a Tool for Programmed Cell Death Induction upon Temozolomide and Quercetin Treatment. *Toxicol. Appl. Pharmacol.* **2013**, *273* (3), 580–589. <https://doi.org/10.1016/j.taap.2013.10.003>.
- (46) Andrieu, C.; Taieb, D.; Baylot, V.; Ettinger, S.; Soubeyran, P.; De-Thonel, A.; Nelson, C.; Garrido, C.; So, A.; Fazli, L.; et al. Heat Shock Protein 27 Confers Resistance to Androgen Ablation and Chemotherapy in Prostate Cancer Cells through EIF4E. *Oncogene* **2010**, *29* (13), 1883–1896. <https://doi.org/10.1038/onc.2009.479>.

- (47) Yi, X.; Zhong, B.; Smith, K. M.; Geldenhuys, W. J.; Feng, Y.; Pink, J. J.; Dowlati, A.; Xu, Y.; Zhou, A.; Su, B. Identification of a Class of Novel Tubulin Inhibitors. *J. Med. Chem.* **2012**, *55* (7), 3425–3435.
- (48) Zhong, B.; Chennamaneni, S.; Lama, R.; Yi, X.; Geldenhuys, W. J.; Pink, J. J.; Dowlati, A.; Xu, Y.; Zhou, A.; Su, B. Synthesis and Anticancer Mechanism Investigation of Dual Hsp27 and Tubulin Inhibitors. *J. Med. Chem.* **2013**, *56* (13), 5306–5320.
- (49) Zhong, B.; Lama, R.; Kulman, D. G.; Li, B.; Su, B. Lead Optimization of Dual Tubulin and Hsp27 Inhibitors. *Eur. J. Med. Chem.* **2014**, *80*, 243–253.
<https://doi.org/10.1016/j.ejmech.2014.04.038>.
- (50) Concannon, C. G.; Gorman, A. M.; Samali, A. On the Role of Hsp27 in Regulating Apoptosis. *Apoptosis* **2003**, *8* (1), 61–70.
- (51) Rogalla, T.; Ehrnsperger, M.; Preville, X.; Kotlyarov, A.; Lutsch, G.; Ducasse, C.; Paul, C.; Wieske, M.; Arrigo, A.-P.; Buchner, J. Regulation of Hsp27 Oligomerization, Chaperone Function, and Protective Activity against Oxidative Stress/Tumor Necrosis Factor α by Phosphorylation. *J. Biol. Chem.* **1999**, *274* (27), 18947–18956.
- (52) Faiella, L.; Piaz, F. D.; Bisio, A.; Tosco, A.; De Tommasi, N. A Chemical Proteomics Approach Reveals Hsp27 as a Target for Proapoptotic Clerodane Diterpenes. *Mol. Biosyst.* **2012**, *8* (10), 2637. <https://doi.org/10.1039/c2mb25171j>.
- (53) Idippily, N. D.; Zheng, Q.; Gan, C.; Quamine, A.; Ashcraft, M. M.; Zhong, B.; Su, B. Copalic Acid Analogs Down-Regulate Androgen Receptor and Inhibit Small

Chaperone Protein. *Bioorganic Med. Chem. Lett.* **2017**.

<https://doi.org/10.1016/j.bmcl.2017.04.046>.

- (54) Lelj-Garolla, B.; Mauk, A. G. Self-Association and Chaperone Activity of Hsp27 Are Thermally Activated. *J. Biol. Chem.* **2006**, *281* (12), 8169–8174.
- (55) Nappi, L.; Aguda, A. H.; Nakouzi, N. Al; Lelj-Garolla, B.; Beraldi, E.; Lallous, N.; Thi, M.; Moore, S.; Fazli, L.; Battsogt, D.; et al. Ivermectin Inhibits HSP27 and Potentiates Efficacy of Oncogene Targeting in Tumor Models. *J. Clin. Invest.* **2019**, *130* (2), 699–714. <https://doi.org/10.1172/JCI130819>.
- (56) Stope, M. B.; Schubert, T.; Staar, D.; Rönnau, C.; Streitböcher, A.; Kroeger, N.; Kubisch, C.; Zimmermann, U.; Walther, R.; Burchardt, M. Effect of the Heat Shock Protein HSP27 on Androgen Receptor Expression and Function in Prostate Cancer Cells. *World J. Urol.* **2012**, *30* (3), 327–331.
- (57) Yoshida, T.; Shiraishi, T.; Nakata, S.; Horinaka, M.; Wakada, M.; Mizutani, Y.; Miki, T.; Sakai, T. Proteasome Inhibitor MG132 Induces Death Receptor 5 through CCAAT/Enhancer-Binding Protein Homologous Protein. *Cancer Res.* **2005**, *65* (13), 5662–5667.
- (58) Hess, K. R.; Broglio, K. R.; Bondy, M. L. Adult Glioma Incidence Trends in the United States, 1977–2000. *Cancer Interdiscip. Int. J. Am. Cancer Soc.* **2004**, *101* (10), 2293–2299.
- (59) Rodríguez-Lozano, D. C.; Piña-Medina, A. G.; Hansberg-Pastor, V.; CAMACHO-ARROYO, I. Testosterone Promotes Glioblastoma Cell Proliferation, Migration and Invasion through Androgen Receptor Activation. *Front. Endocrinol.*

(Lausanne). **2019**, *10*, 16.

- (60) Li, J.; Fu, X.; Cao, S.; Li, J.; Xing, S.; Li, D.; Dong, Y.; Cardin, D.; Park, H.-W.; Mauvais-Jarvis, F. Membrane-Associated Androgen Receptor (AR) Potentiates Its Transcriptional Activities by Activating Heat Shock Protein 27 (HSP27). *J. Biol. Chem.* **2018**, *293* (33), 12719–12729.
- (61) Yaksh, T. L.; Dirig, D. M.; Conway, C. M.; Svensson, C.; Luo, Z. D.; Isakson, P. C. The Acute Antihyperalgesic Action of Nonsteroidal, Anti-Inflammatory Drugs and Release of Spinal Prostaglandin E2 Is Mediated by the Inhibition of Constitutive Spinal Cyclooxygenase-2 (COX-2) but Not COX-1. *J. Neurosci.* **2001**, *21* (16), 5847–5853.
- (62) Chung, Y. G.; Kim, H. K.; Lee, H. K.; Lee, K. C. Expression of Androgen Receptors in Astrocytoma. *J. Korean Med. Sci.* **1996**, *11* (6), 517–521.
- (63) Zalcman, N.; Gutreiman, M.; Shahar, T.; Weller, M.; Lavon, I. Androgen Receptor Activation in Glioblastoma Can Be Achieved by Ligand-Independent Signaling through EGFR—A Potential Therapeutic Target. *Int. J. Mol. Sci.* **2021**, *22* (20), 10954.
- (64) Liu, X.; Feng, C.; Liu, J.; Cao, L.; Xiang, G.; Liu, F.; Wang, S.; Jiao, J.; Niu, Y. Androgen Receptor and Heat Shock Protein 27 Co-Regulate the Malignant Potential of Molecular Apocrine Breast Cancer. *J. Exp. Clin. Cancer Res.* **2018**, *37* (1), 1–12.
- (65) Kiliccioglu, I.; Konac, E.; Dikmen, A. U.; Sozen, S.; Bilen, C. Y. Hsp-27 and NF-KB Pathway Is Associated with AR/AR-V7 Expression in Prostate Cancer Cells.

Gene **2019**, *697*, 138–143.

- (66) U.S. Department of Health and Human Services, F. and D. A. Bioanalytical Method Validation Guidance for Industry. *U.S. Dep. Heal. Hum. Serv. Food Drug Adm.* **2018**, No. May, 1–41.
- (67) Zeng, R.; Liu, Z.; Sun, Y.; Xu, C. Differential Expression and Function of AR Isoforms in Prostate Cancer. *Oncol. Rep.* **2012**, *27* (2), 492–498.
- (68) Sun, H.; Werner, C.; Dresser, J.; Wilder-Romans, K.; Baskin-Bey, E.; Eisner, J.; Lawrence, T.; Spratt, D.; Speers, C.; Wahl, D. EXTH-15. TARGETING ANDROGEN SIGNALING IN GLIOBLASTOMA (GBM) USING SEVITERONEL (SEVI), A CYP17 LYASE AND ANDROGEN RECEPTOR (AR) INHIBITOR, ALONE AND IN COMBINATION WITH RADIATION (RT). *Neuro. Oncol.* **2018**, *20* (Suppl 6), vi88–vi88.
<https://doi.org/10.1093/neuonc/noy148.364>.
- (69) Zhao, N.; Wang, F.; Ahmed, S.; Liu, K.; Zhang, C.; Cathcart, S. J.; DiMaio, D. J.; Punsoni, M.; Guan, B.; Zhou, P. Androgen Receptor, Although Not a Specific Marker for, Is a Novel Target to Suppress Glioma Stem Cells as a Therapeutic Strategy for Glioblastoma. *Front. Oncol.* **2021**, *11*, 1696.
- (70) Kamada, M.; So, A.; Muramaki, M.; Rocchi, P.; Beraldi, E.; Gleave, M. Hsp27 Knockdown Using Nucleotide-Based Therapies Inhibit Tumor Growth and Enhance Chemotherapy in Human Bladder Cancer Cells. *Mol. Cancer Ther.* **2007**, *6* (1), 299–308.
- (71) Chauhan, D.; Li, G.; Shringarpure, R.; Podar, K.; Ohtake, Y.; Hideshima, T.;

- Anderson, K. C. Blockade of Hsp27 Overcomes Bortezomib/Proteasome Inhibitor PS-341 Resistance in Lymphoma Cells. *Cancer Res.* **2003**, *63* (19), 6174–6177.
- (72) Li, Y.; Dano, R.; Li, C.; Zhang, W.; Lathia, J. D.; Wang, B.; Su, B. Pharmacokinetic and Brain Distribution Study of an Anti-Glioblastoma Agent in Mice by HPLC – MS / MS. **2022**, No. November 2021.
<https://doi.org/10.1002/bmc.5310>.
- (73) Brännert, D.; Langer, C.; Zimmermann, L.; Bargou, R. C.; Burchardt, M.; Chatterjee, M.; Stope, M. B. The Heat Shock Protein 70 Inhibitor VER155008 Suppresses the Expression of HSP27, HOP and HSP90 β and the Androgen Receptor, Induces Apoptosis, and Attenuates Prostate Cancer Cell Growth. *J. Cell. Biochem.* **2020**, *121* (1), 407–417.
- (74) Bahnassy, S.; Thangavel, H.; Quttina, M.; Khan, A. F.; Dhanyalayam, D.; Ritho, J.; Karami, S.; Ren, J.; Bawa-Khalfe, T. Constitutively Active Androgen Receptor Supports the Metastatic Phenotype of Endocrine-Resistant Hormone Receptor-Positive Breast Cancer. *Cell Commun. Signal.* **2020**, *18* (1), 1–11.